1-1-2020

The Influence Of Screw Configuration And Other Mechanistic Approaches On The Morphology And Release Of Drugs From Polymeric Matrices Utilizing Hot-Melt Extrusion Technology

Joseph Morott

THE INFLUENCE OF SCREW CONFIGURATION AND OTHER MECHANISTIC APPROACHES ON THE MORPHOLOGY AND RELEASE OF DRUGS FROM POLYMERIC MATRICES UTILIZING HOT-MELT EXTRUSION TECHNOLOGY

A Dissertation
Submitted in Partial Fulfillment of the Requirements
for the Degree of Doctor of Philosophy
in the Department of Pharmaceutics and Drug Delivery
The University of Mississippi School of Pharmacy

Joseph Thomas Morott, Jr.

Oxford, Mississippi

May 2020

ABSTRACT

Twin-screw extrusion, often referred to as Hot-Melt Extrusion within the pharmaceutical industry, is an efficient, continuous and solvent-free process that has been investigated extensively for its solubility enhancement applications, and, to a lesser degree, for its potential to replace more conventional “batch” technologies. The research contained herein focuses on the latter of these with attention paid to the effects of screw configuration. In this research, the twin-screw extrusion process was utilized to produce taste masked formulations of a BCS I API, which necessitated the prevention of amorphous phase formation. The resulting granules were subsequently incorporated into an immediate release orally disintegrating tablet (ODT) platform. This processing technology was also evaluated as an alternative platform for the production of dry granulations, henceforth referred to as Twin-Screw Dry Granulation (TSDG). This novel processing approach was investigated using Quality by Design (QbD) principles; however, as the QbD paradigm in product oriented, the process was assessed by the successful production of a drug intermediate and, ultimately, an optimized target formulation. The TSDG process was utilized to produce a high drug loaded sustained release solid oral dosage form in which the crystalline lattice was preserved. Moreover, as a fundamental purpose of granulating technologies is the improvement of the flowability of one or more of the granule constituents, the resulting granules were assessed for enhanced flowability when compared to the very poorly flowing API. Finally, the effects of screw configuration on API morphology was evaluated for the effects of system dependence as the observed existing literature focuses on single systems wherein the effects of screw configuration on API morphology are not assessed for their variations from one carrier system to another.

Moreover, the effects of screw configuration were evaluated from the standpoint of the preservation of the API crystalline lattice as the observed existing information on screw configuration within the pharmaceutical literature focuses on solubility enhancement via conversion of the API crystalline lattice into either a molecularly dispersed solid solution or an amorphous solid dispersion.

DEDICATION

To my parents, Joseph T. Morott, Sr. & Toni S. Sullivan, Ph.D., for not only teaching me the values of education and hard work, but also for their endless encouragement and support. To my high school sweetheart and wife, Heather Marie Morott, and my two sons, Alexander Casey Morott & Kaleb Thomas Morott, you have forfeited far more of my time than could be expected, so that I could pursue my dream of becoming a credentialed pharmaceutical scientist. I give you all credit.

ACKNOWLEDGEMENTS

I would like to express my deep and sincere gratitude to my advisor Dr. Michael Andrew Repka for allowing me to pursue this opportunity at the University of Mississippi. I suspect that I have learned much more from you than you know. I want to further thank you for all the opportunities that you afforded me while at *Ole Miss*, not to mention your enduring patience.

I would like to express sincere appreciation to Dr. John O'Haver. If ever I find myself back in an academic setting, you are the standard that I will attempt to hold myself to. Our long and frequent conversations in your office often gave me the encouragement I needed.

To Dr. Soumyajit Majumdar, your continuous positive regard and desire for excellence are a source of inspiration to the graduate and professional students alike. You may never know how much your kind words meant to me.

To Dr. Narasimha Murthy, I have met few individuals that are as driven and untiring as you are. It is truly inspiring seeing how much you accomplish while still making time for the rest of life. Thank you for granting me patience as both a graduate student and teaching assistant.

In no particular order, I would like to acknowledge my lab mates in the department, Manjeet Pimprade, Jiannan Lu, Xin Feng, Hemlata Patil, Priyanka Thipsay, Nagendra Punyamurthula, Anh Vo, and Ketaki Patwardhan thank you for helping to quell the moments of frustration and doubt with kind conversation. I will miss our reciprocating support.

If I have forgotten to give credit, acknowledgement or appreciation where it is due, I apologize. There were simply too many names to recall during this exciting, yet hectic, part of my journey.

I can only hope to someday inspire others the way that you all have inspired me. Without a single doubt, these years at the University of Mississippi will remain among my most cherished memories. For old times' sake, from the heart, *"Hotty Toddy"!*

TABLE OF CONTENTS

SECTION **PAGE**

Abstract…..……..……..ii

Dedication……..…...iv

Acknowledgements..……..……v

List of Abbreviations……..…….xii

List of Tables…….....xv

List of Figures…….……xvi

CHAPTER 1: Introduction to Extrusion……1

1.1 Extrusion as a Processing Technology……...……1

1.2 Types of Extrusion…….1

1.2.1 Ram Extrusion……..……2

1.2.2 Screw Extrusion……...2

1.2.3 Single Screw Extrusion……3

1.2.4 Twin-Screw Extrusion……...…….…….7

1.2.5 Pharmaceutical Applications of Hot-Melt Extrusion…….……...9

CHAPTER 2: The Effects of Screw Configuration and Polymeric Carriers on Hot-Melt Extruded Taste-Masked Formulations Incorporated into Orally Disintegrating Tablets…....11

2.1 Abstract……11

2.2 Introduction…….….12

2.3 Materials and Methods…….……..…..14

2.3.1 Materials……...……14

2.3.2 Thermogravimetric (TGA) & Differential Scanning Calorimetry (DSC) Analysis…….….15

2.3.3 Hot-Melt Extrusion Processing……..……...16

2.3.4 Post-Extrusion Drug Content……18

2.3.5 High Performance Liquid Chromatography (HPLC) Analysis……18

2.3.6 Powder X-Ray Diffraction (PXRD) Analysis…….……...……..18

2.3.7 Fourier Transform Infrared (FTIR) Spectroscopy & Mid Infrared Chemical Imaging…….…….……19

2.3.8 Dissolution Testing of Milled Extrudates…….……19

2.3.9 Preformulation for Tableting……19

2.3.10 Tablet Compression……19

2.3.11 Tablet Properties…….20

2.3.12 Electronic Tongue Analysis…….……...…21

2.3.13 ODT Oral & Gastric Dissolution……21

2.3.14 Physical and Chemical Stability…….22

2.3.15 Statistical Analysis of Dissolution Data…….22

2.4 Results and Discussion……23

2.4.1 Hot-Melt Extrusion & Screw Configuration…….……23

2.4.2 Thermogravimetric & DSC Analysis……23

2.4.3 Polymer Screening……23

2.4.4 PXRD Analysis…….……25

2.4.5 FT-IR & Mid Infrared Chemical Imaging……....27

2.4.6 E-Tongue & Oral Dissolution Testing of Milled Extrudates……31

2.4.7 Addition of Release Modifying Agents……33

2.4.8 Tableting API-Excipient Compatibility…….……..35

2.4.9 Tablet Properties…….……..36

2.4.10 ODT Oral & Gastric Tablet Dissolution…….38

2.4.11 Physical and Chemical Stability…….40

2.5 Conclusion……...41

CHAPTER 3: A Quality by Design Investigation of a Novel Twin-Screw Dry Granulation Process……..……...42

3.1 Introduction…….……42

3.2 Materials and Methods…….……45

3.3 Methods…….…..……..46

3.3.1 API-Excipient Compatability…….…….……..46

3.3.2 Fourier Transform Infrared Spectroscopy (FT-IR)……...…46

3.3.3 Preliminary Range Screening of Formulation and Process Variables…..…46

3.3.4 Experimental Design (DoE) & Analysis…….……..47

3.3.5 Physical Mixture Preparation……47

3.3.6 Twin-Screw Dry Granulation (TSDG)…….47

3.3.7 Scanning Electron Microscopy (SEM)…….48

3.3.8 Dry Granulation Flow Property Measurements……..…..……48

3.3.9 Tablet Compression……..……49

3.3.10 Tablet Properties…….……..……..49

3.3.11 Dissolution Testing……..……...50

3.4 Results & Discussion……..…….50

3.4.1 Preliminary Range Finding Studies & Observations……50

3.4.2 Twin-Screw Lubrication……...……52

3.4.3 Screw Design……53

3.4.4 Quality by Design…….55

3.4.5 Experimental Design (DoE) & Analysis……..55

3.4.6 Main Effects Screening DoE……56

3.4.7 Tablet Compression……..57

3.4.8 Tablet Properties……...57

3.4.9 Characterization DoE……58

3.4.10 Percent Fines……...60

3.4.11 Hausner Ratio……..61

3.4.12 Compressibility……...62

3.4.13 Angle of Repose……..63

3.4.14 Time to 80% Dissolution……63

3.4.15 Fourier Transform Infrared Spectroscopy (FT-IR)…….65

3.4.16 Scanning Electron Microscopy (SEM)……...66

3.4.17 Numeric Prediction of Optimization & Confirmation…….…….68

3.4.18 Design Space…….…….71

3.5 Conclusion……..72

CHAPTER 4: The Effects of Screw Configuration on API Morphology within Polymeric Matrices…….……..73

4.1 Introduction…….……73

4.2 Materials & Methods…….……..74

4.3 Hot-Melt Extrusion…….…….……74

4.3.1 Thermogravimetric Analysis……..…….…….74

4.3.2 Differential Scanning Calorimetry (DSC)…….……...75

4.3.3 Hot-Melt Extrusion Processing…….……75

4.3.4 FT-IR & Mid-Infrared Chemical Imaging……75

4.4 Results and Discussion……76

4.4.1 Thermogravimetric Analysis……76

4.4.2 Hot-Melt Extrusion Processing……76

4.4.3 FT-IR & Mid-Infrared Chemical Imaging……...76

CHAPTER 5: Summary and Conclusion…….…...85

Bibliography…….…..……..87

Vita……...……99

LIST OF ABBREVIATIONS

ANOVA……...…Analysis of Variance

API…….....Active Pharmaceutical Ingredient

ASD…….Amorphous Solid Dispersion

ATR…….Attenuated Total Reflectance

BCS……..Biopharmaceutical Classification System

BHT…….……...Butylated Hydroxytoluene

CMA……..……..Critical Material Attribute

CPP…….....Critical Processing Parameter

CQA……..….Critical Quality Attribute

CSD……..Crystalline Solid Dispersion

D_o.…….……..……Outer Diameter of Flighted/Conveying Screw Elements

D_i.…….……..……Inner Diameter of Flighted/Conveying Screw Elements

DoE……...Design of Experiments

DSC.....Differential Scanning Calorimetry

EC……..…Ethyl Cellulose

FMEA……....Failure Mode Effect(s) Analysis

FOV…….Field of View

FPA…….…..Focal Plane Array

FTIR…….Fourier Transform Infrared Spectroscopy

HME……...Hot-Melt Extrusion

HPC……...Hydroxypropyl Cellulose

HPLC……....High Performance Liquid Chromatography

i.e……..id est

L/D…….……...Length to Diameter Ratio

MIR……...Mid-Infrared

MSE……...…….Multi-Screw Extruder

MW…….……..Molecular Weight

NCE…….…New Chemical Entity

ODT…….….Orally Disintegrating Tablet

PVP…….….Polyvinylpyrrolidone

PXRD……..Powder X-Ray Diffraction

QbD……..Quality by Design

QTPP…….…Quality Target Product Profile

RH……Relative Humidity

RPM…….Revolutions per Minute

SC……...…Sildenafil Citrate

SEM……..Scanning Electron Microscope

SSE……..……..Single Screw Extruder

SSF……Simulated Salivary Fluid

Tg……..……Glass Transition

TGA…….Thermogravimetric Analysis

Tm……..…….Melting Temperature

TSDG……Twin-Screw Dry Granulation

TSE……..…….……..Twin-Screw Extruder

USP……..……...……..United States Pharmacopeia

NF……...National Formulary

UV/Vis…….....Ultra Violet/Visible

VA……...…….…..Polyvinyl acetate

XRPD…….……X-Ray Powder Diffraction

ZnSe…….Zinc Selenide

List of Tables

Table…….....Page

2-1: Polymer Screening & Extrusion Parameters……..16

2-2: Artificial Salivary Dissolution Media (adjusted to pH 6.8)……...……22

2-3: ODT Formulation Including the Varying Percentages of Super Disintegrant and Filler Used…….…….…….36

2-4a: ODT Tablet Properties with PVP XL…….……..……37

2-4b: ODT Tablet Properties with PVP XL-10…….……37

3-1: Quality Target Product Profile (QTPP)…….……..…45

3-2: Initial Risk Assessment…….…..…55

3-3: Main effects assessed by pareto analysis of screening DoE (Min. Run Res. IV)…….…….57

3-4: Tablet friability and hardness data from the screening DoE with extragranular magnesium stearate……..……..……58

3-5: 2^3 Full factorial with 4 center points; screw design 1: Figure 2d; screw design 1: Figure 2e……...……..…59

3-6: Response ranges and statistically significant main effects & interactions from the characterization DoE……..……60

3-7: Numerically predicted formulation and process parameters resulting from the input acceptable ranges on screw design 1; *Confirmation*: Confirmatory Results……..……69

List of Figures

Figure……....Page

1-1: Schematic Representation of a Rudimentary Ram Extrusion Process……..……...2

1-2: Schematic Representation of a Single Screw Extruder……4

1-3: Single Screw Extruder Sections……...5

1-4: Single Helix Conveying Element……6

2-1a-c: Figures 2-1a-1c: Images of the three screw configurations evaluated during HME process optimization. Figure 2-1a: ThermoFisher "Standard Configuration" 40:1 L/D. Figure 2-1b: All conveying elements; 40:1 L/D. Figure 2-1c: From Left to Right: 110mm of conveying elements; 22mm of perpendicularly arranged mixing elements; 165mm of conveying elements; 25:1 L/D..17

2-2: SC release profile of preliminary polymer screening formulations in artificial saliva media adjusted to pH 6.8.……..……24

2-3a-b: a; PXRD diffractogram of pure crystalline SC. b; PXRD diffractograms of binary mixtures of ethylcellulose & SC as a function of screw configurations……26

2-4: FTIR Spectra of Crystalline & Amorphous SC…….…..…..…..……..28

2-5a-c: Chemical image (5.5 µm spatial resolution) of a binary mixture of ethylcellulose & SC highlighting the intensity of the carbonyl present in crystalline SC processed using screw configuration 2 (Figure 2-1b). Figure 5b: Chemical image (5.5 µm spatial resolution) of a binary mixture of ethylcellulose & SC highlighting the intensity of the carbonyl present in crystalline SC processed using screw configuration 3 (Figure 2-1c). Figure 2-5c: Chemical image (1.1 µm

spatial resolution) of a binary mixture of ethylcellulose & SC highlighting the intensity of the carbonyl present in crystalline SC processed using screw configuration 3 (Figure 2-1c).….....30

2-6: Graphical illustration of PCA results from e-tongue analysis illustrating each samples distance from artificial salivary fluid as a function of screw design. ……...……31

2-7: Dissolution data of binary mixtures of ethylcellulose and SC as a function of screw design…….32

2-8: E- Graphical illustration of PCA results from e-tongue analysis illustrating each samples distance from artificial salivary fluid as a function of individual pore former in each formulation. ……..……...……34

2-9: Dissolution release profile of milled extrudate (20% SC, 60% ethylcellulose & 20% calcium carbonate) in artificial salivary media (pH 6.8).……..……...……..35

2-10a: Dissolution profile of optimized SC ODT formulation in artificial salivary fluid (pH 6.8)…….39

2-10b: Gastric release profile of optimized SC ODT formulation in gastric media (pH 2)…..….39

3-1a-b: (Top) and 3-1b (Bottom): Graphic Illustration of the Observed Differences between a Polymer Melt on the Mixing Elements (3-1a) and the Compacted Powder Mass Formed During the TSDG Process (3-1b)…….…….51

3-2a-e: a: ThermoFisher preconfigured screw design; b: all conveying screw design; c: single mixing zone screw design; d: two mixing zone screw design; e: modified final mixing zone screw design……54

3-3: Percent Fines contour plot and response surface graph with Screw Design 1 (Figure 3-2b)……..…61

3-4: Compressibility contour plot and response surface graph with screw design 1 (Figure 3-2 e)….……...……62

3-5: Time to 80% Dissolution Contour plot and Response surface graph with Screw Design 1 (Figure 3-2 e)……...…..…….64

3-6: Mid-Infrared Spectral Evaluation of Sildenafil Citrate's Post Processing Physical Phase…….……..……..……...…66

3-7: A-D: 4A Physical Mixture (100X), 4B Hot-Melt Granule (100X), 4C Dry Granule (100X); 4D Dry Granule (300X)……...…….....68

3-8: Individual independent variable and dependent variable desirability values…….……..…..70

3-9: Desirability function contour plot and corresponding response surface…….……71

3-10: Overlay plot of the resulting design space……72

4-1: FT-IR spectra of Eudragit E PO (EPO), Carbamezapine (CBZ) and Caffeine Citrate (CC).77

4-2: FT-IR spectral overlay of Eudragit E PO (EPO) and Caffeine Citrate (CC)…….78

4-3: FT-IR spectral overlay of Eudragit E PO (EPO) and Carbamezapine (CBZ)……79

4-4: IR chemical images take of CC from the Beginning, Middle and End of Mixing zone…....80

4-5: IR chemical images take of CC from the Beginning, Middle and End of Mixing zone……81

4-6: IR chemical images take of CBZ from the Beginning, Middle and End of Mixing zone….82

4-7: IR chemical images take of CBZ from the Beginning, Middle and End of Mixing zone…..83

CHAPTER 1.

INTRODUCTION TO EXTRUSION

1.1 Extrusion as a Processing Technology

Extrusion is a commonly utilized processing technology spanning a wide variety of industries including, but not limited to, ceramics, food, metals, paper, plastics, various chemically reacted products, and more recently pharmaceuticals [1-10]. In the simplest terms, extrusion is the process of forcing material through a die into a material of uniform cross-sectional geometry. The ubiquity of this process is owed, in part, to over 100 years of industrial application, as well as the numerous variations of the process that are commercially available.

1.2 Types of Extrusion

While it is important to acknowledge the many subclasses of the extrusion process that exist (e.g. direct, indirect, hydrostatic, sheet, forward, backward, blow film, over jacketing, hot, cold, etc.), a description and discussion of each is beyond the scope of any single text. Therefore, as described within this work there are two fundamental sub-classes of this process that are defined by the method in which the in-process material is moved along the barrel and exits the extruder. Namely, these are ram extrusion and screw extrusion. While research contained in this work focuses exclusively on screw extrusion, which can be further subdivided into single and multi-screw processes, a brief description of ram extrusion is provided for completeness.

1.2.1 Ram Extrusion

A typical ram type extruder (Figure 1-1) is essentially a piston inside of an extruder barrel which, in order to accommodate the forward compressive motion of the piston, is necessarily a complimentary shape, typically a cylinder. The piston, when in its retracted position, allows the barrel to be filled with the in-process material. In a “hot” process, this material typically remains within the extruder barrel until achieving a specified temperature and is then compressed by the piston through the extruder die. In contrast, a “cold” process does not require the material to achieve a molten state and, as such, is compressed through the die at ambient temperatures.

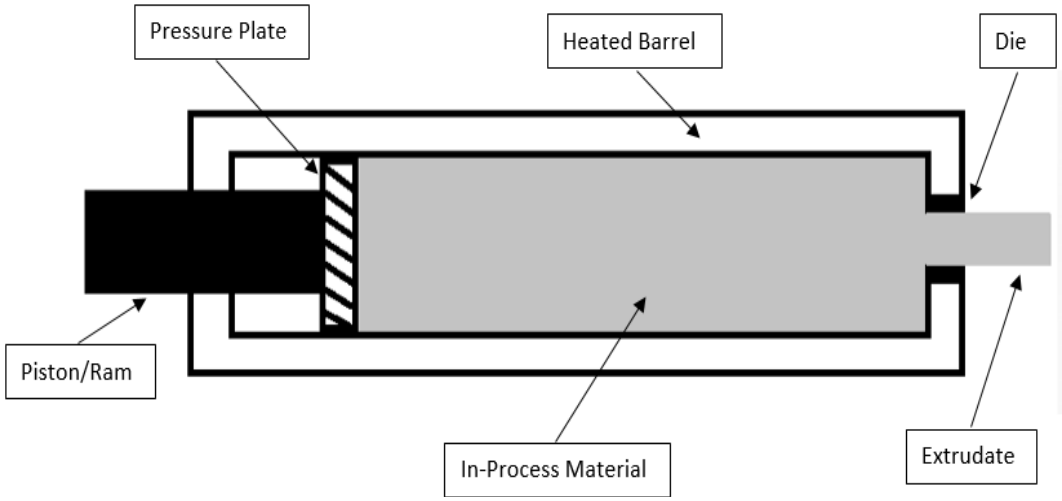

Figure 1-1, Schematic representation of a rudimentary ram extrusion process

1.2.2 Screw Extrusion

Screw extruders can be divided into three primary subclasses defined as follows:

1. Single-screw Extruders: High pressure systems containing only one screw/auger within the extruder barrel.
2. Twin-Screw Extruders: Relatively low-pressure systems containing exactly two screws within the extruder barrel. Often further categorized by the relative direction

of rotation (*i.e.* counter-rotating & co-rotating) and the degree of intermeshing of the screws within the barrel (*i.e.* intermeshing & non-intermeshing).

3. Multi-Screw Extruders: Static or rotating center shafts. Further classification can be more complex and is typically dependent on the number of screws employed.

Regardless of the number of screws employed in the process, there are some commonalities across the screw extrusion platform. Within each there is a minimum of one screw which is under constant torque requirements and is responsible for pumping the in-process materials. To achieve this, a standard assembly consisting of the following basic components, or some variation thereof, is commonly employed.

1. Motor (drive unit): provides the required torque to the screw(s)
2. Barrel: contains the screws and in-process materials;
3. Die: Attached to the end of the barrel to force the in-process materials into the desired geometry.

1.2.3 Single Screw Extrusion

Single screw extruders (SSE) were the first type of screw enabled extruders to utilize an Archimedean type screw for material processing [11]. Single screw extruders are similar in function to the previously discussed ram extruders with the primary difference being the presence of a rotating screw within the heated barrel (Figure 1-2). The most notable difference is the replacement of the ram piston with the continuous rotation of a screw, which provides a clear avenue for truly continuous processing as the in-process material is not required to remain stagnant until reaching the desired processing temperature. Instead, the feed material is in constant motion during the various unit processes (e.g. conveying, plasticizing, melting, devolatization, etc.). The

screw's rotation is powered by a motor, which is typically geared down, thereby reducing the motor speed to the desired screw speed (rpm). The gearing is usually housed within a box and surrounded by an oil, which serves to lubricate and cool the gears. Single screw type extruders function primarily as pumps where the rate of screw rotation provides the forward conveying capacity of the in-process material(s). In addition to the heated barrel, the shear imparted to the in-process material from the rotation of the screw within the barrel provides another source of energy to melt the polymer.

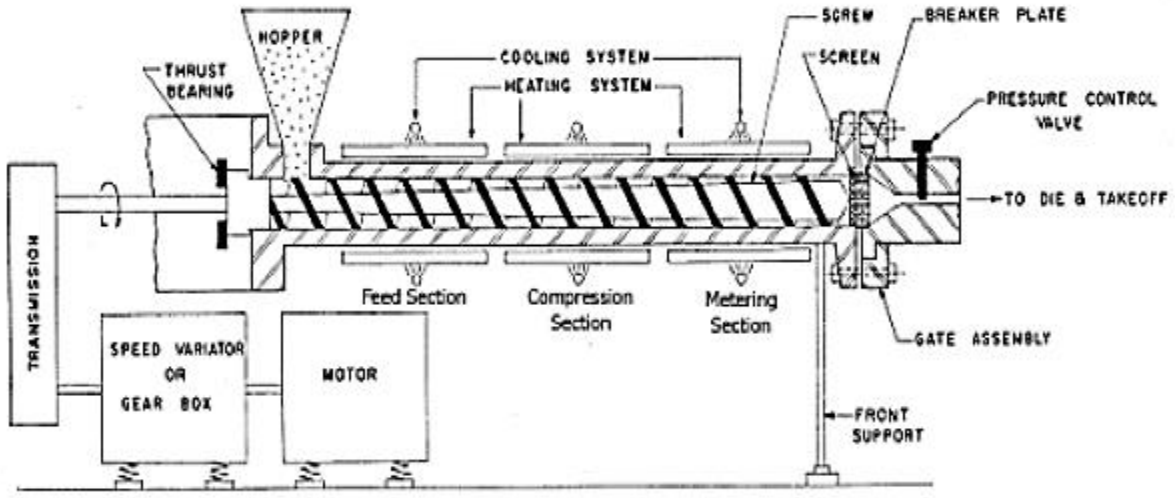

Figure 1-2, Schematic representation of a single screw extruder (SSE) [14].

Owing to the simplicity of their design, they are also the most commonly utilized type of extruder [12]. This type of extruder employs a single one-piece screw which is continuously rotated within the extruder barrel. In its simplest form, the screw itself consists of conveying sections only. However, various alterations have been employed to improve on this basic design thereby enabling enhanced mixing and distributive properties [13]. A SSE is usually characterized as a stable high-pressure system capable of consistent output operating in "flood fed" manner

whose material throughput determined by the revolutions per minute (rpm) of the screw within the barrel. It is important to note that a SSE can be operated in a “starve fed” manner, though this application is less common. In a starve fed mode of operation, the material throughput becomes less dependent on the screw rpm and becomes almost entirely dependent on the introduction of new material into the extruder hopper, otherwise referred to as the feed rate.

Multiple unit operations are achieved within the SSE, such as feeding raw material, downstream conveying or the raw materials or polymer melt, melting of the raw materials, devolatization and pumping; however, the dispersive and distributive mixing capabilities are generally considered inferior to that of their multi-screw counterparts.

The screw within a SSE is typically consists of three distinct sections or zones (Figure 1-3), which can vary in geometry, but are typically defined as Feeding, Transitioning and Metering The feed section possesses deeper flights to transport the relatively less dense powder material away from the feed throat to subsequent sections. The transitioning section provides gradual conversion from the deep flighted feed section, which contains the unmelted pellets or powder, to the metering section.

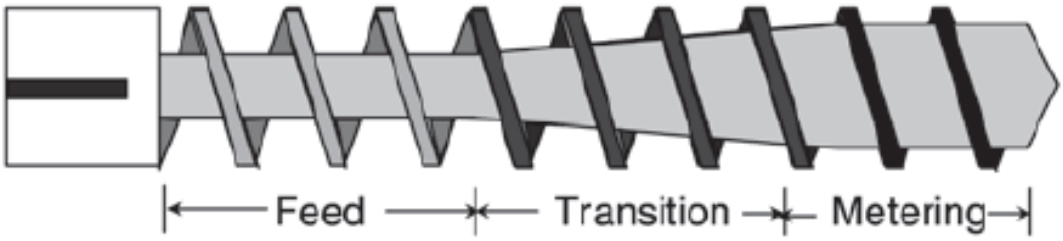

Figure 1-3, Single screw extruder (SSE) sections [14].

Additionally, the transition section provides the initial compression of the polymer melt prior to the metering process. The metering section is the final section in SSE and possesses the shallowest

flight depth to facilitate a pressure builds in the polymer melt, which in turn functions to facilitate extrusion through the die at a consistent rate.

While the ratios of the flight to the root of the SSE screw may vary, it ultimately consists solely of conveying elements unless otherwise modified. The graphical depiction and nomenclature of which, is as follows (Figure 1-4):

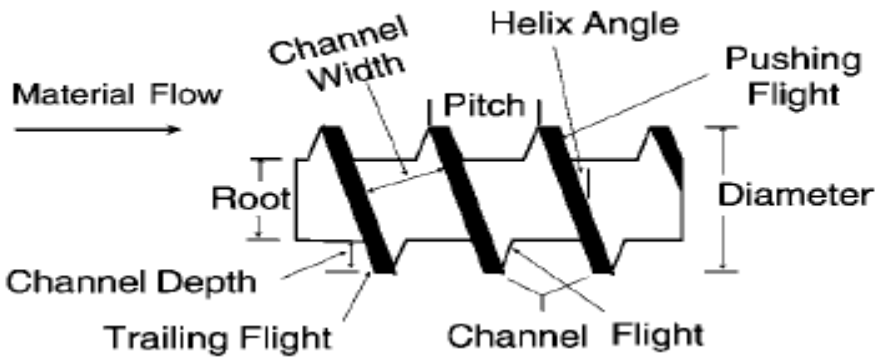

Figure 1-4, SSE single helix conveying element [14].

- Channel Depth: The distance from the tip of the flight to the root
- Channel Width: The distance between successive flights
- Trailing Flight: Back edge of the flight
- Pushing Flight: Front edge of the flight
- Pitch: The distance required for one full 360^{o} rotation of the flight around the screw root
- Helix Angle: the angle formed between the flight and a line perpendicular, or normal, to the screw root.
- Screw Diameter (D_o): The distance between the furthest flights on a screw root

- Root Diameter (D_i): The distance from the channel bottom on one side of the screw to the channel bottom on the other side of the screw.
- D_o/D_i: The ratio of the outer diameter to the inner diameter

The screw itself is typically further characterized by an L/D, or length to diameter ratio. Note that the length of the screw in Figure 1-3 is taken to be the entire flighted length of the screw, which typically runs from the base near the feeding section to the tip near the die, and the diameter is taken to be the screw diameter (D_o). The most common ratios used in industry are 25:1 and 40:1, though others are common as well.

1.2.4 Twin-Screw Extrusion

Twin-screw extruders have two screws placed side by side within the barrel of the extruder. Functionally, the addition of another screw serves to enhance the compounding ability of the process, but at the expense of reduced die pressures. In order to take advantage of this enhanced compounding capacity, the barrel of the extruder is often connected to one or more powder, pellet, flake, liquid or gas feeding system(s).

With the addition of the second screw within the extruder, a variety of orientations between the screws became possible. The first distinction to draw is the difference between co-rotating and counter rotating screws while another distinction is the distance between the screws (i.e. intermeshing). Co-rotating screw extruder rotate the screws in the same direction, be it either clockwise or counter clockwise with respect to the vantage point of the observer. Counter rotating screws rotate in opposing directions, that is, one will rotate clockwise while the other rotates counter clockwise.

While extruders with more than two screws are common, it has become apparent that the twin-screw extruder has become the extruder of choice within the pharmaceutical industry[54]. Where single screw extruders typically function as continuous pumps, twin-screw extruders commonly function as continuous compounders.

For the purposes of this thesis, further conversation will be limited to the fully intermeshing co-rotating parallel twin-screw extruders, henceforth referred to as a twin-screw extruder, hot-melt extruder or extruder. This type of extruder has two screws that lie parallel down the length of the extruder barrel. They are fully intermeshing, which provides a self-wiping mechanism for more efficient processing and decreased material residence times within the extruder. In order to facilitate the fully intermeshing corotating mechanics of this process, the additional requirement that the twin-screws are of identical configurations with an offset about the screw shaft's axis is necessitated. Interestingly, this simplifies the process setup.

Where applicable, the extrusion process has numerous inherent advantages over alternative processing techniques including relative simplicity, economical design, simplicity of scale-up, small processing foot print, reduced processing time and obvious potential continuous processing. More recently, this processing technique has been implemented by the pharmaceutical industry.

Although extrusion itself is generally considered to be a unit operation, where extrudates typically go through further downstream processing, it is most easily viewed as a series of sub-unit operations. Within the context of twin-screw extrusion, these sub-unit operations are, in simplest terms, material feeding into the extruder, material conveying and downstream metering, melting, mixing, venting, and shaping. Feeding solid or liquid raw materials into the extruder is typically accomplished by either gravimetric (weight loss) or volumetric (volume displacement) systems.

1.2.5 Pharmaceutical Applications of Hot-Melt Extrusion

Extrusion has attracted considerable attention in the pharmaceutical industry owing to the aforementioned reasons. While this process ultimately yields an extrudate of one form or another, these intermediate extrudate has been utilized to arrive at a wide variety of dosage forms including tablets, pellets, films, implants and granulations [15-26]. In addition to utilizing extrusion as an alternative to more conventional technologies present in the pharmaceutical industry, it is also being investigated for novel processing approaches. Namely, extrusion has been widely explored as a fusion based technique for arriving at the production of solid dispersions.

The formation of solid dispersions has attracted considerable interest within the pharmaceutical industry over recent years. This is due, in part, to the nature of many of the new chemical entities (NCEs) currently under investigation. These NCEs are typically arrived at through computational chemistry, commonly used to predict the binding affinity of an NCE to a biological target, or high throughput screening, which utilizes automated processes to assay the biological activity of numerous compounds over a short period of time. Both approaches tend to result in compounds that demonstrate exceptional biological characteristics but suffer from poor aqueous solubility [27-28]. Unfortunately, the lack of aqueous solubility translates into poor bioavailability, which preempts the successful development of viable drug products [27,28]. To address the issue of poor aqueous solubility, numerous physicochemical manipulations have been investigated including nanoparticle formation [29], various salt forms [30,31], co-crystallizations 31,32], pre-solubilized formulations [33-35], and API polymorphisms [35,59]. More recently, the formation of solid dispersions has attracted substantial attention in both academia and industry. Solid dispersions were initially described by Chiou & Riegleman as a solid system in which one or more APIs are dispersed into an inert carrier [36]. The carrier itself can exist in an amorphous,

crystalline or semi-crystalline (i.e. with both amorphous and crystalline regions) state, while the API(s) can be in an amorphous, crystalline or molecularly dispersed state within the carrier. Phase separated dispersions can be further categorized into two subclasses, amorphous and crystalline dispersions, while the molecularly dispersed API exists as a solid solution. These systems are commonly differentiated by their respective thermograms, in which, typical phase transition behavior can be identified. A crystalline solid dispersion would typically exhibit a glass transition (T_g) for the polymeric carrier and a melting endotherm (T_M) for the crystalline API. In contrast, an amorphous solid dispersion would typically show a glass transition for each of the amorphous components, both the amorphous/semi-crystalline carrier and the amorphous API. A molecular level solution would present only a single phase transition for the carrier as the molecularly dispersed API would not be subject to any phase changes.

There are two broadly cited methods of producing solid dispersions, which are solvent based systems and fusion based systems. Solvent based methods have historically been utilized to arrive at solid dispersions due to their simplicity in concept. First, both the carrier and API are dissolved in a common solvent, which is then followed by solvent removal. The rate of solvent removal requires consideration with regard to the type of dispersion desired. For example, it is generally accepted that rapid removal of the solvent tends to result in either a molecular or amorphous dispersion as the intermolecular forces between API molecules are provided insufficient time to orient into a crystalline lattice. Lattice formation is further inhibited by the presence of the polymeric carrier, which functions by interacting with the API via intermolecular forces, by kinetically hindering the movement of drug molecules, or by a combination of mechanisms.

CHAPTER 2.

THE EFFECTS OF SCREW CONFIGURATION AND POLYMERIC CARRIERS ON HOT-MELT EXTRUDED TASTE-MASKED FORMULATIONS INCORPORATED INTO ORALLY DISINTEGRATING TABLETS

2.1 Abstract

The primary aim of this research was to produce successfully taste masked formulations of Sildenafil Citrate (SC) using hot-melt extrusion (HME) technology. Multiple screw configurations and polymeric carriers were evaluated for their effects on taste masking efficiency, which was assessed by both E-tongue analysis and *in vitro* dissolution in simulated salivary fluid (SSF, pH 6.8 artificial saliva). The screw configurations were further assessed for their effects on the morphology of the API using PXRD, FT-IR and mid-infrared chemical imaging. It was determined that the screw configuration had a profound effect on the taste masking efficiency of the formulations as a result of altering the physical state of the API. Selected extruded formulations using ethylcellulose (EC) with a pore former were further formulated into orally disintegrating tablets (ODTs), which were optimized by varying the grade and percentage of the superdisintegrant used. An optimized disintegration time of approximately 8 seconds was achieved. The final ODT formulation exhibited excellent taste masking properties with over 85% drug release in gastric media as well as physical tablet properties. Interestingly, friability, which

tends to be a common concern when formulating ODTs, was well within the acceptable limits (<1%) for common tablets.

2.2 Introduction

The perception of taste, or palatability, of a pharmaceutical dosage form is a significant concern in terms of patient compliance. The development of successfully taste-masked formulations remains to be a particularly formidable challenge when formulating oral dosage forms for pediatric populations, who actively refuse to ingest drugs with an unpleasant taste, and/or geriatric populations, who tend to exhibit unique perceptions of taste [37,38]. A 2003 survey of Pediatricians conducted by the American Association of Pediatrics concluded that the unpleasant taste of oral dosage forms was the single greatest obstacle in completing a prescribed therapy due to a lack of patient compliance [37]. This problem is further accentuated when attempting to formulate orally dissolving/disintegrating platforms (i.e. dissolvable films, orally disintegrating tablets, etc.) wherein more traditional methods of taste-masking, such as tablet film coating, are not feasible. These rapidly dissolving platforms have received considerable attention as they do not require equipment for dosing (oral syringes, measuring cups, etc.), chewing or additional liquids in order to be administered. This is because these dosage forms are intended to completely dissolve or disintegrate utilizing only the saliva available in the oral cavity. While convenient for all populations, this quality makes them ideal for patients who suffer from dysphagia, which is common in both pediatric and geriatric populations, where patient compliance is an issue (i.e. psychiatric disorders, etc.), or for chronic conditions that are characterized by random and rapid onset such as anxiety attacks or migraine headaches [39-44]. Unfortunately, ODTs tend to be

relatively fragile and suffer from increased friability which, in turn, leads to more expensive packaging requirements.

Sildenafil Citrate (SC), a phosphodiesterase type 5 inhibitor with a markedly bitter taste, has been marketed to both pediatric and geriatric populations as Revatio®, for the treatment of pulmonary arterial hypertension, and Viagra®, for the treatment of erectile dysfunction, respectively [45-48]. As a BCS I drug, SC presents an additional difficulty in terms of taste masking as it readily goes into solution while in the oral cavity thereby allowing it to interact with taste receptors more rapidly. Moreover, SC is used to treat the aforementioned chronic conditions which necessitate repeated exposure to the drug and excipients used in these formulations. This is a particular concern in both pediatric and geriatric populations where a heightened sensitivity to even the most modest toxicity may exist [49, 50].

Hot-melt extrusion has emerged as a novel and appealing pharmaceutical processing technology in recent years [51]. HME processes are characterized by the pumping of raw materials along a rotating screw, or screws, inside a barrel at elevated temperatures. The molten material is then forced through a die into a substance of uniform shape and character where it is then collected for further use [52]. HME is an attractive processing option for pharmaceutical applications as it is a potentially continuous process, does not necessitate the use of water or toxic organic solvents, is easily scaled up, provides relatively short processing times, and many of the polymeric carriers employed during processing are generally recognized as safe [52, 53]. This technology is best recognized for its ability to enhance the solubility of poorly water soluble APIs; however, it can also be extended to BCS I compounds in which solubility enhancement is not required [54]. This application is explored in this research through the modification of screw configurations for the

purpose of maintaining the API's crystallinity while also achieving acceptable homogeneity in the extrudates. Here, three configurations and their effects on the physical state of SC are investigated.

To be suitable for taste masking applications, however, the selected polymeric carrier must have two qualities. First, it must inhibit interaction of the API with taste receptors in the mouth. Second, it must not appreciably inhibit dissolution in the GI tract. Successful taste masking via HME technology would minimize both ensuing processing steps as well as the quantity of flavor enhancing excipients required to produce an acceptably palatable end product. In this current research, Plasdone™ S-630 copovidone, Aqualon™ N7 ethylcellulose (EC) and multiple grades of Klucel™ (HF, EF & ELF) hydroxypropylcellulose (HPC) polymers, were evaluated for their effectiveness in taste masking. The most suitable of the polymeric carriers, ethylcellulose, as evaluated by taste masking efficiency, was selected for additional experimentation and ultimately for formulation into an ODT.

2.3 Materials And Methods

2.3.1 Materials

Copovidone (Plasdone™ S-630), hydroxypropylcellulose (Klucel™ ELF, EF, & HF), ethylcellulose (Aqualon™ N7), Polyplasdone™ XL & XL-10 and Sildenafil Citrate were kindly gifted by Ashland Specialty Ingredients (Wilmington, DE). Mannitol (Pearlitol™ 300-DC) was donated by Roquette America Inc. (Keokuk, IA). Sucralose was gifted from JK Sucralose (Jiangsu Provence, China). Monoammonium Glycyrrhizinate (Magnasweet®) was donated by Mafco Worldwide CORP. (Camden, NJ). Butylated hydroxytoluene (BHT) was purchased from Sigma-Aldrich (St. Louis, MO). Magnesium Stearate was purchased from Spectrum Laboratory Products Inc. (Gardena, CA.). Calcium carbonate, magnesium oxide, calcium chloride dihydrate,

magnesium chloride hexahydrate, sodium chloride, potassium carbonate, sodium phosphate dibasic heptahydrate, sodium phosphate monobasic monohydrate as well as all solvents used in these studies (analytical grade methanol, acetonitrile & water), were purchased from Fisher Scientific (Norcross, GA). Natural & artificial mint flavoring was gifted by Flavors of North America (Carol Stream, IL).

2.3.2 Thermogravimetric (TGA) & Differential Scanning Calorimetry (DSC) Analysis

TGA (Pyris 1 TGA Perkin Elmer) was utilized to determine the thermal stability of the individual polymers, BHT, mannitol, magnesium oxide, calcium carbonate and pure SC. Binary mixtures (1:1 w/w) of the individual excipients with SC, as well as complete physical mixtures, were examined at the temperatures required for melt extrusion processing. During TGA, each of the weighed samples was heated from 25^{o}C to 180^{o}C at a rate of 20^{o}C/min. in a platinum pan under an inert nitrogen atmosphere purge of 20ml per minute. The samples were held at 180^{o}C for 5 minutes to simulate the thermal stresses encountered during HME.

DSC (Diamond DSC, Perkin Elmer) was utilized to confirm the thermal stability of replicate TGA samples. The samples, weighing 4-5 mg each, were placed in hermetically sealed aluminum pans and placed under an inert nitrogen atmosphere at a purge rate of 20ml per minute. These samples were heated from 25^{o}C to 180^{o}C at a rate of 20^{o}C/min., held at 180^{o}C for 5min. and cooled to room temperature. The thermograms of the samples were analyzed for deviations from samples of the pure substances, as well as for other thermal events. Calibration of the instrument was performed with an Indium reference.

2.3.3 Hot-Melt Extrusion Processing

Prior to HME processing, the polymers were sieved with a USP #35 mesh screen to remove any aggregates that may have formed. The compounds necessary for each physical mixture (Table 2-1) were placed in a V-shell blender (GlobePharma, Maxiblend®) and mixed at 20 rpm for 20 minutes. API content uniformity in the physical mixtures was assessed by HPLC analysis using a Waters HPLC-UV system (Waters Corp, Milford, MA). A fully intermeshing co-rotating twin-screw extruder (11 mm Process 11™, ThermoFisher Scientific) was used to process the physical mixtures. The barrel temperature profile and screw speed were based on the physical properties of polymeric carrier in each of the preliminary physical mixtures (Table 2-1) and a 3mm rod die was attached to the end of the barrel. Three screw configurations were investigated for their effects on the physical state of SC post extrusion (Figure 2-1a-c).

Table 2-1. Polymer screening formulations and extrusion parameters

Carrier	Drug Load	Temperature Range	Screw Speed (rpm)
Plasdone ® S-630 copovidone	25%	80-110ºC	100
Klucel™ ELF HPC	25%	90-120 ºC	100
Klucel™ EF HPC	25%	90-140 ºC	100
Klucel™ HF HPC	25%	90-160 ºC	100
Aqualon™ N7 EC	25%	90-160 ºC	100
Aqualon™ N7 EC	40%	90-160 ºC	100
Aqualon™ N7 EC + $CaCO_3$ (20%)	20%	140-160 ºC	100

After allowing the extruder to reach a steady state, material was collected from the extruder as uniform cylindrical extrudates. The extrudates were allowed to cool to ambient temperature and stored in foil lined polyethylene bags for further processing. The extrudates were later milled using a comminuting mill (Fitzpatrick, Model L1A). The milled extrudates were sieved to a particles size range of 300-425µm using what was retained between US #35 and US #40 sieves. The milled and sieved extrudates were stored in glass vials with a foil lined cap for future use.

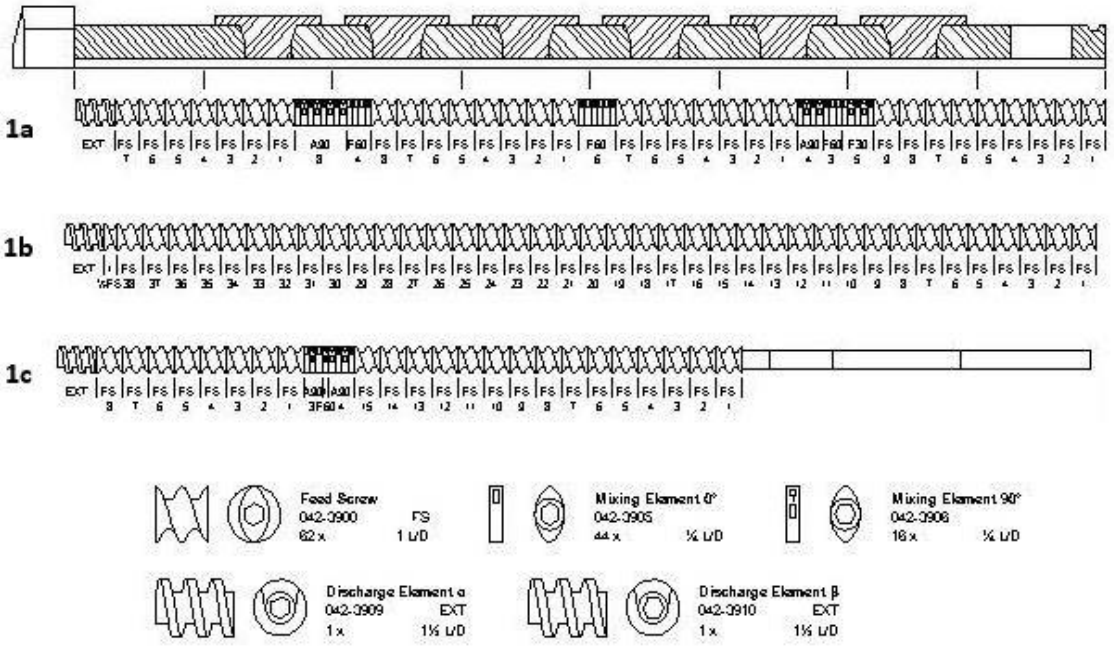

Figures 2-1a-1c: Images of the three screw configurations evaluated during HME process optimization. Figure 2-1a: ThermoFisher "Standard Configuration" 40:1 L/D. Figure 2-1b: All conveying elements; 40:1 L/D. Figure 2-1c: From Left to Right: 110mm of conveying elements; 22mm of perpendicularly arranged mixing elements; 165mm of conveying elements; 25:1 L/D.

2.3.4 Post-Extrusion Drug Content

A randomly selected portion of each of the extruded formulations was crushed into a fine powder using a mortar & pestle and analyzed for post-extrusion drug content. A known amount of the extruded formulations was dissolved in 1:1 methanol:water, diluted with additional 1:1 methanol:water and filtered using 0.2 µm, 13 mm PTFE membrane filters (Whatman, Piscataway, NJ) and analyzed using HPLC analysis. The same method was used to evaluate the finished ODT formulations.

2.3.5 High Performance Liquid Chromtography (HPLC) Analysis

The SC content in dissolution samples was analyzed using a Waters (Waters Corporation, Milford, MA, USA) high performance liquid chromatography (HPLC) system equipped with an autosampler, UV detector and a Phenomenex® Luna 5µ C18 (150 x 4.6 mm) column. An isocratic mode of elution with a mobile phase consisting of acetonitrile and water (60:40) at a flow rate of 1.0ml/min. was employed to quantify the drug at a wavelength of 273 nm. The data was acquired and processed using Waters Empower 3 software suite [55].

2.3.6 Powder X-Ray Diffraction (PXRD) Analysis

Powder X-Ray Diffraction (Bruker AXS, Madison, MI) was utilized to determine the physical state of SC post extrusion. The X-ray diffraction apparatus used CuKα radiation at 35 mA and 40 kV, 2°/min, and diffraction angles (2θ) of 5-50.

2.3.7 Fourier Transform Infrared (FTIR) Spectroscopy & Mid Infrared Chemical Imaging

Mid infrared spectral analysis was conducted on an FT-IR bench (Agilent Technologies Cary 660, Santa Clara, CA.). The bench was equipped with an ATR (Pike Technologies MIRacle ATR, Madison, WI), which was fitted with a single bounce diamond coated ZnSe internal reflection element. Chemical imaging was conducted using an infrared microscope (Agilent Technologies Cary 620 IR, Santa Clara, CA.) equipped with a 64 x 64 pixel focal plane array (FPA) with and without a germanium micro-ATR.

2.3.8 Dissolution Testing of Milled Extrudates

The milled and sieved extrudates were tested for *in vitro* drug release in both 150ml of SSF (pH 6.8 artificial saliva, Table 2) and 900ml of pH 2 media (0.01N HCl) with USP apparatus I (Hanson SR8) at 37 ± 0.5°C with a rotation speed of 100 rpm (n=6) [56, 57].

2.3.9 Preformulation for Tableting

Binary (1:1 w/w) mixtures of the milled extrudates with each of the excipients employed for tableting, as well as complete physical mixtures representative of the final tablet formulations, were stored under accelerated stability conditions (40°C ± 2°C/75% RH ± 5% RH) for one month. These samples were then qualitatively analyzed by FT-IR and quantitatively analyzed by HPLC.

2.3.10 Tablet Compression

Prior to direct tablet compression, the milled extrudates were mixed with mannitol, sucralose and Monoammonium Glycyrrhizinate in a V-shell blender at 20 rpm for 20 min.

Magnesium Stearate was added during the last 2 minutes of blending. The API content uniformity was determined by HPLC analysis. ODTs were prepared on a ten-station Piccola tablet press (SMI) using 8.0 mm standard concave tooling and a compression force of 5.5 kN.

2.3.11 Tablet Properties (Friability, Hardness, Disintegration & Weight Variation)

A dual scooping projection Vanderkamp friabilator (Vankel Industries Inc. Chatham, NJ) filled with 22 300mg ODTs in one side, to meet USP requirements, was used to assess tablet friability. The friabilator, which rotates at 25 rpm, was allowed to rotate continuously for four minutes. The tablets were accurately weighed prior to the test, and carefully de-dusted and reweighed after the test.

Tablet hardness was assessed using a Schleuniger hardness tester. Each tablet tested was placed firmly against the stationary anvil prior to beginning the test, and all debris from the previous test was carefully removed before performing replicate tests (n=10).

Weight variation was measured on a microbalance. 20 tablets were weighed, and their average determined. The weight of the individual tablets was then compared to the average and evaluated within USP specified tolerances for uncoated tablets (± 7.5%).

Tablet disintegration time was measured on a disintegration tester (Dr. Schleuniger Pharmatron). The beakers were filled with one liter simulated salivary fluid (pH 6.8 buffer solution, Table 2). The unit was thermally equilibrated to 37 ± 2°C (n=6) prior to tablet disintegration testing. Each tube of the apparatus was used to hold one tablet and each tablet was covered with a perforated plastic disc. The test was concluded when no particles were retained by the 10-mesh in the bottom of each tube. Prior to beginning the test, it was determined that the basket oscillations were between the recommended 28-32 cycles per minute.

2.3.12 Electronic Tongue Analysis

The electronic tongue samples were assayed on an Astree e-tongue (Alpha M.O.S.) equipped with sensor set #2 (pharmaceutical analysis) composed of seven sets of sensors (ZZ, AB, BA, BB, CA, DA, & JE) on a 48 position auto sampler. The individual sample volumes were 25ml and the acquisition times were set at 120s. The data generated on the e-tongue was analyzed using principle component analysis on the AlphaSoft V12.3 software suite (Mathworks Inc., Massachusetts, USA). Each sample was run at least three times, and three replicates of these samples were utilized for statistical purposes. The sensors and sample containers were thoroughly cleaned with deionized water between each sample assay. The individual assayed samples were diluted for 60 seconds in 25 ml of phosphate buffer solution (pH 6.8) in order to simulate oral conditions, and the supernatant liquid was filtered through 2.5 µm syringe filters.

2.3.13 ODT Oral & Gastric Tablet Dissolution

In vitro oral drug release was measured using dissolution apparatus I (Hanson SR8) set to 100 rpm and equipped with UV-Vis probes (Rainbow Dissolution Monitor, pION) collecting every 5 seconds for 60 seconds at 273nm. The dissolution medium consisted of SSF (150ml of artificial saliva pH 6.8, Table 2-2) and was maintained at 37 ± 0.5°C (n=6). *In vitro* gastric release was evaluated using dissolution apparatus I (Hanson SR8) set to 100 rpm. The dissolution medium consisted of 0.01N HCl (900ml) and the temperature was held at 37 ± 0.5°C. Samples were collected at 5, 10, 15 & 30 minute time points (n=6).

Table 2-2. Artificial saliva dissolution media (adjusted to pH 6.8)

Compounds	Concentration (g/L)
$CaCl_2 \cdot 2H_2O$	0.228
$MgCl_2 \cdot 6H_2O$	0.061
NaCl	1.017
$K_2CO3 \cdot 1.5H_2O$	0.603
$Na_2HPO_4 \cdot 7H_2O$	0.204
$NaH_2PO_4 \cdot H_2O$	0.273

2.3.14 Physical and Chemical Stability

The final ODT formulations, as well as milled extrudates containing the API, were stored under standard ($25^{O}C$/65% RH) and accelerated ($40^{O}C$/75% RH) stability conditions for 6 months in closed glass containers. The dissolution similarity factor (f_2) was utilized to compare the post-stability dissolution profiles of the ODTs. The milled extrudates were utilized for physical stability analysis of the API.

2.3.15 Statistical Analysis of Dissolution Data

The dissolution data, whether collected using Uv-Vis probes (section 2.2.12), or more conventional HPLC analysis (section 2.2.4, 2.2.7 & 2.2.12), were subjected to statistical analysis using the Similarity Factor (f_2) which allows for an accurate comparison of immediate release dissolution profiles.

2.4. Results and Discussion

2.4.1 Hot-Melt Extrusion & Screw Configuration Selection

2.4.2 Thermogravimetric & DSC Analysis

Prior to HME processing, an understanding of the thermal behavior of the API and any employed excipients is critical as thermal degradation of the constituents, or an unexpected chemical reaction between the constituents, can be thermally induced. The TGA thermograms of the samples were observed for changes in weight. The thermograms indicated that the drug, excipients and physical mixtures were chemically stable under the thermal conditions that would be employed for HME processing as only negligible weight loss near 100^{o}C (<1%), which was attributed to adsorbed water, was observed. Thermal degradation of SC occurred at approximately 194^{o}C. DSC data supported the findings of TGA analysis as no unexpected thermal events were observed under the same conditions. It was concluded that the temperatures necessary to process the carriers were suitable to employ. Thermal degradation of SC was observed to occur with the onset of melting at approximately 194^{o}C. The simultaneous melting and decomposition of SC has been previously reported and is recognized as thermally induced dissociation of Sildenafil base and citrate wherein citrate is responsible for the observed degradation [58].

2.4.3 Polymer Screening

Binary Mixtures of the individual polymers with SC were extruded and evaluated for *in vitro* drug release in artificial salivary fluid (Figure 2). While each of the polymers that was investigated showed promising taste masking potential during preliminary screening at up to one minute, the subsequent accelerated release exhibited by Plasdone S-630 was a source of concern. A comparison the S-630 dissolution profile with 25% and 40% drug loaded ethylcellulose

demonstrated a significant difference in terms of similarity factors (f_2 = 20 & 36, respectively). It was, therefore, removed from further consideration. Relative to ethylcellulose, the HPCs (grades HF, EF and ELF), too, showed a heightened, but steady, release (f_2 = 45, 42 & 39, respectively, when compared to 25% drug loaded ethylcellulose). It was concluded that the initial *in vitro* drug release studies of the various carriers indicated that ethylcellulose, with 0.2% BHT as an antioxidant, provided the greatest taste masking potential and was selected for additional study. A comparison of two drug loadings (25% & 40%) in ethylcellulose was evaluated (Figure 2-2). At 1.5 minutes of oral dissolution the 40% drug load showed more rapid dissolution (approximately 5%). This finding was not statistically significant when the profiles were compared using the similarity factor (f_2 = 71). The lower drug loading (25% API), which was suitable for the targeted dose of SC, was selected for additional study.

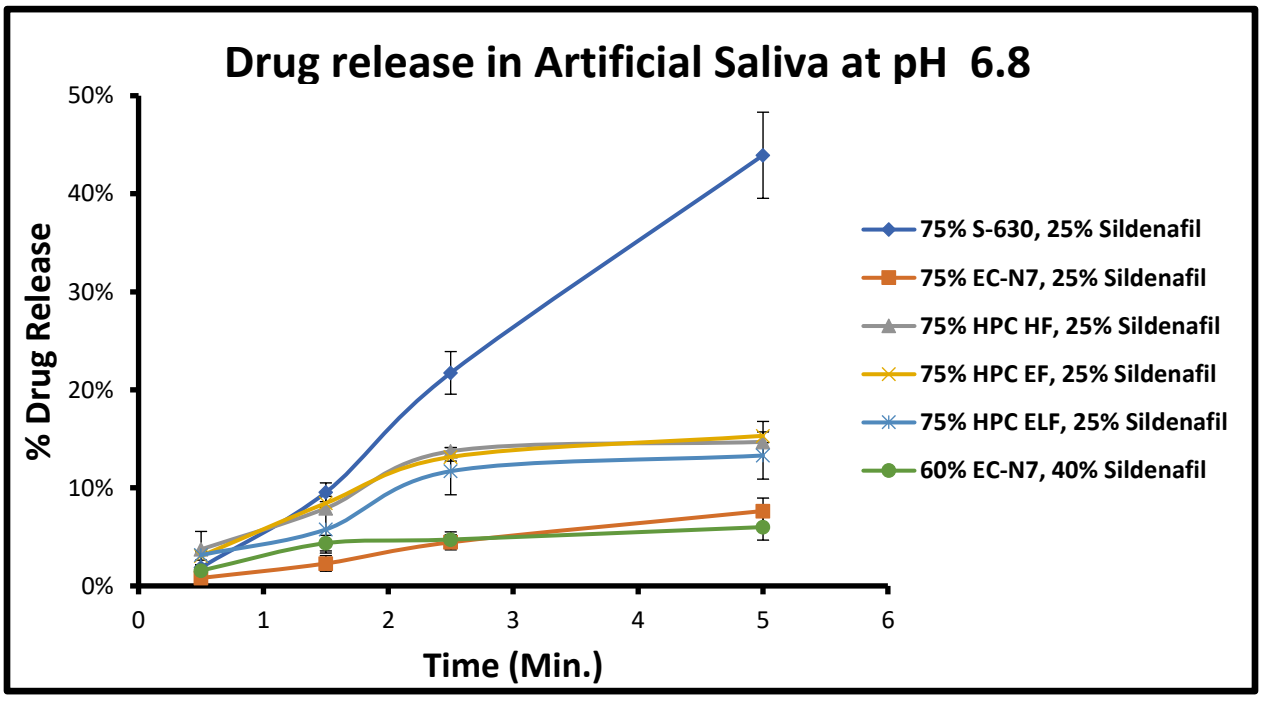

Figure 2-2: SC release profile of preliminary polymer screening formulations in artificial saliva media adjusted to pH 6.8.

2.4.4 PXRD Analysis

X-Ray diffraction was used to examine the effects of the three screw configurations on the physical state of SC in the carrier post-extrusion. Figure 3a shows the diffractogram for pure SC for comparison with the extruded formulations. The effect of the three screw configurations on the physical state of SC was considerable. The screw configuration in Figure 2-1a (ThermoFisher Standard Screw configuration; 40:1 L/D) resulted in highly amorphous phase SC, which was both unnecessary and undesirable in the case of a BCS I API and was, therefore, not utilized for future processing. The amorphous form, being more readily soluble, would only serve to hinder any taste masking effects imparted by the carrier. Additionally, the amorphous form of an API is inherently less thermodynamically stable and, consequently, subject to recrystallization into various polymorphs, which have differing physical properties, if they exist [59]. This observed conversion was attributed to not only the length of the screw, and thus increased residence time in the extruder, but more significantly, the presence of three high shear mixing zones which, depending on configuration, are primarily responsible for the conversion of crystalline phases of an API to their morphologically altered, or amorphous, phases [52].

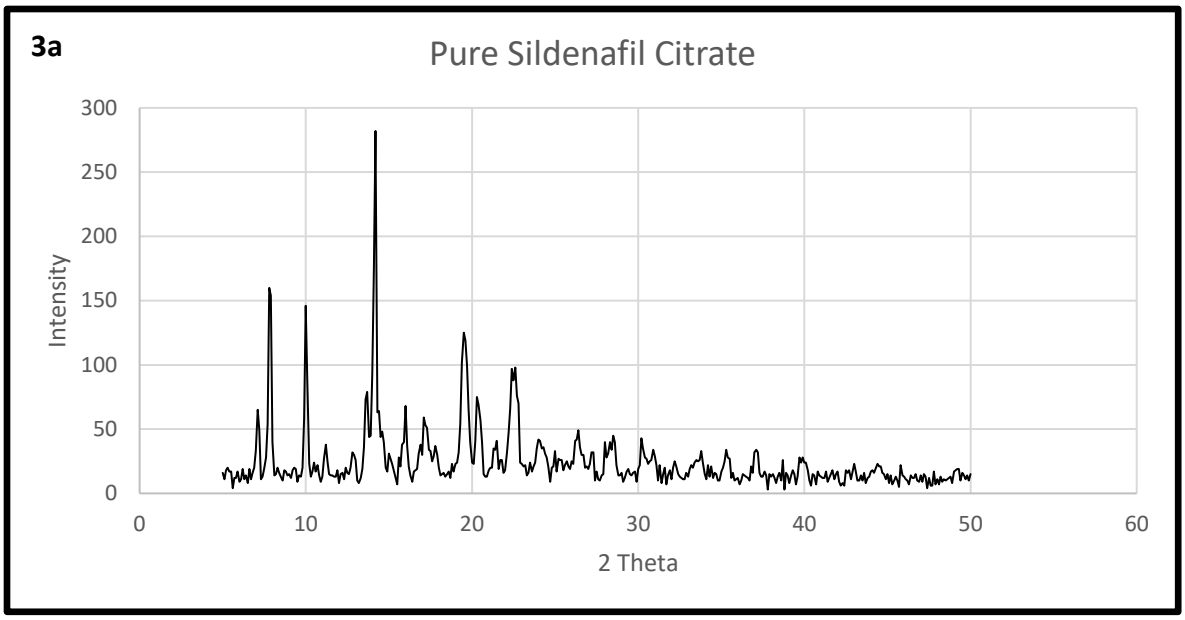

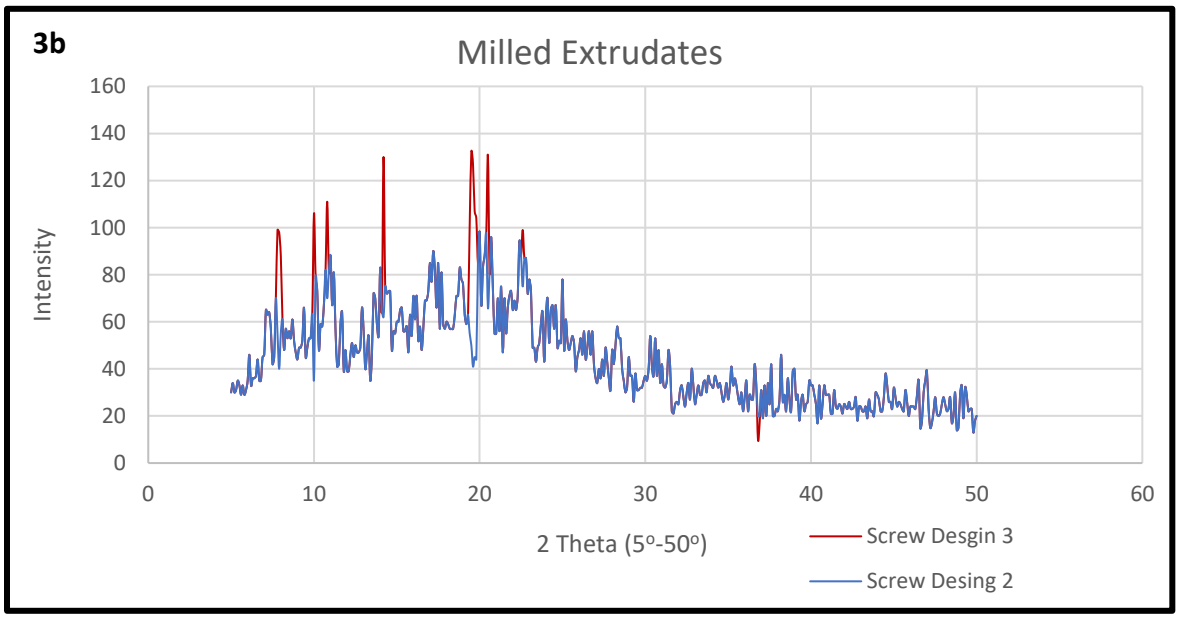

Figures 2-3a-b: a; PXRD diffractogram of pure crystalline SC. b; PXRD diffractograms of binary mixtures of ethylcellulose & SC as a function of screw configurations.

The screw configuration in Figure 1b preserved a considerable portion of the crystalline phase of the API; however, there remained noticeable amorphicity of SC in the carrier as depicted in Figure 3b. It was speculated that the combination screw length and shear that can occur along the

flight of conveying elements and the barrel of the extruder was responsible for the amorphicity noted in the diffractogram. Screw design 3 (Figure 2-1c) was designed to be shorter than the previous two (25:1 L/D) while still imparting sufficient distributive mixing to the melt. Indeed, despite the employment of a single mixing section in Figure 1c, in which the mixing elements were perpendicularly arranged, the diffractogram for screw configuration 3 showed enhanced preservation of the crystalline structure of SC in the carrier matrix as can be seen in the diffractogram.

2.4.5 FT-IR & Mid Infrared Chemical Imaging

Mid-infrared (MIR) spectra of crystalline and amorphous SC were collected and compared. Differences in these MIR infrared spectra allowed for differentiation between the phases in the extruded material. This was accomplished using a series of spectral derivatives to exploit the differences highlighted in the spectra (Figure 2-4). It has been previously reported that the unbound carbonyl, located at 1697cm^{-1} in the more organized crystalline structure, becomes shifted when it is free as is the case with Sildenafil base [58].

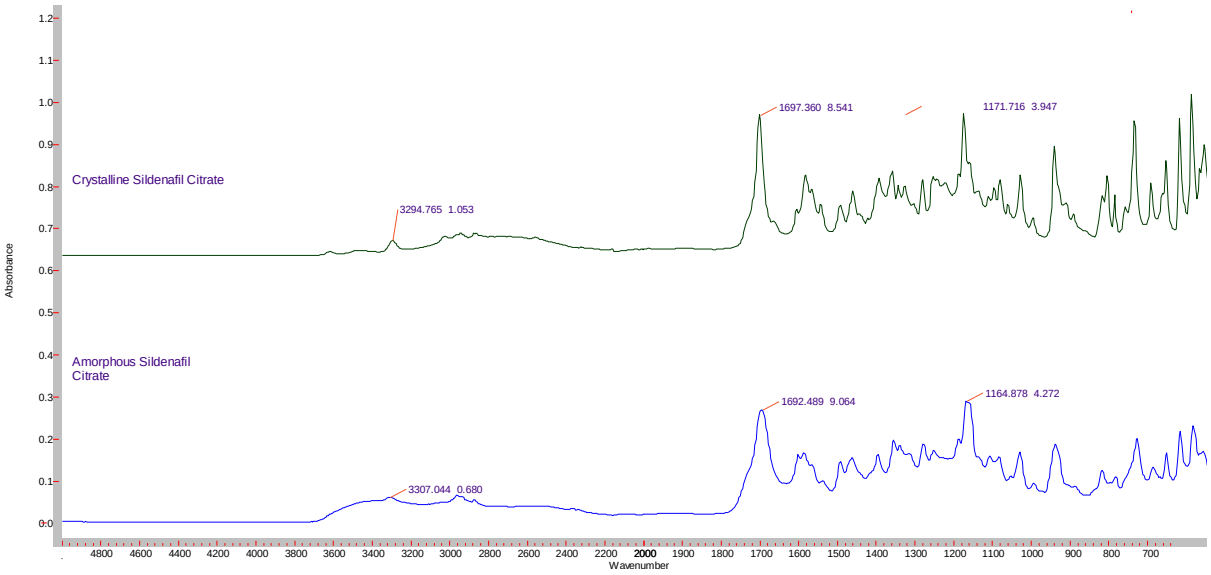

Figure 2-4: FTIR spectra of crystalline and amorphous SC.

Additionally, virtually all of the intermolecular bonding is attributed to interaction between COOH groups in the citrate portion and the carbonyl and the amine group, which appears at 3294cm^{-1} in the crystalline form, and is shifted to 3307cm^{-1} in the amorphous form. The sulfone group, which appears at 1171cm^{-1} in the crystalline form has shifted to 1164cm^{-1} in the amorphous form. In this study, the amorphous form of SC was produced using the well-known solvent evaporation technique. The infrared images (Figures 5a-c) were produced by taking spectral derivatives of the obtained spectra and isolating spectral bands representative of the crystalline phase alone. The amorphous phase carbonyl center is shifted to 1692cm^{-1} as opposed to 1697cm^{-1} in the crystalline phase.

Figures 2-5a represents an infrared image of crystalline SC in the polymer matrix, post extrusion using screw configuration 2 (Figure 2-1b), taken at 5.5 µm spatial resolution in transmission mode with a total field of view (FOV) of 350 x 350 µm. The light blue area represents

a lack of crystalline API due to either complete absence of SC or the presence of the amorphous phase. This seems to correspond well with XRD data and analysis of the same material.

Figure 2-5b, representative of screw configuration 3 (Figure 2-1c), illustrates a more uniform distribution of crystalline SC in the carrier. Here it can be seen that there exists good homogeneity of SC in the polymeric carrier as indicated by the relatively modest intensity of the carbonyl centered at 1697 cm^{-1} that this image is taken with respect to. Additionally, the pockets of crystallinity are less apparent at this spatial resolution. However, Figure 5c represents an infrared image taken with a Ge micro ATR at 1.1 μm spatial resolution with a total FOV of 70 x 70 μm. On closer inspection, it is apparent that there is a slight inhomogeneity of SC in the carrier as the low intensity blue areas correspond to a complete lack of crystalline SC in that region. Additionally, the elevated yellow and regions in the images correspond to pockets of crystalline SC. These small pockets of inhomogeneity are presumably due to preserving the crystalline structure of SC. Interestingly, this inhomogeneity showed no effect during content uniformity testing by HPLC analysis and was, therefore, considered negligible. This was presumed to be due to the small sample size used for the imaging analysis relative to the sample size utilized for HPLC analysis.

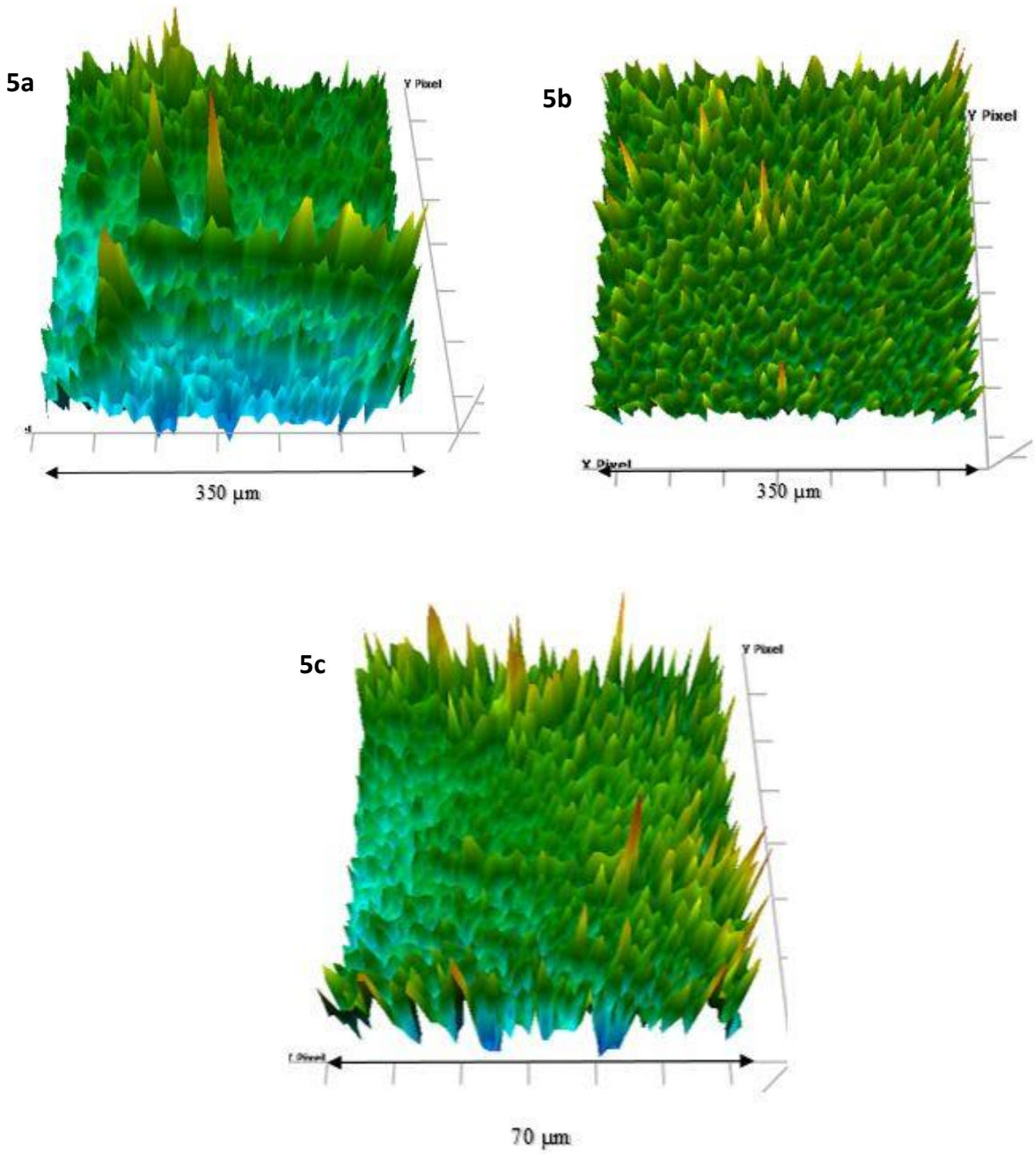

Figure 2-5a-c: Chemical image (5.5 µm spatial resolution) of a binary mixture of ethylcellulose & SC highlighting the intensity of the carbonyl present in crystalline SC processed using screw configuration 2 (Figure 2-1b). Figure 5b: Chemical image (5.5 µm spatial resolution) of a binary mixture of ethylcellulose & SC highlighting the intensity of the carbonyl present in crystalline SC processed using screw configuration 3 (Figure 2-1c).

Figure 2-5c: Chemical image (1.1 µm spatial resolution) of a binary mixture of ethylcellulose & SC highlighting the intensity of the carbonyl present in crystalline SC processed using screw configuration 3 (Figure 2-1c).

3.1.5 E-Tongue & Oral Dissolution Testing of Milled Extrudates

Electronic tongue evaluation and *in vitro* dissolution of the milled extrudates, which consisted of 20% SC loading in ethylcellulose, on the basis of screw configuration supported the physical characterization studies (FT-IR & XRD). The distance chart (Figure 2-6) graphically illustrates the principal component analysis results taken as a comparison of the reference or blank (artificial saliva solution).

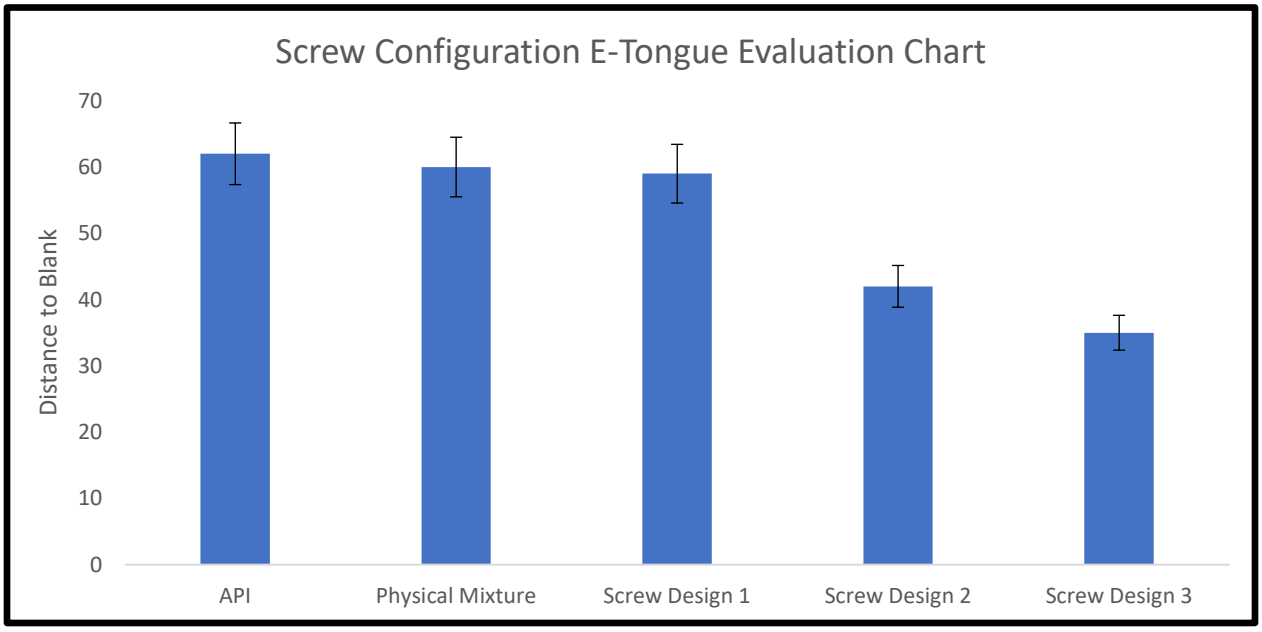

Figure 2-6: Graphical illustration of PCA results from e-tongue analysis illustrating each samples distance from artificial salivary fluid as a function of screw design.

Here it is presumed that the greater the distance to the blank, the less efficient the screw configuration is for taste masking purposes. It can be seen that pure SC and the physical mixture are poorly taste masked as they exhibit the greatest distance from the blank, as would be expected. Screw configuration 1 also produced a poorly taste masked product due to the conversion of the crystalline lattice of SC to the amorphous form, which goes into solution more rapidly.

Screw configurations 2 & 3 produced comparable results on the basis of e tongue and *in vitro* oral dissolution (Figure 2-7); however, the results were not in complete agreement. E-tongue analysis indicated that screw configuration 3 produced a superior taste masked product, which was attributed to improved encapsulation of SC in the polymeric carrier. Additionally, FT-IR analysis indicated that the crystalline lattice was more effectively preserved when employing this configuration, which further explains the differences in e-tongue analysis. On the other hand, the dissolution data indicated screw configuration 2 produced a slightly better product in terms of taste masking.

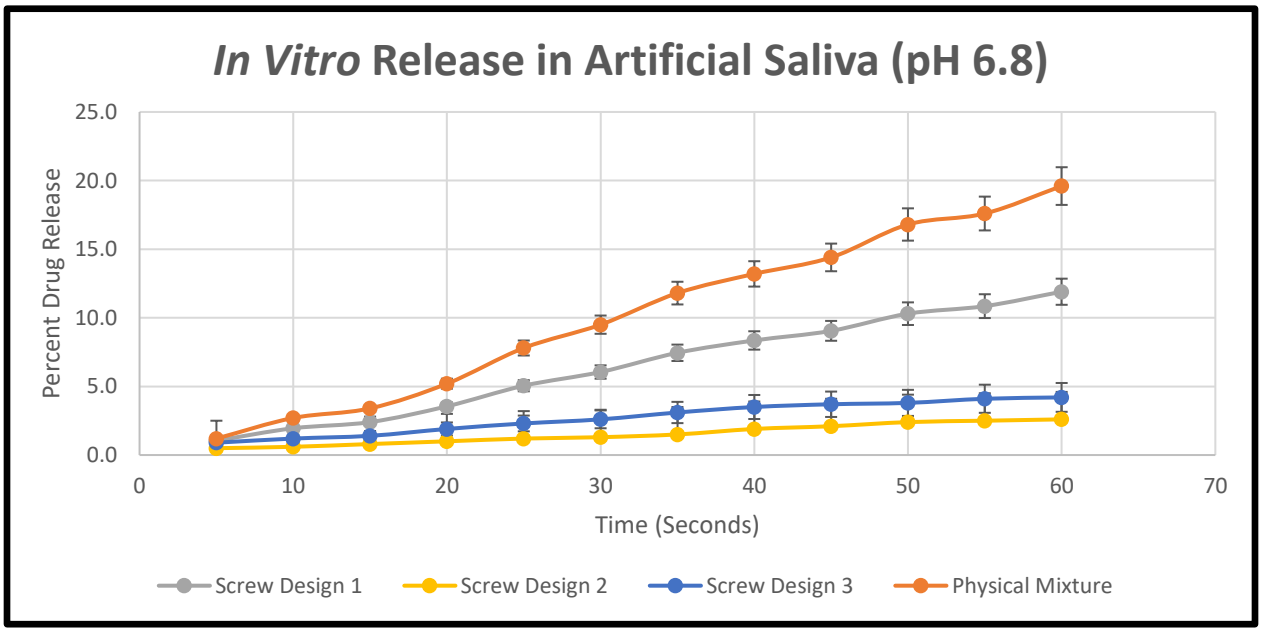

Figure 2-7: Dissolution data of binary mixtures of ethylcellulose and SC as a function of screw design.

Upon closer examination of the dissolution profiles for these screw configurations at 30 seconds, which is the maximum amount of time the formulation is expected to remain in the oral cavity, there exists a negligible difference (<1%) between the two profiles, which was further supported by the similarity factor comparison ($f_2 = 73$). These observations along with the physical characterization data, wherein it was shown that screw configuration 3 produced a more uniform crystalline dispersion, aided in deciding that screw configuration 3 would be utilized for further processing. Interestingly, there seems to exist a strong correlation between the e-tongue analysis, wherein greater distance would be indicative of greater interaction of the API with the taste sensors, and dissolution data, which indicates the amount of API in solution available for the perception of taste.

2.4.7 Addition of Release Modifying Agents

While ethylcellulose, an erodible polymer, was selected due to a very low release profile in artificial saliva, it became necessary to incorporate a release modifying agent for more rapid drug diffusion as gastric drug release was correspondingly low. Magnesium oxide and calcium carbonate were selected as potential pore formers due to being practically insoluble near salivary pH while being completely soluble at or near gastric pH. Mannitol was also used as a pH independent pore former. Additionally, it was postulated that any dissolution of mannitol in the oral cavity could have potentially served as an additional taste masking agent as a result of being a sugar alcohol with a sweet flavor.

Initial e-tongue screening of the individual pore formers within the extruded matrices (20% each) demonstrated promising results (Figure 2-8) for both magnesium oxide and calcium carbonate. However, magnesium oxide produced highly erratic results during gastric dissolution screening

and was therefore removed from consideration for further taste masking application. Based on the distance chart results for the pore formers, mannitol was also excluded from further consideration. It was observed that the quantity of mannitol needed for adequate pore forming capacity was assisting in solubilizing SC during the melt extrusion processing, which hindered the taste masking capacity of the formulations. This observation explains why mannitol ranked very closely to pure SC during the e-tongue analysis.

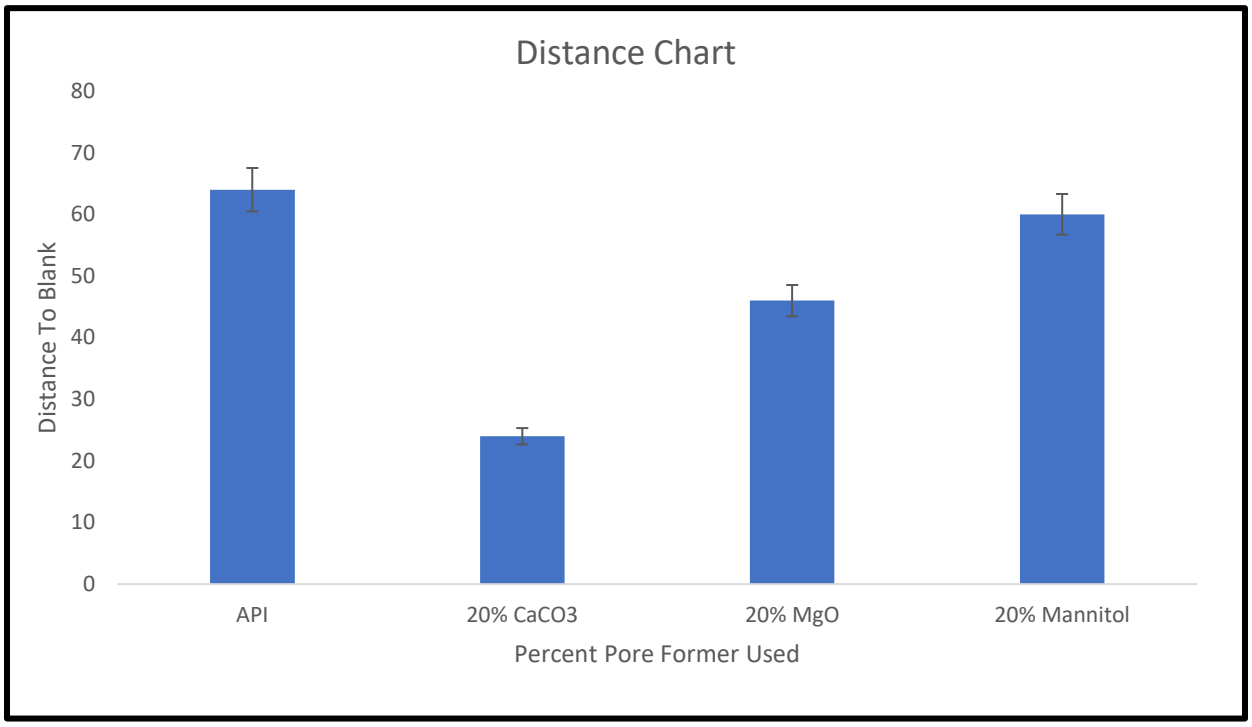

Figure 2-8: Graphical illustration of PCA results from e-tongue analysis illustrating each samples distance from artificial salivary fluid as a function of individual pore former in each formulation.

Oral dissolution data for calcium carbonate agreed well with the e-tongue results (Figure 2-9) without producing the unpredictable results associated with magnesium oxide. These data were

as hypothesized as calcium carbonate is insoluble near neutral pH, which should prevent the formation of diffusion promoting pores, thus keeping the exterior of the matrix intact. Because of these observations, calcium carbonate as the pore former was selected for additional studies.

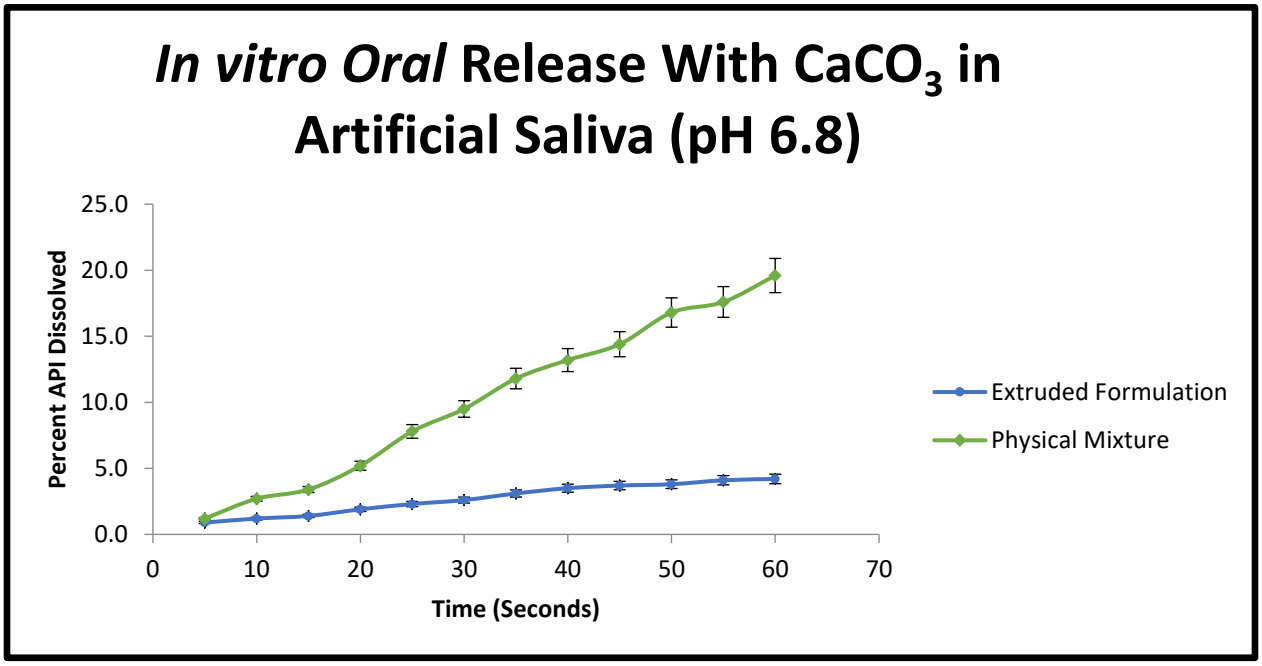

Figure 2-9: Dissolution release profile of milled extrudate (20% SC, 60% ethylcellulose & 20% calcium carbonate) in artificial salivary media (pH 6.8).

2.4.8 Tableting API-Excipient Compatibility

After storage for one month under accelerated stability conditions (40ºC/75% RH), HPLC analysis was conducted to evaluate the compatibility of the extruded formulations with the excipients selected for direct compression tableting (Table 2-3). All API-excipient compatibility samples were dried in the presence of desiccant prior to investigation in order to remove adsorbed water which would interfere with both qualitative spectral analysis and quantitative chromatographic data analysis. API-excipient compatibility studies were evaluated qualitatively by FTIR analysis

wherein the spectra were observed for the appearance and/or disappearance of previously unobserved characteristics. When no changes in the infrared spectra were observed, these samples were further evaluated quantitatively using HPLC analysis. No incompatibilities were noted.

Table 2-3. ODT formulation including the varying percentages of super disintegrant and filler used

Constituents	Concentration
PVP (Grades XL & XL-10)	2.5, 5 & 10%
Sucralose	1%
Magnasweet	1%
Nat. & Art. Mint Flavor	1%
Milled Extrudate	41.7% (Equivalent to 25mg of SC)
Mannitol (300DC)	52.3, 49.8 & 44.8%
Magnesium Stearate	0.5%

2.4.9 Tablet Properties

Tablets containing varying levels of super disintegrant (PVP XL & XL-10) were evaluated for common tablet properties (Tables 4a & 4b respectively). The percentage of super disintegrant evaluated ranged from 2.5-10. As noted earlier, friability tends to be a common concern when formulating ODT platforms. To the contrary, these formulations exhibited excellent friability (0.8-0.32) despite having somewhat low hardness values (2.68-6.56 kp). The low hardness values are attributed to the poor compressibility and high loading (41.7%) of the milled extrudates in the ODT formulations. Interestingly, the disintegration times for the ODTs were within the acceptable limits for ODT designation (approximately 8-33 seconds depending on formulation), which are

generally taken to be less than 30 seconds. While the tablets formulated with PVP XL-10 demonstrated improved hardness and friability values, those formulated with PVP XL demonstrated superior disintegration times, which is a primary concern when formulating rapidly dissolving platforms. Remarkably, tablets containing 5.0% PVP XL had average disintegration times of 8.6 seconds. With the other properties within the acceptable ranges, priority was given to disintegration time. Therefore, ODTs containing 5.0% PVP XL were selected for oral and gastric dissolution studies.

Table 2-4(a). Tablet properties as a function of the percentage of PVP XL incorporated

	2.5% PVP XL	5.0% PVP XL	10% PVP XL
Disintegration Time (sec.)	11.3±1.01	8.6±0.62	9.3±1.63
Percent Friability	0.24±0.01	0.32±0.02	0.19±0.01
Thickness (mm)	4.63±0.06	4.63±0.05	4.67±0.01
Hardness (kp)	3.57±0.64	2.67±0.30	2.89±0.55
Loss on Drying (w/w)	2.22±0.46	2.37±0.42	2.66±0.63

Table 2-4(b). Tablet properties as a function of the percentage of PVP XL 10 incorporated

	2.5% PVP XL-10	5.0% PVP XL-10	10% PVP XL-10
Disintegration Time (sec.)	33.3±5.10	27.7±2.71	30.0±3.99
Percent Friability	0.08±0.02	0.23±0.001	0.13±0.01
Thickness (mm)	4.64±0.02	4.63±0.09	4.66±0.14
Hardness (kp)	6.56±0.50	5.68±0.31	5.90±0.48
Loss on Drying (w/w)	2.17±3.00	2.34±0.20	2.61±0.52

2.4.10 ODT Oral & Gastric Tablet Dissolution

Oral and gastric dissolution profiles (Figures 2-10a-b) were evaluated for finished product (ODT containing 5% PVP XL) drug release. While the oral dissolution study was conducted for 60 seconds, a disintegration time of approximately 8 seconds indicates that the formulation would remain in the oral cavity for 30 seconds or less. At this time, the tablets exhibited a mere 2% drug release. The gastric release profile of the tablets indicates that excellent release can be obtained by incorporating the milled extrudates into rapidly dissolving platforms. In this case, more than 80% drug release was realized with 60 minutes.

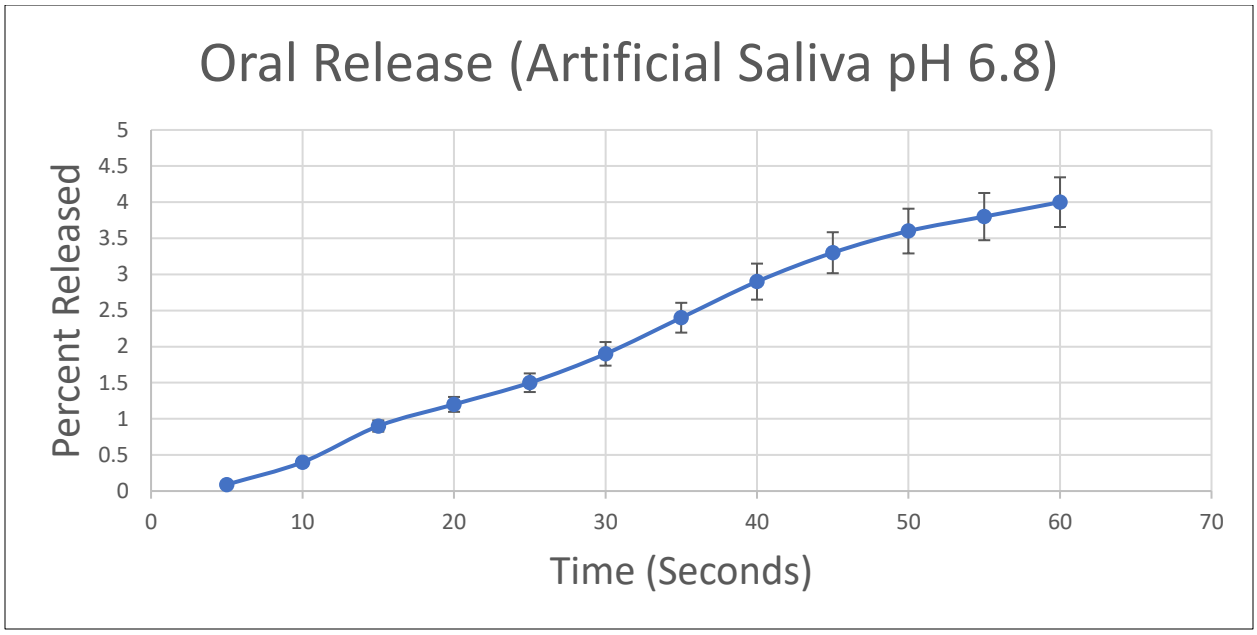

Figure 2-10a: Dissolution profile of optimized SC ODT formulation in artificial salivary fluid (pH 6.8)

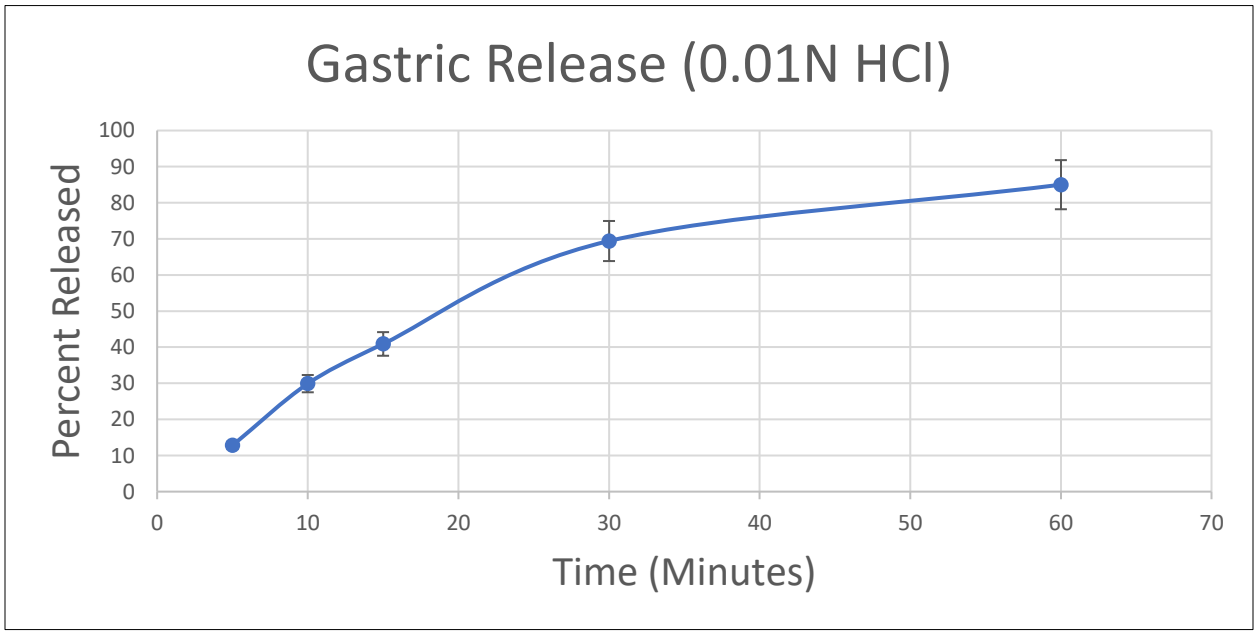

Figure 2-10b: Gastric release profile of optimized SC ODT formulation in gastric media (pH 2).

2.4.11 Physical and Chemical Stability

The milled extrudates were assessed for physical stability of the API by both FT-IR and PXRD analysis. There was no observable difference in the spectra generated by either method indicating that that the specific polymorphic crystalline lattice had been preserved after both standard and accelerated stability testing, as would be expected. The milled extrudates were also assessed for chemical stability by HPLC analysis using the method outline in section 2.2.4, and their similarity factor was calculated ($f_2 = 89$).

4. CONCLUSION

In this study, HME was successfully employed as a processing technology for the production of taste masked formulations containing SC. This was accomplished by embedding the API in ethylcellulose along with a pH dependent pore former. The crystallinity of SC, and presumably the subsequent physical stability, was found to be dependent on the screw configuration and pore former used. FT-IR spectroscopic imaging, in tandem with conventional XRD analysis, proved to be very valuable in the evaluation of the melt-extruded formulations as it was demonstrated that preserving the crystalline structure of SC was critical for arriving at successfully taste masked formulations. The addition of calcium carbonate into the extruded formulations proved to be especially advantageous in that its pH dependent solubility helped prevent drug dissolution under oral conditions (pH 6.8) while promoting drug dissolution under gastric conditions (pH 2). The ODT formulations demonstrated uncharacteristic but excellent friability profiles without sacrificing disintegration time, which is critical for ODT formulations. E-tongue assessment of taste masking efficiency, in conjunction with dissolution data, was found to be extremely valuable and mutually supportive.

CHAPTER 3.

A QUALITY BY DESIGN INVESTIGATION OF A NOVEL TWIN-SCREW DRY GARANULATION PROCESS

3.1 Introduction

Historically, extrusion processes have found considerable applicability in a multitude of processing fields. A few examples might include metal & plastic profile extrusion, ceramic extrusion, cooking & confectionary extrusion, plastic & rubber compounding extrusion, polymer synthesis reaction extrusion, and finally, with over a century of industrial refinement, pharmaceutical extrusion [1-11]. The extrusion processing platform, be it ram, single or multi-screw, has a sound reputation for being economical, efficient, continuous and, most importantly, consistently reliable for the repeated production of high quality products. The later of these qualities, being a source of ill repute and vulnerability for the pharmaceutical industry as evidenced by the ubiquity of drug recalls, has led to the FDA's substantial push for QbD guided process development [60, 61]. While most of the primary requirements for developing a QbD based process are conceptual in nature (QTPP, FMEA, DoE), and thus easily implemented in a wide array of processes, those required by the enhanced QbD requirements, namely in-line process monitoring and process controls, are relatively foreign to conventional pharmaceutical processing technologies. By contrast, these in-process analytics and controls are not only integrated into extrusion systems, but are also fundamental to the process.

Twin-screw extrusion has attracted considerable attention in the pharmaceutical industry as an alternative processing technology where bioavailability enhancement is required and multiple review articles cover this application aspect in detail [62-65]. More recently, the innumerable advantages inherent to extrusion processing (economical processing, small scale-up footprint, reduced in-process times, solvent free/green processing, reduced processing steps, continuous processing, etc.) have led to applicability studies where solubility enhancement is either not required, undesirable or where this processing technology simply imparts its advantages over more conventional processing platforms. Indeed, investigations in twin-screw granulation processes are rapidly increasing, and for good reason [66-83]. With approximately 70 percent of pharmaceuticals being solid dosage forms, and the primary physical modification of the bulk ingredients being a granulation process of one form or another, any advancement in granulation technology is going to have significant implications [84].

Granulation processes are commonly employed in the pharmaceutical industry as a means to increase particle size, reduce segregation, improve flowability and enhance compressibility. Dry granulations are often considered useful for formulations that have acceptable compression properties, but suffer from poor flowability. Unlike wet granulations, dry granulations do not require the formation of a wet mass along with the subsequently necessary drying operations, and are also suitable for hydrolysable compounds. Typically, a dry granulation process consists of the addition of mechanical energy to a formulation containing a dry binder. The resulting agglomerated mass is then often subjected to one or more milling, sieving and blending operations.

The primary objective of this work was to investigate the previously unreported utility of a fully intermeshing, co-rotating, twin-screw extruder for the development of a Twin-Screw Dry Granulation (TSDG) process. TSDG fundamentally differs from the more conventional

pharmaceutical applications of twin-screw extruders (*i.e.* Hot-Melt Extrusion; HME) in that the formulation's constituents are not processed into a continuous melt within the barrel, but are instead compacted into discrete agglomerates. In further contrast to HME processes, wherein the in-process melt functions as the lubricant for the barrel and rotating screws, an additional powder lubricant was required to prevent the observed metal on metal contact during TSDG processing. The TSDG process differs substantially from its wet granulation counterpart as well in that no solvents or binder solutions are required. This is particularly advantageous in that the need for subsequent, and often lengthy, drying operations is circumvented along with analytical determinations of residual organic solvents when used. Moreover, this dry processing approach does not preclude the incorporation of hydrolytically sensitive actives or excipients. Careful attention to screw design was required as there existed a balance between simply pushing the powdered formulation through the extruder (powder in-powder out), the formation of melted material and the formation of a dry granulated material.

A Quality by Design approach was implemented in order to arrive at a well-defined process yielding a product of predefined character and quality. In this case study, Sildenafil Citrate, a BCS class I API, was utilized as a model drug for the granulating process. The selection of this API was beneficial in that it exhibits poor flowability, which makes it ideal for a granulating process wherein high drug loading is desired. Additionally, a BCS I API poses the possible challenge of undesirable amorphous phase formation, an application for which twin-screw extruder processing is both well-known and suited.

The objectives outlined in the quality target product profile (QTPP) were to produce a high drug loaded, sustained release formulation in which the API's pre-existing crystalline lattice was preserved (Table 1). The resulting granules were assessed for surface morphology, API phase

changes, chemical interactions, conventional granule properties (i.e. compressibility index, angle of repose, Hausner ratio), and finally utilized to produce a high drug loaded sustained release solid oral dosage form.

Table 3-1: Quality Target Product Profile (QTPP)

QTPP Element	Target	Justification
Dosage form	Tablet	Pharmaceutical equivalence requirement: same dosage form
Route of administration	Oral	Pharmaceutical equivalence requirement: same route of administration
Dosage strength	100 mg	
Pharmacokinetics	In vitro dissolution – 12-18hrs 80% release	
Stability	At least 6 months 40C/75RH accelerated stability	
Drug Product quality attributes	Physical Attributes	Tablets (size, color, shape)
	Identification	Positive identification for sildenafil citrate
	Assay	90.0-110.0 (Compendial requirement)
	Content Uniformity	AV $\leq$ 15.0 (USP<905>)
	Degradation Products	Monitor and report (CQA)
	DSC	Monitor and report (CQA)
	TGA	Monitor and report (CQA)
	XRPD	Monitor and report (CQA)
	NIR	Monitor and report (CQA)
	Residual Solvents	Will not be monitored for this study
	Drug Release	Extended Release
	Microbial Limits	Will not be monitored for this study
	Water Content	Will not be monitored for this study
Container Closure System	NA	
Administration/concurrence with labeling	NA	
Alternate methods of administration	NA	

3.2 Materials & Methods

Hydroxyethyl cellulose (Natrasol™ 250 L), ethyl cellulose (Aqualon™ N7), hydroxypropyl cellulose (Klucel™ HF) and Sildenafil Citrate were generously donated by Ashland Specialty

Ingredients (Wilmington, DE). Magnesium Stearate, hydrochloric acid and the solvents used in this study (analytical grade methanol & water), were purchased from Fisher Scientific (Norcross, GA).

3.3 Methods

3.3.1 API-Excipient Compatibility

Binary (1:1 w/w) mixtures of the API with each of the excipients, as well as complete physical mixtures representative of the final tablet formulations, were stored under accelerated stability conditions (40°C ± 2°C/75% RH ± 5% RH) for one month. These samples were then analyzed by FT-IR spectroscopy.

3.3.2 Fourier Transform Infrared Spectroscopy (FT-IR)

Mid infrared spectral collection was performed on an FT-IR bench (Agilent Technologies Cary 660, Santa Clara, CA.). The bench was equipped with an ATR (Pike Technologies MIRacle ATR, Madison, WI), which was fitted with a single bounce diamond coated ZnSe internal reflection element. The spectra were collected over a range of 4000-650cm^{-1}. Spectral analysis was conducted using the Resolutions Pro software suite (Agilent Technologies, CA.).

3.3.3 Preliminary Range Screening of Formulation & Process Variables

Prior to a formal DoE, preliminary studies were conducted to evaluate acceptable process parameter ranges (*e.g.* screw configurations, screw speeds, feed rates, etc.) and formulation variables (*e.g.* polymer ratios, inter/extra-granular lubricant, API morphology, etc.).

3.3.4 Experimental Designs (DoE) & Analysis

Experimental designs were created and evaluated using DoE software (StatEase, Design-Expert® Version 8.0.6, Minneapolis, MN). A fractional factorial design (Min Run Res IV) with two center points was used as a screening design for the elucidation of main effects, which resulted in a total of 16 experimental runs. A full factorial 2 level (2^3) with four center points was utilized to evaluate interactions between the previously selected main effects and curvature present within the design. The full factorial design necessitated an additional 12 experimental runs. Finally, the results from the full factorial design were used to produce contour plots, response surface plots, and to predict an optimized formulation and process.

3.3.5 Physical Mixture Preparation

Prior to TSDG processing, the polymers were sieved using a USP #35 (500 µm) mesh screen to remove any aggregates that may have formed. The components necessary for each physical mixture were geometrically diluted using a glass mortar and pestle.

3.3.6 Twin-Screw Dry Granulation (TSDG)

A fully intermeshing, co-rotating, twin-screw extruder (11mm Process 11™, ThermoFisher Scientific) was used to process the physical mixtures. The extruder experiments were conducted without a die on the extruder barrel. After allowing the extruder to reach a steady state, material was collected from the extruder in the form of granules and/or fine powder. The granules were stored in polyethylene bags for further processing and/or analysis.

3.3.7 Scanning Electron Microscopy (SEM)

SEM was used to assess the surface morphology of the final optimized formulation in three different forms. These were the physical mixture, a representative melt extruded sample, and the optimized dry granulated sample. Prior to sample mounting, the surfaces of the samples was cut with a razor in order to provide a flat surface to focus upon. Adhesive carbon tape was used to mount the samples onto an aluminum stage. These samples were then sputter coated with gold under an argon atmosphere using a Hummer 6.2 Sputter Coater (Ladd Research Industries, Williston, VT, US). The coater was kept under a high-vacuum evaporator equipped with an omni-rotary stage tray to help ensure uniform coating. Finally, the images were captured using a JSM-5600 scanning electron microscope (JEOL USA, Inc., Waterford, VA, US) at an accelerating voltage of 5 kV. The samples were evaluated at multiple magnifications.

3.3.8 Dry Granulation Flow Property Measurements

The powder/granulation flow peoperties were measured and assessed in accord with the current USP-NF[37] guidelines. The bulk volume (V_o) of 25 g of granules was measured in 50 ml of graduated glass cylinder. The bulk density (ρ_b) was calculated using the following equation:

$$\text{Bulk density } (\rho_b) = \frac{\text{amount of granules weighed (25 g)}}{\text{bulk volume } (V_o)}$$

The graduated glass cylinder was tapped 100 times and the reduced volume of the granules was measured. Tapped density (ρ_t) was calculated by using the volume of the granules after tapping 100 times (V_f) using the following equation:

$$\text{Tapped density } (\rho_t) = \frac{\text{weight of granulation/powder (25 g)}}{\text{tapped volume } (V_f)}$$

Carr's (compressibility) index (CI) and Hauser's ratio (HR) were calculated using the following equations:

$$\mathrm{CI} = \frac{(\rho_t - \rho_b)}{\rho_t} \times 100 \qquad HR = \frac{\rho_t}{\rho_b}$$

The angle of repose was measured using a funnel method outlined in the USP-NF[37]. The height of the funnel was placed above the horizontal surface such that the upper tip of the resulting cone lightly touched the tip of the funnel. The weighed granules were poured freely through the funnel onto the horizontal base. The diameter and the height of the cone was measured and the angle of repose (θ) was calculated by the following equation, where 'h' and 'r' are the height and radius of the formed cone, respectively:

$$Tan\,(\theta) = \frac{h}{r}$$

3.3.9 Tablet Compression

The tablets were prepared on a single station tablet press (Globe) using 8.0 mm flat face tooling and standard concave tooling. The compression force varied per the experimental design requirements in the screening study, which were evaluated at 100, 200 & 300 kg/cm^2 in the main effects screening study. Compression forces greater than 300 kg/cm^2 resulted in formulation leakage around the compression tooling. The compression force was held constant in the optimization study (200 kg/cm^2).

3.3.10 Tablet Properties

A dual scooping projection Vanderkamp friabilator (Vankel Industries Inc. Chatham, NJ) filled with 33 200mg tablets in one side, to meet USP requirements, was used to assess tablet friability.

The friabilator was allowed to rotate continuously for four minutes at 25rpm. The tablets were accurately weighed prior to the test, and carefully de-dusted and reweighed after the test.

Tablet hardness was assessed using a Schleuniger hardness tester. Each tablet tested was placed firmly against the stationary anvil prior to beginning the test, and all debris from the previous test was carefully removed before performing replicate tests (n=10).

Weight variation was measured on a microbalance. Twenty tablets were weighed, and their average determined. The weight of the individual tablets was then compared to the average and evaluated within USP specified tolerances for uncoated tablets (± 7.5%).

3.3.11 Dissolution Testing

The tableted formulations were assessed for *in vitro* drug release in 900ml gastric media (0.01N HCl) using USP apparatus I (Hanson SR8) at 37 ± 0.5°C with a basket rotation speed of 100 rpm over a 24 hour period. The dissolution vessels were equipped with UV-Vis fiber optic probes (Rainbow Dissolution Monitor, pION) and the detector was set at a wavelength (λ_{Max}) of 290nm.

3.4 Results & Discussion:

3.4.1 Preliminary Range Finding Studies & Observations

Prior to utilizing a statistical experimental design, it was necessary to conduct a series of prescreening and range finding studies as no prior knowledge was available to suggest appropriate formulation and/or operational parameters for this novel process. As would be anticipated, observations that are unique to this dry granulating approach were made.

Figures 3-1a & 3-1b below provide a visual comparison of the in-process materials, and illustrate the observed differences between the formation of a typical polymer melt, depicted in Figure 3-

1a, and a compacted dry mass, Figure 3-1b, of the same composition. It should be noted that presence of mixing elements was necessary to provide the compaction forces which resulted in the formation of the dry granules. As can be seen in Figure 3-1b, uncompacted powder is metered out by the conveying elements and subsequently compacted by the mixing elements, where the compact takes on the matte appearance similar to that of a roller compacted ribbon. Discrete granules (Figure 3-1b) can be seen along the conveying elements moving beyond this compaction zone and toward the discharge elements of the screws.

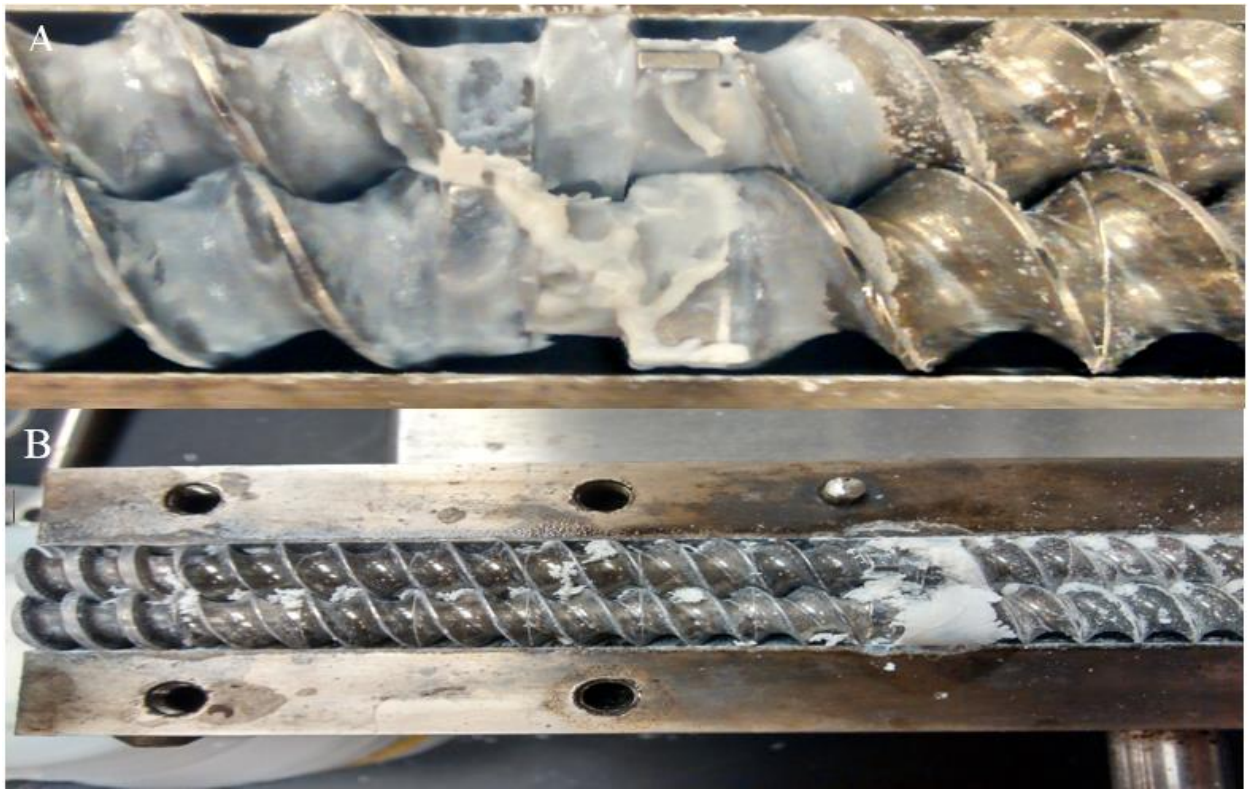

Figure 3-1a (Top) and 3-1b (Bottom): Graphic Illustration of the Observed Differences between a Polymer Melt on the Mixing Elements (3-1a) and the Compacted Powder Mass Formed During the TSDG Process (3-1b).

Additionally, the ability to easily mill the compact back into a fine powder further indicates that a dry agglomerate is being formed. In contrast, the material on the mixing zone in Figure 3-1a has

the glossy appearance that commonly results from the complete melting of polymers. The melted mass could not be easily removed, nor crushed back into a fine powder. This is a common occurence during HME processes as pharmaceutical polymers tend to have a relatively high affinity for metal after achieving a molten state.

During processing, it was consistently observed that dry powder exited the barrel prior to the appearance of granules, indicating that a buildup of back pressure was required to facilitate the agglomeration process. This differs from HME processes in that, while the generation of back pressure is common with extruders in general, during a melt extrusion or melt granulation process agglomerated material typically appears immediately when output is achieved. Additionally, the torque values measured during a melt extrusion process tend to become elevated at steady state as the polymeric carriers become molten and viscous. On the other hand, during the TSDG process the torque values remained exceptionally low with relatively large fluctuations ranging from 0.72-3.12 Nm. This observation was brought to greater acuity when the optimized formulation was both dry granulated and melt extruded with the barrel temperature profile being the only adjusted variable. The polymer melt produced consistent torque values of approximately 5.3 Nm. While seemingly low, the torque values resulting from the melt process are also a function of the reduced feed rate, which were representative of the feed rate employed during the TSDG process.

3.4.2 Twin-Screw Lubrication

During a melt extrusion process, the melt itself serves as the lubricant for the moving parts during processing; however, during a TSDG process this is not the case as no melted material is present. During these preliminary studies, observable metal-on-metal contact between the extruder screws and barrel frequently occurred. In order to prevent product degradation and/or contamination, as

well as damage to the processing equipment itself, it became desirable to incorporate a solid lubricant. Similar concerns are commonly addressed during tableting processes by the addition of nominal quantities of a solid lubricant such as magnesium stearate or stearic acid. Likewise, the addition of magnesium stearate was investigated for the mitigation of these effects. While the addition of modest quantities of magnesium stearate (0.2%) eliminated the previously observed metal-on-metal noises emanating from the extruder, it was observed that a narrow range of its utility existed as the addition of relatively larger quantities (0.5%) resulted in unfavorable quantities of fine particles (often greater than 50%). This was attributed to excessive lubrication of the powder mass by the magnesium stearate, which, in turn, resulted in decreased compactability of the dry mass within the extruder. The addition of even larger quantities (1.0%) frequently prevented the formation of granules entirely. Likewise, the method of its addition also produced varying effects on the granulating process. More specifically, the addition of magnesium stearate into the physical mixture needed to occur during the final stage of blending as earlier addition would also prevent granulation. Finally, limiting the quantity of dry lubricant present while granulating, and the utter absence of a lubricating melt, required limiting the extruder's screw speed to a maximum of 200 rpm.

3.4.3 Screw Design

Screw configuration demonstrated profound effects on the process. Figure 3-2a-e illustrates the various screw configurations explored during this research. Figure 3-2a shows a configuration that is similar to those used in typical polymer processing or HME operations as the numerous mixing elements impart considerable shear to the in-process materials. This configuration consistently resulted in the formation of a melt material at any appreciable screw speed. On the other hand, the

screw design in Figure 3-2b, which consisted of all conveying elements, served to merely pump the powdered material through the extruder's barrel.

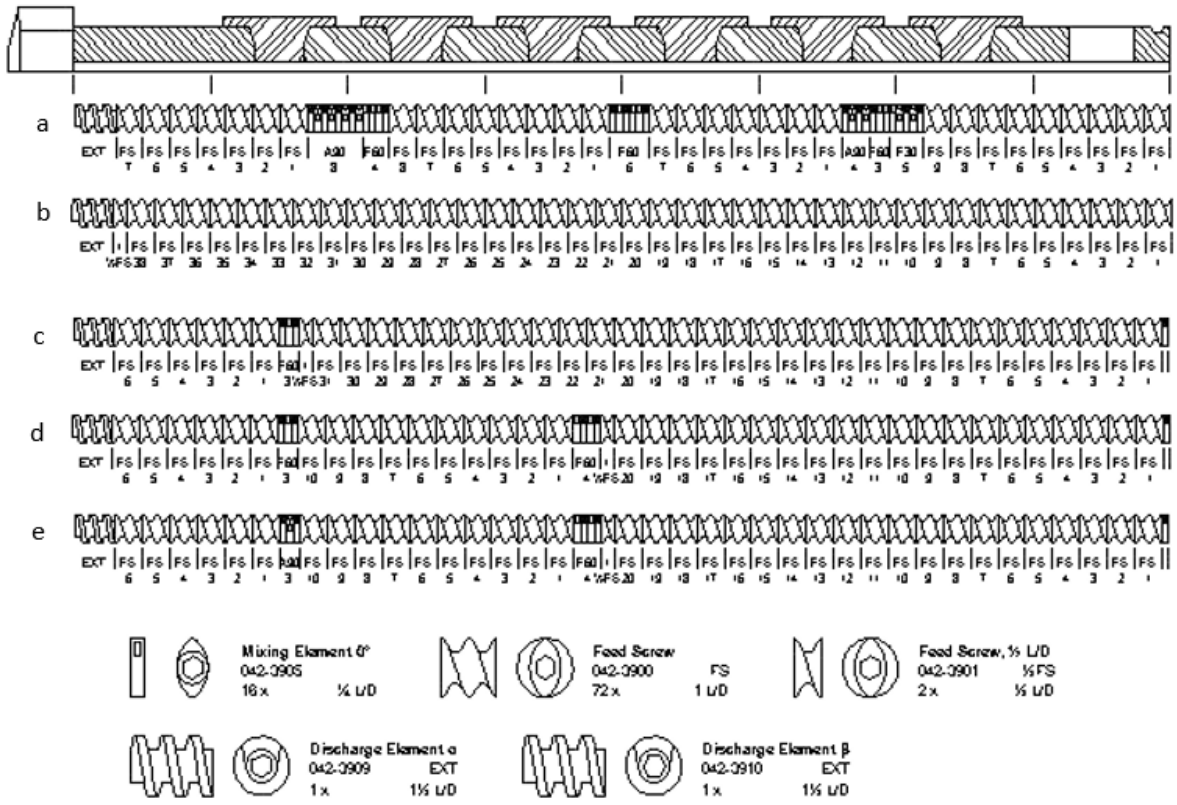

Figure 3-2a-e: a: ThermoFisher Preconfigured Screw Design; b: All Conveying Screw Design; c: Single Mixing Zone Screw Design; d: Two Mixing Zone Screw Design; e: Modified Final Mixing Zone Screw Design.

Beginning again with configuration 3-2b, three mixing paddles were added near the discharging end of the barrel, which resulted in a third configuration (Figure 3-2c). This configuration was capable of yielding granules. From this observation, it was apparent that an alternative approach to screw configuration, relative to HME applications, was required to produce a dry granulation. Two additional configurations capable of producing granules were developed (Figures 3-2d & 3-2e). In Figure 3-2d, an additional mixing zone has been added closer to the feeding hopper. The

configuration in 3-2e is a modified version of 3-2d where the mixing elements near the discharge section of the screw has been altered in order to evaluate effects of mixing element offset angle.

3.4.4 Quality by Design

In general, QbD studies involve the systematic utilization of various elements and tools (e.g. QTPP, Risk Assessment, DoE, etc.). This phase of investigation began with the identification of the product's critical quality attributes (CQAs) in the quality target product profile (QTPP, Table 1). Based on the predefined CQAs, excipients possessing the critical material attributes (CMAs) were selected. In the same fashion, the critical processing parameters were identified and selected for further study. Based on these observations, an initial risk assessment (Table 3-2) was performed to openly identify the variables perceived to pose that greatest risk to the CQAs. The CMAs & CPPs (inputs) were statistically analyzed through the DoE process where variation therein was assessed for variations in the CQAs (outputs).

Table 3-2: Initial Risk Assessment

Drug Product CQAs	Process steps		
	Twin Screw Granulation	Milling	Compression
Size	Low	Low	Low
Assay	High	Low	Low
Content Uniformity	Low	High	High
Drug Release	High	High	High

3.4.5 Experimental Designs (DoE) & Analysis

Prior to implementing the DoE, multiple factors were fixed. For example, the percent of intra-granular magnesium stearate used to lubricate the powder mixture, as well as the screws, was held at constant at 0.2% during the compaction process, while extra-granular magnesium stearate was

held constant at 0.5% for compression purposes. Additionally, it had been previously observed that variation in tablet tooling (standard concave vs. flat face) produced no observable variations in the tablets physical properties (disintegration, hardness & friability). This was attributed to the relatively large quantities of binder in the formulations. All of the polymers that were evaluated (ethyl cellulose, hydroxypropyl cellulose & hydroxyethyl cellulose) were capable of producing granules using the process and formulation ranges that were employed; however, in order to reduce the number of experiments required by a DoE, the subsequent experiments were limited polymeric blends consisting of HPC and HEC only.

3.4.6 Main Effects Screening DoE

A fractional factorial design (Minimum Number of Runs with Resolution IV; Min Run Res IV) with two center points was utilized as a screening design in order to determine the main effects from the formulation and process variables. The ranges of the responses and their main effects are listed in Table 3-3. Crystallinity, hardness and friability were not evaluated during the optimization/characterization phase of the DoE as they consistently produced acceptable values within the ranges under investigation. Additionally, these ranges would only be further restricted, rather than broadened, in subsequent studies.

\

Table 3-3 Main effects assessed by pareto analysis of screening DoE (Min. Run Res. IV).

Response	Range	Main Effect
Crystallinity	NA	NA (Always Maintained)
Percent Fines	12 – 49%	Polymer Ratio
Hausner Ratio	1.05 – 1.39	Screw Configuration
Compressibility Index	4.76 – 28.17	Screw Configuration
Angle of Repose	22.0 – 38.7	Polymer Ratio
Tablet Friability	0.0 0.3%	Drug Loading
Tablet Hardness	8.6 – 18.7kp	Screw Config., Compression Force, Drug Loading
Time to 80% Dissolution	3.0 – 15.3 hr.	Polymer Ratio, Drug Loading

3.4.7 Tablet Compression

Initially, tablets were compressed without the addition of extra-granular excipients; however, this resulted in the occasionally observed picking and sticking (the adherence of granulated particles to the tablet tooling) upon tablet ejection. The addition of 0.5% extra-granular magnesium stearate prevented these previously observed failures.

3.4.8 Tablet Properties

The granules produced in the initial screening design were mixed with and additional 0.5% extra-granular magnesium stearate and pressed into tablets using the appropriate compression force and the same 8mm flat face tooling. These reformulated tablets were assessed for hardness and friability (Table 3-4).

Table 3-4. Tablet Friability and Hardness Data from the Screening DoE with extragranular magnesium stearate.

Run Order	*Friability (%)*	*Hardness (kp)*
1	0.05	15.8
2	0.18	16.0
3	0.10	15.9
4	0.10	18.7
5	0.0	11.5
6	0.05	12.6
7	0.15	14.0
8	0.30	8.6
9	0.10	13.6
10	0.05	11.2
11	0.0	12.1
12	0.0	11.8
13	0.0	15.0
14	0.05	17.3
15	0.05	13.4
16	0.15	14.4

3.4.9 Characterization DoE

With the completed main effects/screening design results, which reduced the previously investigated six independent variables to three main effects (i.e. screw design, polymer ratio & drug loading), a full factorial (2^3) with four center points (Table 3-5) was created to evaluate potential interactions between the main effects, and, ultimately, to predict an optimized formulation and process.

Table 3-5: 2^3 Full Factorial with 4 Center Points. Screw Design 1: Figure 2d; Screw Design 2: Figure 2e.

Run	*Screw Design*	*Polymer Ratio (HPC:HEC)*	*Drug Loading (%)*	*Fines (%)*	*Hausner Index*	*Compressibility*	*80% Disso. (hr.)*
1	1	3:1	50	13.2	1.3	24.4	12.5
2	2	1.7:1	42.5	14.0	1.3	25.4	11.5
3	2	3:1	35	10.5	1.3	22.4	15
4	2	1:1	35	13.6	1.2	13.5	11.5
5	1	1.7:1	42.5	13.1	1.3	20.5	14
6	1	1.7:1	42.5	10.3	1.3	24.4	12
7	1	1:1	50	17.1	1.3	23.1	8.5
8	2	1.7:1	42.5	13.2	1.3	24.4	12
9	2	1:1	50	10.7	1.3	20.3	6.5
10	1	3:1	35	10.7	1.2	15.6	15
11	2	3:1	50	12.6	1.2	19.2	11
12	1	1:1	35	11.0	1.3	22.5	8

The parameters that did not produce main effects in the screening design (i.e. screw-speed, feed rate & tablet compression force) were presumed to have ngelible effects relative to the main effects and, as such, the mean of their previously utilized ranges was taken and implemented in the characterization study at fixed values. Therefore, the extruder's feeder output was set to 4g/min (previous range: 3-5g/min.), the screw speed was maintained at 150rpm (previous range: 100-200 rpm), and the tablet compression force was held constant at 200kg/cm^2 (previous range: 100-300 kg/cm^2) . The barrel temperature was held at 65^{o}C from zones 2 until granule discharge. The responses, their statistically significant main effects and interactions are summarized in Table 3-6 and further discussed in the ensuing individual sections.

Table 3-6: Response Ranges and Statistically Significant Main Effects & Interactions from the Characterization DoE.

Response	Range	Interaction Type and/or Main Effect(s)
Percent Fines	10.3 – 17.1	Polymer Ratio & Drug Loading (Main Effects); Interaction with Screw Design
Hausner Ratio	1.2 – 1.3	Screw-Configuration, Polymer Ratio & Drug Loading (3-Way Interaction)
Compressibility Index	13.5 – 25.4	Polymer Ratio & Screw Configuration (Main Effects & Two Way Interaction)
Angle of Repose	33.7 – 42.0	Insufficient Variation Within the Model
Time to 80% Dissolution (hr.)	6.5 - 15	Polymer Ratio & Drug Loading (Independent Main Effects; Interaction with Screw Configuration)

3.4.10 Percent Fines

The following values were used in the analysis of variance (ANOVA) of the "percent fines" response variable. A Model F value of 14.64 in the unadjusted model suggests that the model is significant. The "Lack of Fit F-Value" 0.75 indicates that the lack of fit is not significant ($p > 0.0011$). The model is statisitically significant for the response Percent Fines with an "R-Squared" value of 0.7262. The Predicted R-Squared value (0.430) is in reasonable agreement with the Adjusted R-Squared value (0.5698). The adequacy/precision ratio of 7.697 indicates an adequate signal. This model can be used to navigate the design space. The following polynomial equation, which is expressed in terms of coded factors, was generated for the mathematical description of percent fines generated during granulation: Percent Fines = +12.49 -0.67*B –0.98*C -1.18*A*C; where A, B and C are the screw configuration, polymer ratio and drug loaing respectively. In this equation, a positive or negative sign prior to a coded variables coefficient is inversely related to an additive or deleterious effect respectively as the response variable is a measure in increasing in-process fine material. In this case, an decrease in the polymer ratio, which corresponds to a decrease in the high molecular weight binder (HPC HF), corresponds to a increase in fine material, where an increase in drug content corresponds to decrease in fine materials. The above equation is

graphically depicted by both a contour plot and response surface for a visual assessment of these variables (Figure 3-3).

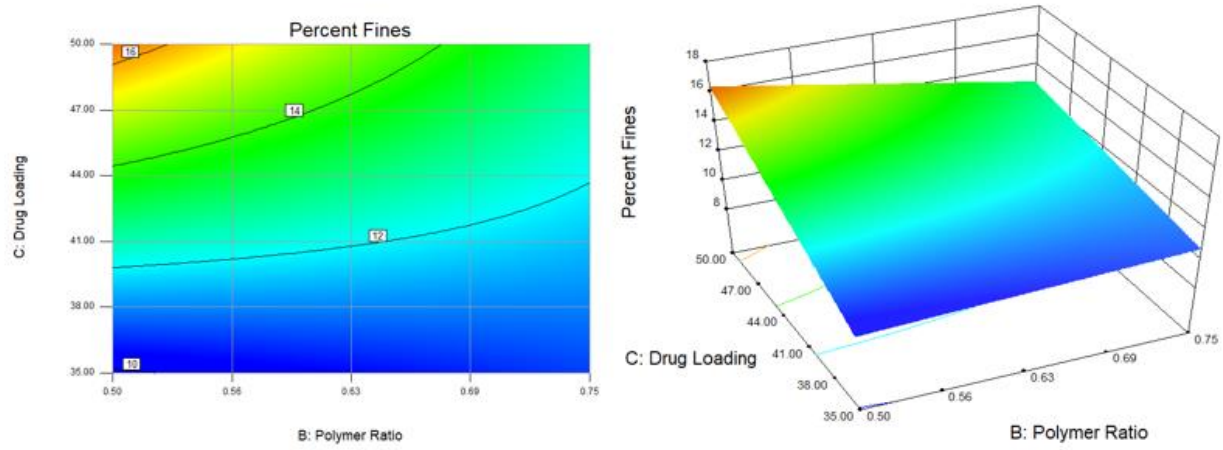

Figure 3-3: Percent Fines contour plot and response surface graph with Screw Design 1 (Figure 3-2 d).

3.4.11 Hausner Ratio

The Hausner Ratio of the granules was evaluated using the procedure outlined by the USP-NF[37]. The full factorial experiments resulted in the range of values of 1.16 – 1.34, which, while satisfying the compendial specifications spanning "Good" to "Passable", did not produce sufficient variation to result in a predictive model (Model F value 1.13, Predicted R^2 -2.27). Given these results, the values for the Hausner ratio were not used to produce a predictive equation. Instead, given that the entire range of values was acceptable, the span of the data points was taken and utilized to inform numerically predicted solution.

3.4.12 Compressibility

The following values were used in the analysis of variance (ANOVA) of the "compressability" response variable. A Model F value of 7.24 in the unadjusted model suggests that the model is significant. The "Lack of Fit F-Value" 0.70 indicates that the lack of fit is not significant ($p > 0.01114$). The model is statisitically significant for the response Percent Fines with an "R-Squared" value of 0.7308. The Predicted R-Squared value (0.4679) is in reasonable agreement with the Adjusted R-Squared value (0.6299). The adequacy/precision ratio of 6.545 indicates an adequate signal. This model can be used to navigate the design space. The following polynomial equation, which is expressed in terms of coded factors, was generated for the mathematical description of compressability of the granulation: Compressability = +22.08 +1.25*A –1.50*B +0.5*C - 1.50*AB; where A, B and C are the screw configuration and polymer ratio and drug loaing respectively.

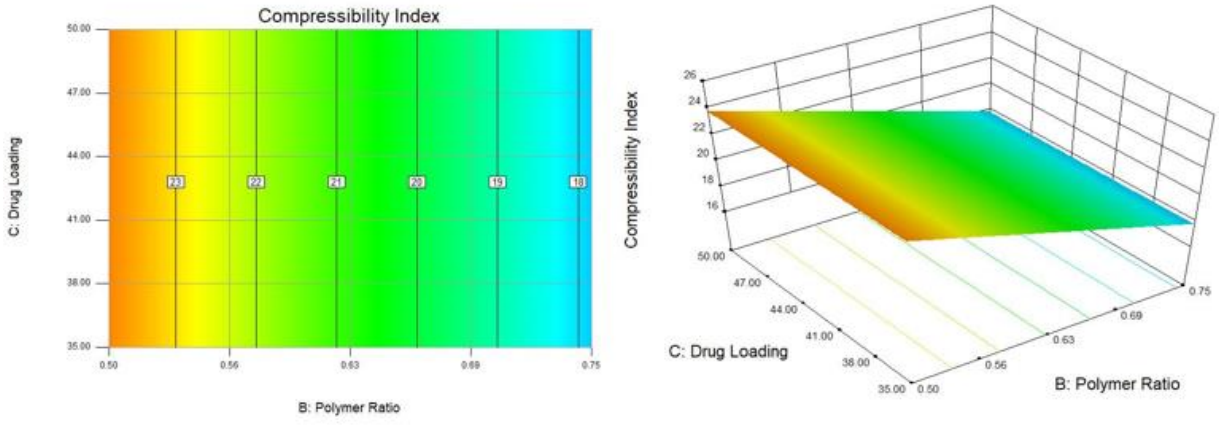

Figure 3-4: Compressibility contour plot and response surface graph with screw design 1 (Figure 3-2 e).

3.4.13 Angle of Repose

The flowability of the granules was evaluated using the Recommended Procedure for Angle of Repose outlined by the USP-NF [86]. The full factorial experiments resulted in the range of values presented in (33.7 – 42.0), which produced insufficient variation to result in a sufficiently predictive model. However, this range of values falls within the qualitatively described ranges for angle of repose in the USP-NF [86]. More specifically, the range presented spans what the USP describes as “Good” to “Fair”. Given these results, the values for the angle of repose were not used to produce a predictive equation. Instead, given that the entire range of values was acceptable, the mean of the data points was taken and utilized to inform numerically predicted solution.

3.4.14 Time to 80% Dissolution

The *in-vitro* drug release was assessed using the conditions outlined for this drug by the FDA [87]. The following values were used in the analysis of variance (ANOVA) of the dissolution predictive model. A Model F value of 14.67 in the unadjusted model suggests that the model is significant. The “Lack of Fit F-Value” 2.20 indicates that the lack of fit is not significant ($p > 0.0011$). The model is statisitically significant for the response Time to 80% Dissolution with an “R-Squared” value of 0.7653. The Predicted R-Squared value (0.5668) is in reasonable agreement with the Adjusted R-Squared value (0.7131). The adequacy/precision ratio of 10.468 indicates an adequate signal. This model can be used to navigate the design space. The following polynomial equation, which is expressed int terms of coded factors, was generated for the mathematical description of tablet dissolution: Time to 80% Dissolution = +11.46 +2.37*B –1.38*C; where B and C are the polymer ratio and drug loaing respectively. In this equation, a positive or negative sign prior to a coded variables coefficient is indicative of an additive or deleterious effect respectively. In this

case, an increase in the polymer ratio, which represents and increase in the high molecular weight polymer (HPC HF), corresponds to prolonging dissolution. Likewise, a decrease in drug content also corresponds to an increase the time it takes to reach 80% dissolution. As might be anticipated when employing a high molecular weight polymer and a BCS I API, an increase in the amount of the high molecular weight polymer was correlated with an increase in dissolution time (indicated by the "+" symbol in the equation), while an increase in drug loading was correlated with a decrease in dissolution time (indicated by the "–" symbol in the equation). This equation is graphically depicted by both a contour plot and response surface for a visual assessment of these variables (Figure 3-5).

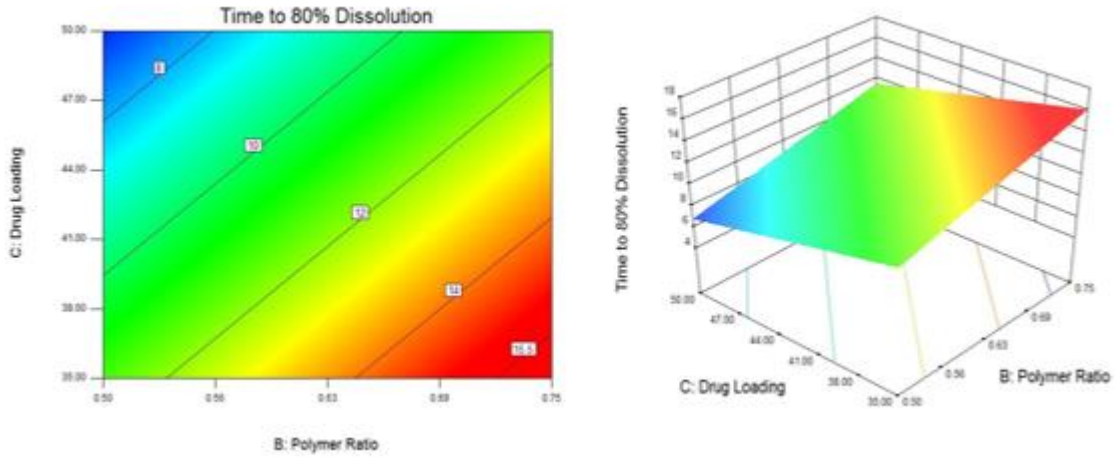

Figure 3-5: Time to 80% Dissolution Contour plot and Response surface graph with Screw Design 1 (Figure 3-2 e)

As might be anticipated when employing a high molecular weight polymer and a BCS I API, an increase in the amount of the high molecular weight polymer was correlated with an increase in dissolution time (indicated by the "+" symbol in the equation), while an increase in drug loading

was correlated with a decrease in dissolution time (indicated by the "–" symbol in the equation). This equation is graphically depicted by both a contour plot and response surface for a visual assessment of these variables (Figure 3-5).

3.4.15 Fourier Transform Infrared Spectroscopy (FT-IR)

FT-IR spectral analysis (Figure 3) clearly illustrates the differences between the crystalline and amorphous phases of Sildenafil Citrate. As would be expected, the amorphous phase exhibits shifted, shorter and broader spectral bands relative to the crystalline phase. These alterations in spectral responses arise from the lack of long range order that is characteristic of the amorphous phase. This allows for the identification of the API's post-processing physical phase, which demonstrates that the API is still crystalline. Interestingly, the physical mixture shows the carbonyl in Sildenafil Citrate, which is centered at $1697cm^{-1}$, in the same position as the carbonyl in the pure crystalline spectrum, whereas the dry granulated carbonyl is centered at $1699cm^{-1}$. While there is obviously a spectral shift occurring, it is shifted in the opposite direction of the carbonyl in the amorphous phase. This may be indicative of hydrogen bonding between the carbonyl in crystalline Sildenafil Citrate and the hydroxyls (ranging from approximately $3600\text{-}3200cm^{-1}$) present in the polymeric carrier(s), which, considering their relative proportions within the mixture, may be assisting in the formation of the granules.

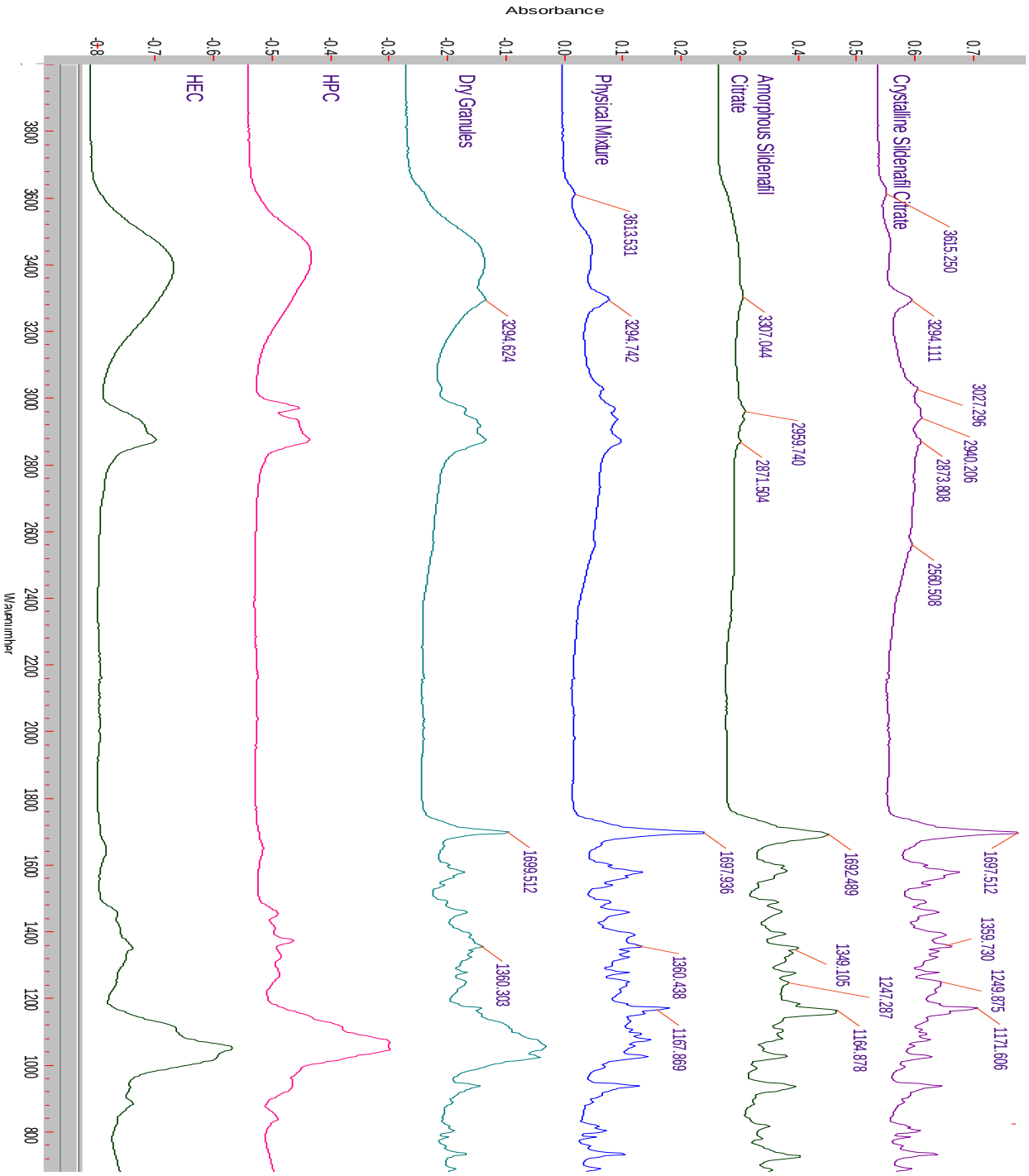

Figure 3-6: Mid-Infrared Spectral Evaluation of Sildenafil Citrate's Post Processing Physical Phase.

3.4.16 Scanning Electron Microscopy (SEM)

Figure 3-7a through 3-7d illustrates the visually observable differences in the surface morphology between the physical mixture, the dry granules and the hot-melt granules, respectively. These samples are representative of the optimized formulation predicted by the full factorial model. In Figure 3-7a it can be observed that the dry granulated material appears to be a compacted agglomerate of the physical mixture presented in Figure 3-7b. The image of the Hot-Melt Granulated material in Figure 3-7c appears homogenous and lacks the observable appearance of its constituents. Further magnification of the Hot-Melt Granulated material revealed no additional information; however, Figure 3-7d, taken at 300X magnification, demonstrates that compacted agglomeration of the primary particles is still apparent in smaller domains.

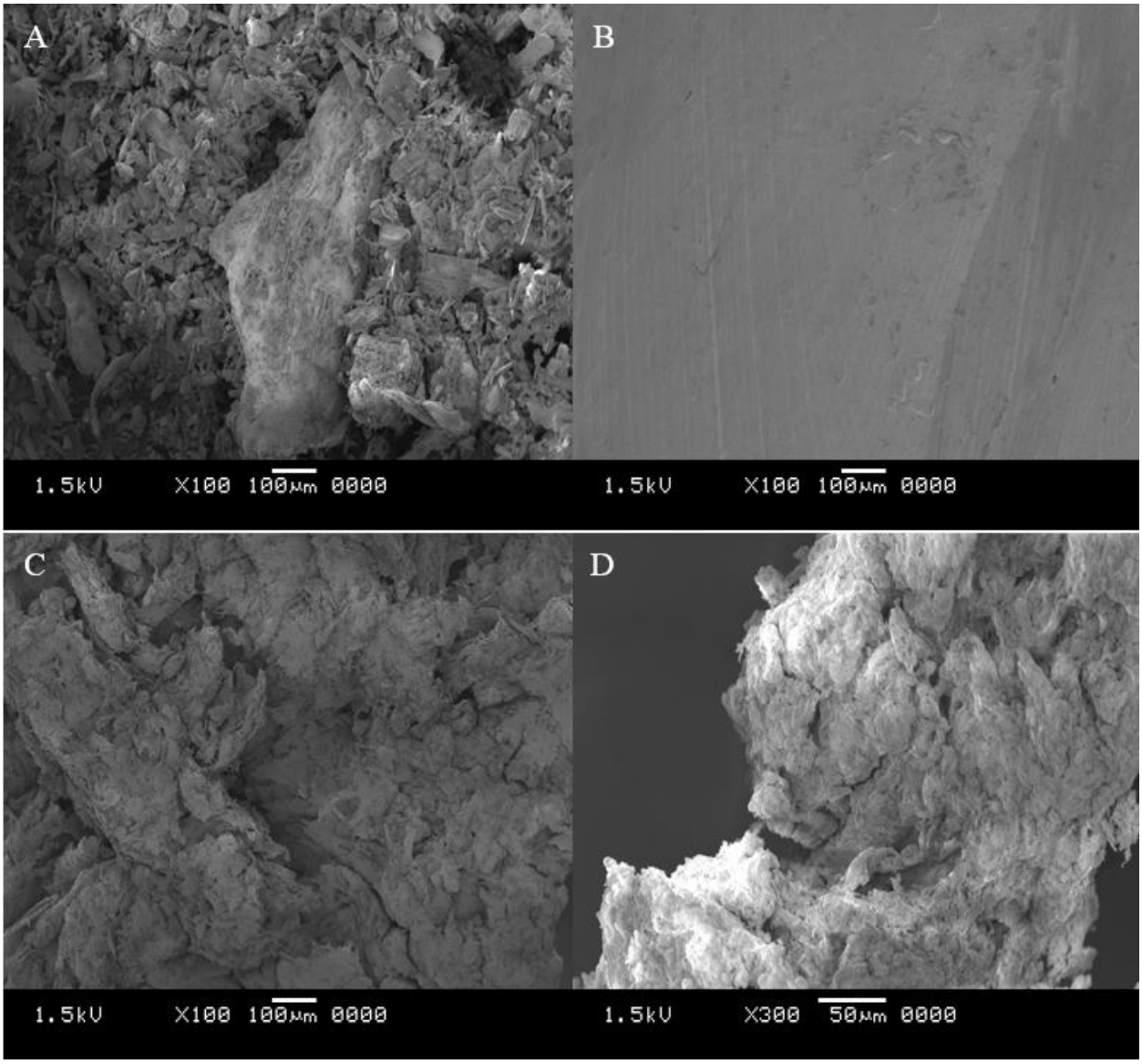

Figure 3-7A-D: 4A Physical Mixture (100X), 4B Hot-Melt Granule (100X), 4C Dry Granule (100X); 4D Dry Granule (300X).

3.4.17 Numeric Prediction of Optimization & Confirmation

The full factorial model was used to predict a set of graphically and numerically optimized formulations (Table 3-7). The criteria for the optimization process were based on the CQAs in the QTPP as well as the acceptable ranges for the measured responses found in the USP. With a

relatively broad range of acceptability for the dissolution profile (80% in 12 – 18 hrs.), the target was set to the median value (15 hrs.). The percentage of fines was set to a range of 10 – 15%, as this is the generally acceptable . The lower limit of the Hausner Ratio was set to the lowest value obtained during this study (1.15) and the upper limit was set to 1.25 as the USP defines this as the cutoff "Fair" flowability. The range for the angle of repose was set such that it encompassed the lowest value attained in this study

Of the most desirable predicted solutions to the predefined ranges and targets, solution 1 was selected as it incorporated the highest drug loading, which was one of the primary objectives of this research, and it possessed the most favorable desirability value (0.558). The predicted values of the proposed formulation and process were then compared to the measured values in during confirmation stage of optimization. The measured values are presented in Table 3-7.

Table 3-7: Numerically predicted formulation and process parameters resulting from the input acceptable ranges on screw design 1; *Confirmation*: Confirmatory Results from Prediction Number 1.

Predicted Solution Number	Polymer Ratio	Drug Load (%)	Percent Fines	Hausner Index	Compress. Index	Time to 80% Disso.	Angle of Repose	Desirability
1	3:1	42.7	11.85	1.25	19.70	13.82	39	0.558
2	3:1	42.6	11.82	1.25	19.63	13.84	39	0.552
Confirmation	3:1	42.7	12.05	1.22	21.1	14	36	NA

Based on the desired input model criteria for the individual independent and dependent variables, the resulting individual desirability values are graphically depicted in Figure 3-8. While the criteria for both the independent variable "drug loading" and the dependent variable dissolution were each given the highest priority of the model variables, which are consistent with the product criteria established in the QTPP, it can be seen that their respective desirability values lie well below that

of the other responses. This is clearly explained by the inversive relationship between the two variables, that is, the time required to reach 80% dissolution decreases as drug loading increases and vice versa, and equal priority having been given to both. As such, a balance, or compromise, between the two criteria was established by the resulting model.

The overall desirability contour plot and response surface (Figure 3-9) was for predicted solution 1 (Table 3-7) was constructed to graphically depict the complete relationship between the independent variables and predefined and prioritized response value ranges. Addtionally, these plots serve to illustrate that an optimal region of overlap is predicted to exist. It is important to note that while the range for desirability is predefined from 0.0 – 1.0, that the obtained value (0.558) is a multiplicative mean rather than additive mean, which is to say that if any value were unable to meet the input specifications, the desirability function would become 0.0. Therefore, it is the existence of some appreciable value greater than 0.0 that is of importance here, which justifies proceeding with predicted solution confirmatory experiment (Table 3-7).

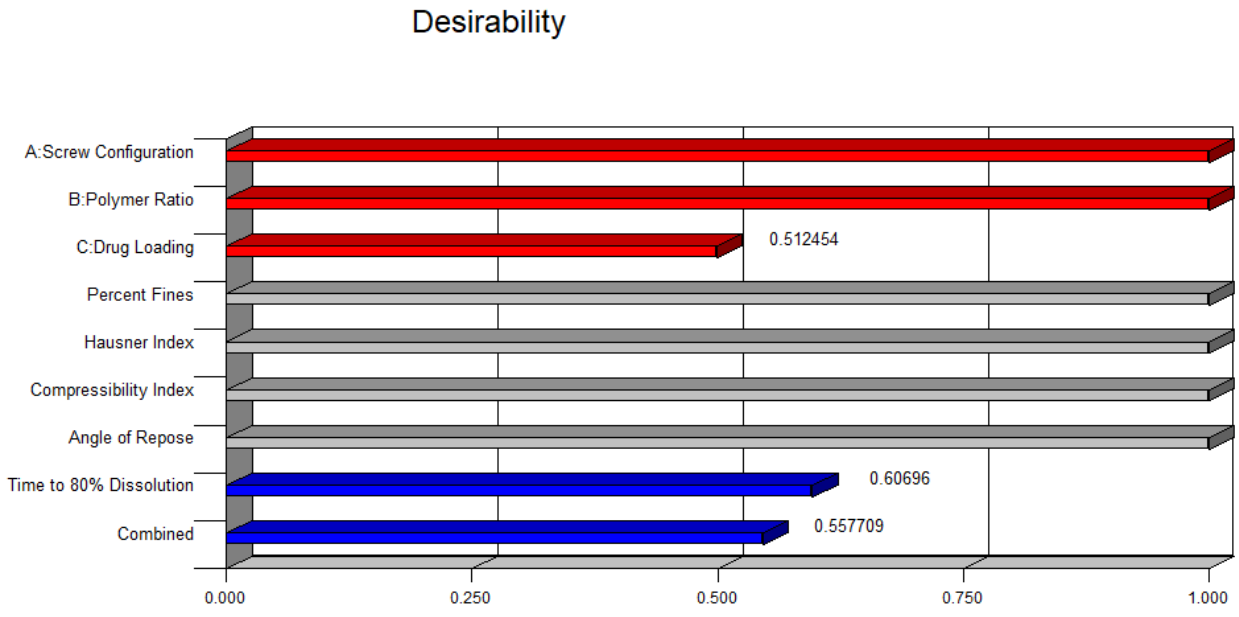

Figure 3-8: Individual independent variable and dependent variable desirability values.

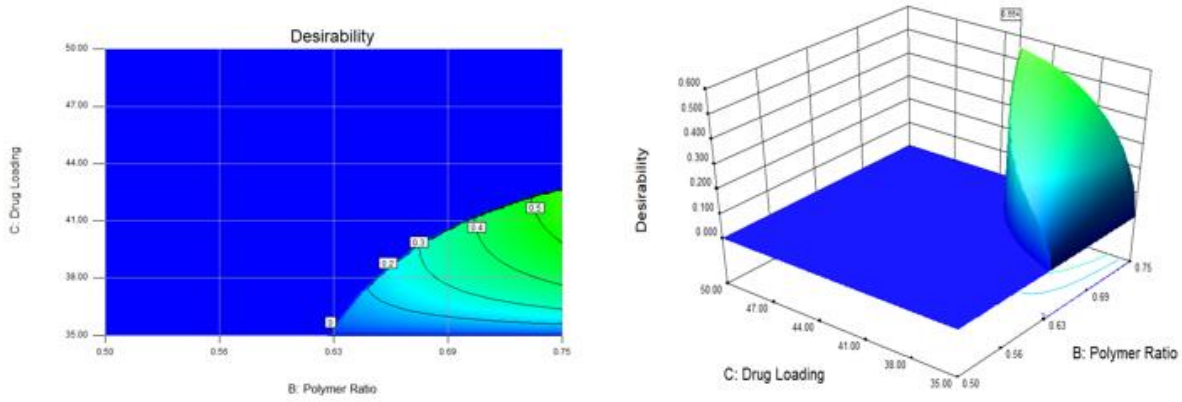

Figure 3-9: Desirability function contour plot and corresponding response surface.

3.4.18 Design Space

When attempting to optimize for multiple variables, it is necessary to find the region where all requirements are met simultaneously. The close agreement of the Predicted Solution values with the values collected from the confirmation experiment (Table 3-7) suggest the suitability of the predictive model. As such, the previous contour plots (Figures 3-3, 3-4 & 3-5) have been superimposed to produce the overlay plot in Figure 3-10. This overlay is representative of what is considered to be the design space, shaded in blue, where the control space being chosen a subset thereof. It can be seen from the plot that the most limiting of the response (dependent) variables were the lower boundry condition set for percent fines (10 -15%) and the upper boundry condition set for Hausner's Ratio (1.34). The compressibility index and angle of repose, within the ranges studied in this factorial design, did not impose on the design space whatsoever.

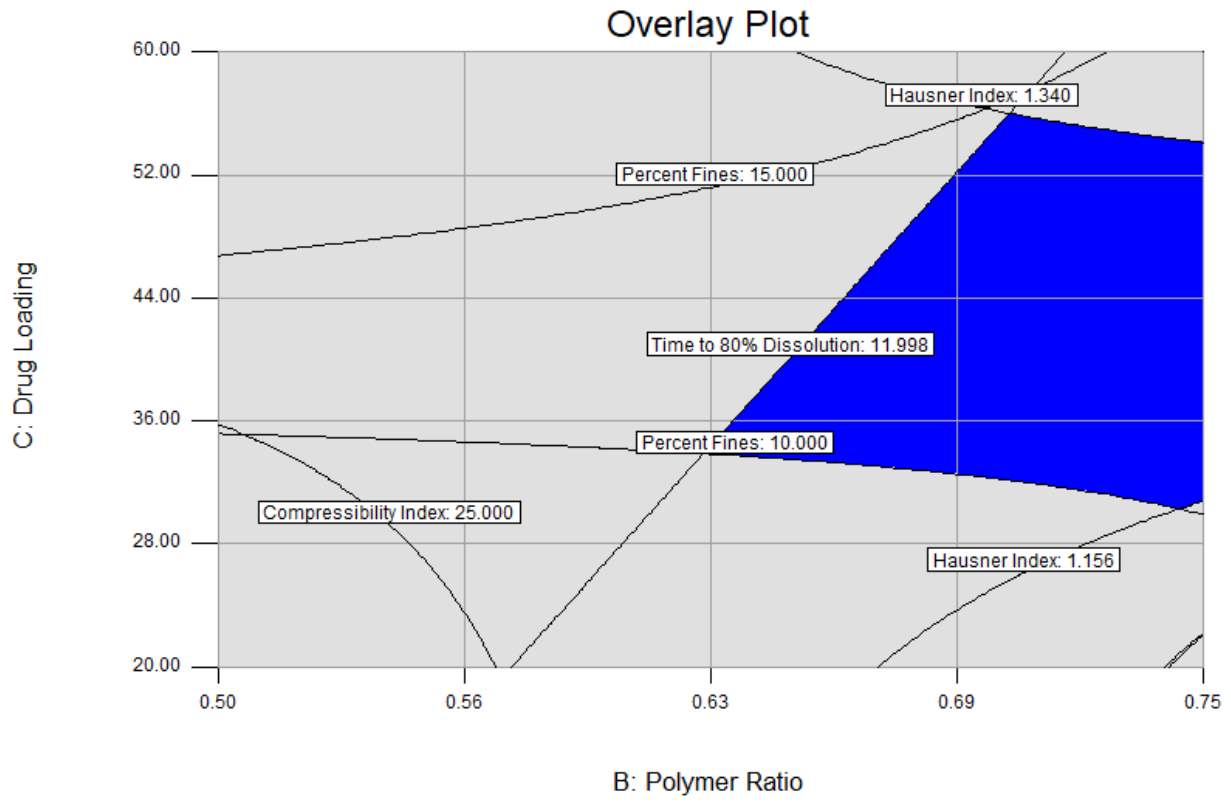

Figure 3-10: Overlay plot of the resulting design space.

3.5 Conclusion

This study explores the previously unreported applicability of a fully intermeshing co-rotating twin-screw extruder for the production of dry granules. Fundamental differences from conventional HME processing were discovered and assessed accordingly. Screw design played an integral role in the formation of the granules, while the extruder feed rate was limited by the absence of a lubricating polymer melt. Utilizing the QbD methodology to investigate this alternative dry granulation process facilitated rapid and efficient method development.

CHAPTER 4.

THE EFFECT OF MIXING BLOCK OFFSET ANGLE ON THE DISTRIBUTION OF CARBAMEZAPINE AND CAFFEINE CITRATE IN A POLYMERIC MATRIX

4.1 Introduction

While screw configuration is widely regarded as a critical processing parameter in extrusion processes, as it plays a vital role in the physicochemical characteristics of the final extrudates, little practical information is available in the literature concerning the effects of screw configuration on pharmaceutical formulations. Moreover, nearly all of that information is focused on the conversion of a crystalline API into its amorphous form with little attention given to the intermediate changes that occur during processing. To some extent this stands to reason as the initial obstacles that HME was investigated to address were related to the poor aqueous solubility of many newer APIs. However, given the numerous processing advanteges that this platform offers, it is well poised to serve as an alternative to many more conventional pharmaceutical processing technologies. Moreover, this particular platform readily embraces the agency's current thinking on pharmaceutical regualtory matters; namely continuous processing. Given some of the additional advantages inherent in HME processing (i.e. , fewer processing steps, simple scalability, avoidance of organic solvents, etc.), it becomes apparent that processing any suitable API by this technique is an attractive option regardless of which BCS class it belongs to. However, in the case of BCS class I and class III APIs, where the formation of an API's amorphous phase might not be desirable, it may be appropriate to preserve the initial crystalline structure as solubility enhancement is not

necessary and common stability issues associated with amorphous forms, such as recrystallization into an undesired polymorphic form, can be avoided. Conversely, a complete understanding of the morphological changes that are induced in such an environment poses the possibility controlled conversion between polymorphs in situ, much like conversion from a crystalline lattice to a molecular or amorphous dispersion is peformed today. The objective of this study is to evaluate the effects of screw configuration on active pharmaceutical ingredient (API) morphology using a fully intermeshing co-rotating twin-screw extruder and FT-IR chemical imaging for spatial determinations. Here the examination takes place within the mixing zones along the co-rotating screw.

4.2 Materials & Methods

Eudragit E PO was generously donated by Evonik (Somerset, NJ.). Carbamezapine and Caffeine Citrate were donated by Ashland Specialty Ingredients (Wilmington, DE).

4.3 Hot-Melt Extrusion

4.3.1 Thermo Gravimetric Analysis (TGA)

Prior to melt extrusion processing, TGA (Pyris 1 TGA Perkin Elmer) was utilized to determine the thermal stability of the individual polymers and API. Binary mixtures (1:1 w/w) of the individual polymers with the API were examined at the temperatures required for melt extrusion processing. During TGA, each of the weighed samples was heated from 25^{o}C to 180^{o}C at a rate of 20^{o}C/min. in a platinum pan under an inert nitrogen atmosphere purge of 20ml per minute. The samples were held at 180^{o}C for 5 minutes to simulate the thermal stresses and residence time encountered during HME processing.

4.3.2 Differential Scanning Calorimetry (DSC)

DSC (Diamond DSC, Perkin Elmer) was utilized to confirm the thermal stability of replicate TGA samples. The samples, weighing 4-5 mg each, were placed in hermetically sealed aluminum pans and placed under an inert nitrogen atmosphere at a purge rate of 20ml per minute. These samples were heated from 25^{o}C to 180^{o}C at a rate of 20^{o}C/min., held at 180^{o}C for 5min. and cooled to room temperature. The thermograms of these samples were analyzed for deviations from the thermograms of the pure substance and other significant thermal events. Calibration of the instrument was performed with an Indium reference.

4.3.3 Hot-Melt Extrusion Processing

Prior to HME processing, the polymer was sieved with a USP #35 mesh screen to remove any aggregated particles. The compounds required for each physical mixture were placed in a V-shell blender (GlobePharma, Maxiblend®) and mixed at 20 rpm for 20 minutes. A fully intermeshing co-rotating twin-screw extruder (11 mm Process 11, ThermoFisher Scientific) was used to process the physical mixtures.

4.3.4 FT-IR & Mid-Infrared Chemical Imaging

Mid-infrared spectral analysis was conducted on an FT-IR bench (Agilent Technologies Cary 660, Santa Clara, CA.). The bench was equipped with an ATR (Pike Technologies MIRacle ATR, Madison, WI), which was fitted with a single bounce diamond coated ZnSe internal reflection element. Chemical imaging was conducted using an infrared microscope (Agilent Technologies

Cary 620 IR, Santa Clara, CA.) equipped with a 64 x 64 pixel focal plane array (FPA) with a germanium micro-ATR.

4.4 Results and Dsicussion

4.4.1 Thermogravimetric Analysis

No thermal events were noted during thermogravimetric analysis of the binary mixtures during the course of this study, which is indicative of thermal stability over the temperature ranges utilized.

4.4.2 Hot-Melt Extrusion Processing

The barrel temperature profile and screw speed were based on the physical properties of polymeric carrier in each of the preliminary physical mixtures and a 2mm rod die was attached to the end of the barrel. After allowing the extruder to reach a steady state, a barrel plug was removed from the top half of the barrel, which exposed the respective mixing zones, and samples were collected directly from the mixing elements for analysis. The samples were either immediately analyzed, or stored in foil lined polyethylene bags for future analysis. Three screw configurations. Each screw design was characterized by three consecutive mixing blocks. Each block was composed of mixing paddles with offset angles of 30^{o} or 90^{o} each. It is important to note that these angles were not investigated in conjunction with eachother, but were examined for the individual angle effects on the dispersion and distribution each active (CC or CBZ) within the EPO matrix.

4.4.3 FT-IR & Mid-Infrared Chemical Imaging

A qualitative examination of the FTIR spectrum for each of compounds indicates that there exists a region of clear spectral resolution for each of the model drugs within the polymer matrix (Figure 4-1).

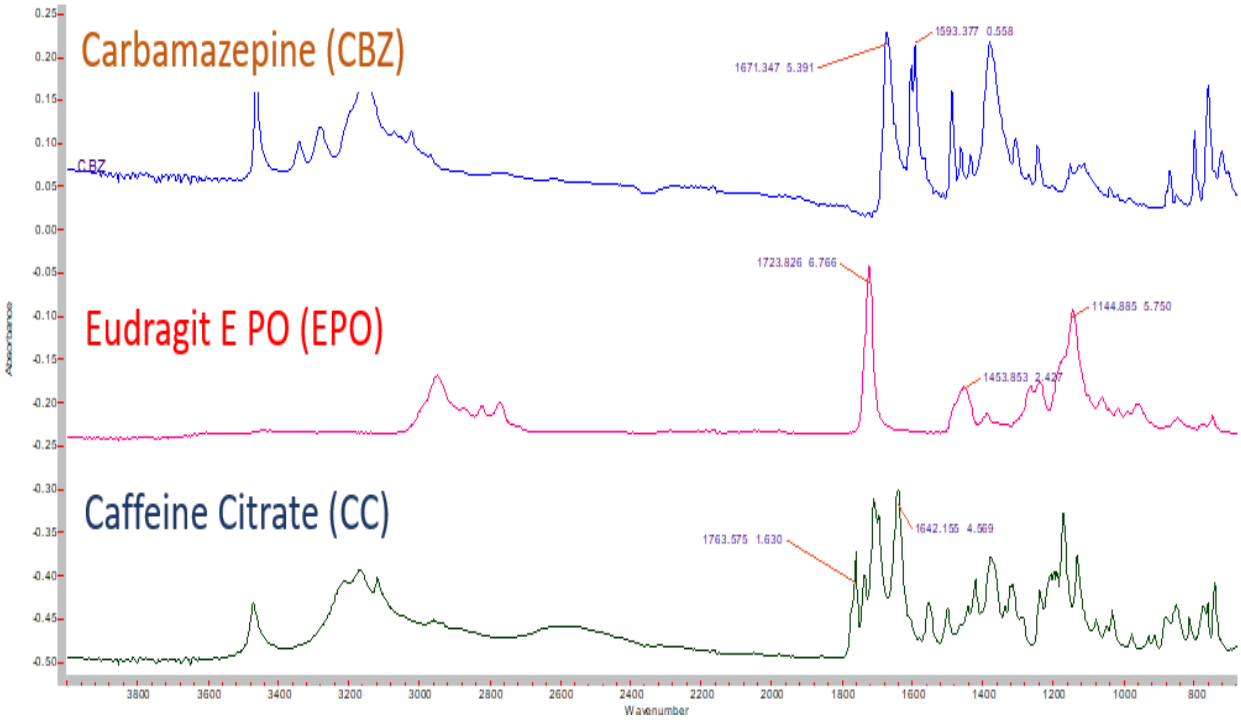

Figure 4-1: FT-IR spectra of Eudragit E PO (EPO), Carbamezapine (CBZ) and Caffeine Citrate (CC).

More specifically, for the mixture of caffeine citrate (CC) and Eudragit E PO (EPO), CC exhibits a very strong peak at 1642cm^{-1} while EPO presents only baseline contributions in this same region. Overalys of the representative spectra can be seen in Figure 4-2 and Figure 4-3, respectively.

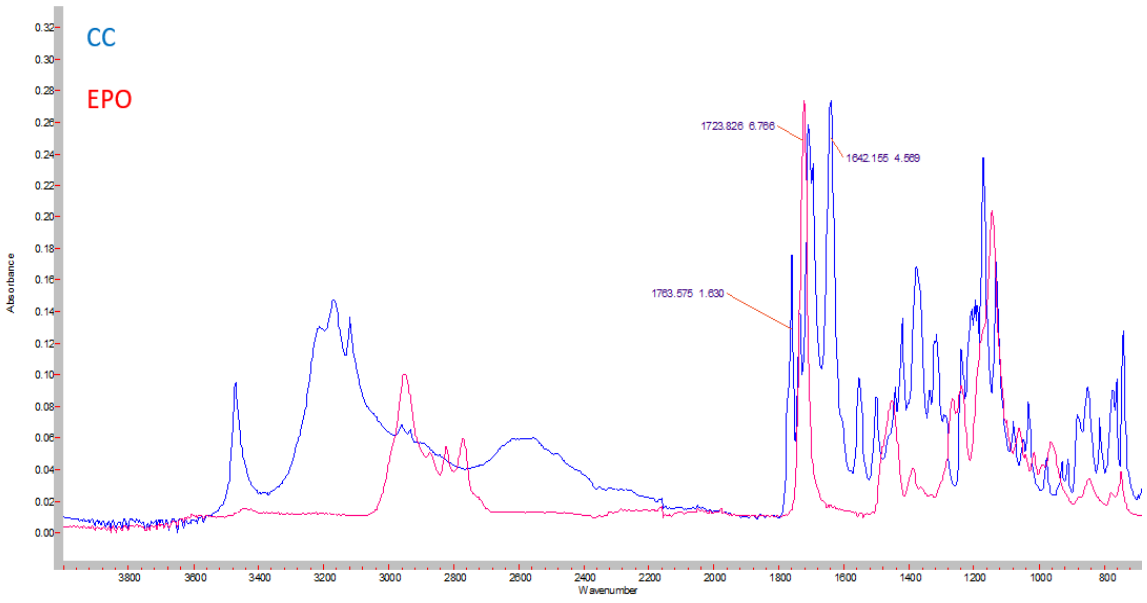

Figure 4-2: FT-IR spectral overlay of Eudragit E PO (EPO) and Caffeine Citrate (CC).

Here it can be seen that while a marginal contribution to the IR spectrum results from EPO (approximately 0.02 AU) at 1642cm^{-1} the majority of the signal (approximately 0.28 AU) is from CC, which allows this peak to be used for spectral imaging. Likewise for the combinations of Carbamezapine (CBZ) and EPO, there is a clear contribution to the IR spectrum from CBZ at 1593cm^{-1} (approximately 0.22 AU) where EPO again presents only baseline contributions (approximately 0.02 AU).

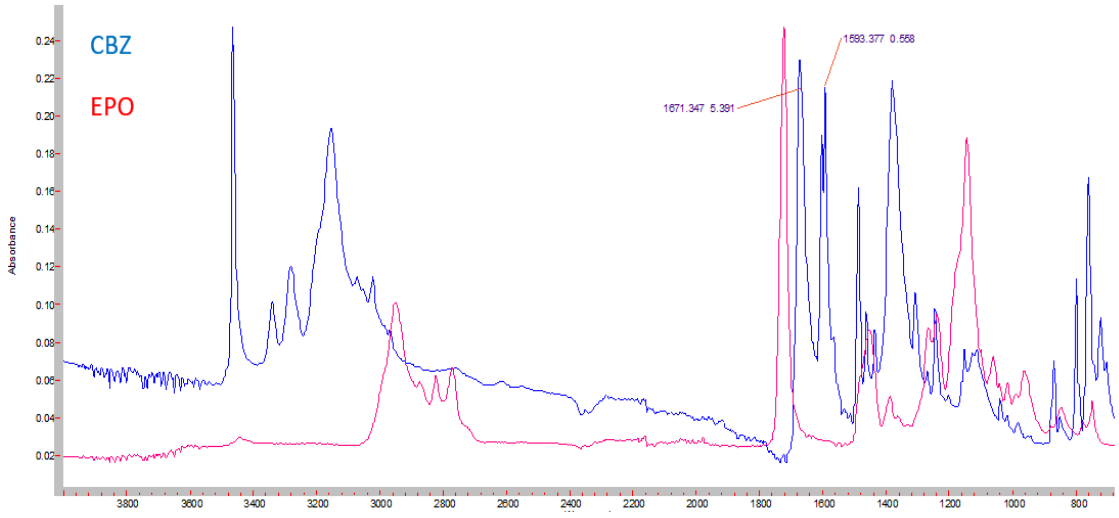

Figure 4-3: FT-IR spectral overlay of Eudragit E PO (EPO) and Carbamezapine (CBZ).

Using these clear distinctions in the spectra allows for the generation of resolved chemical images such as those in Figure 4-4. Here it can be seen that as the in-process melt travels along the mixing block that the active (depicted as a function of intensity for the characteristic peak; 1642cm^{-1}) is not being distributed thoughout the matrix as intensely as it is being dispersed into smaller units within a given area, that is, the blue area that is representative of the absence of this peak is slowly disappearing while the rea areas are declining in intensity. Interestingly, the corresponding DSC thermograms for each of the three regions sampled showed practically no difference in AUC as the in-process material passed through the mxing zone (1.23, 1.23 & 1.14 J/g, respectively) indicating that though the material is being dispersed, it has not yet been converted from its crystalline form to an amorphous form.

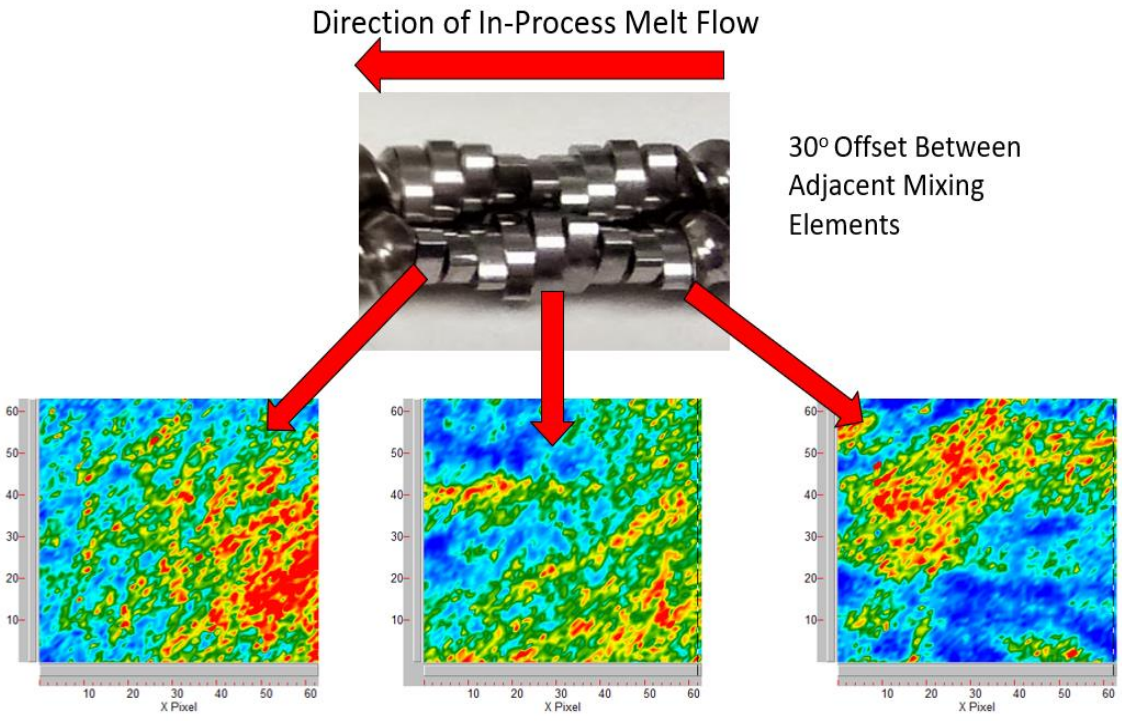

Figure 4-4: IR chemical images take of CC from the Beginning, Middle and End of Mixing zone.

The opposite can be determined from the behavior of CC in EPO when the mixing element angles are chaged to 90° (Figure 4-5). Here we can see that the orientation of the mixing elements is imparting more distributive character to the in-process material as the intensity of the signal from CC is not as diminished as before, but is more distributed throughout the melt.

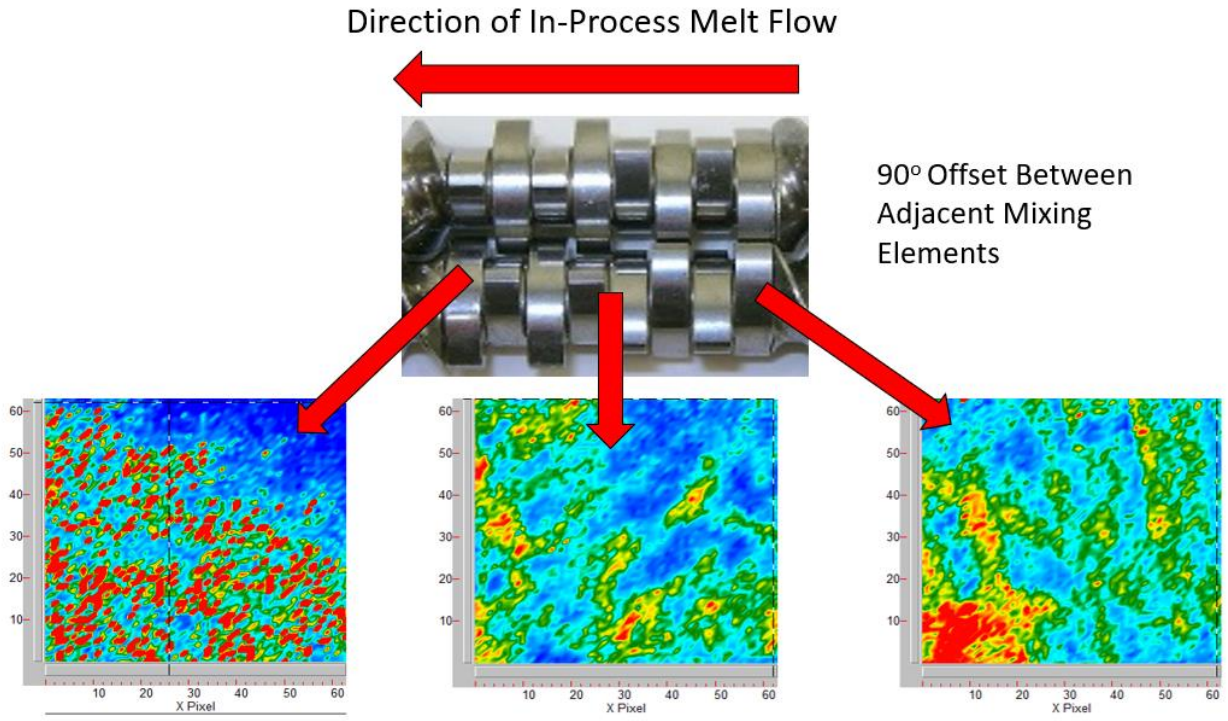

Figure 4-5: IR chemical images take of CC from the Beginning, Middle and End of Mixing zone.

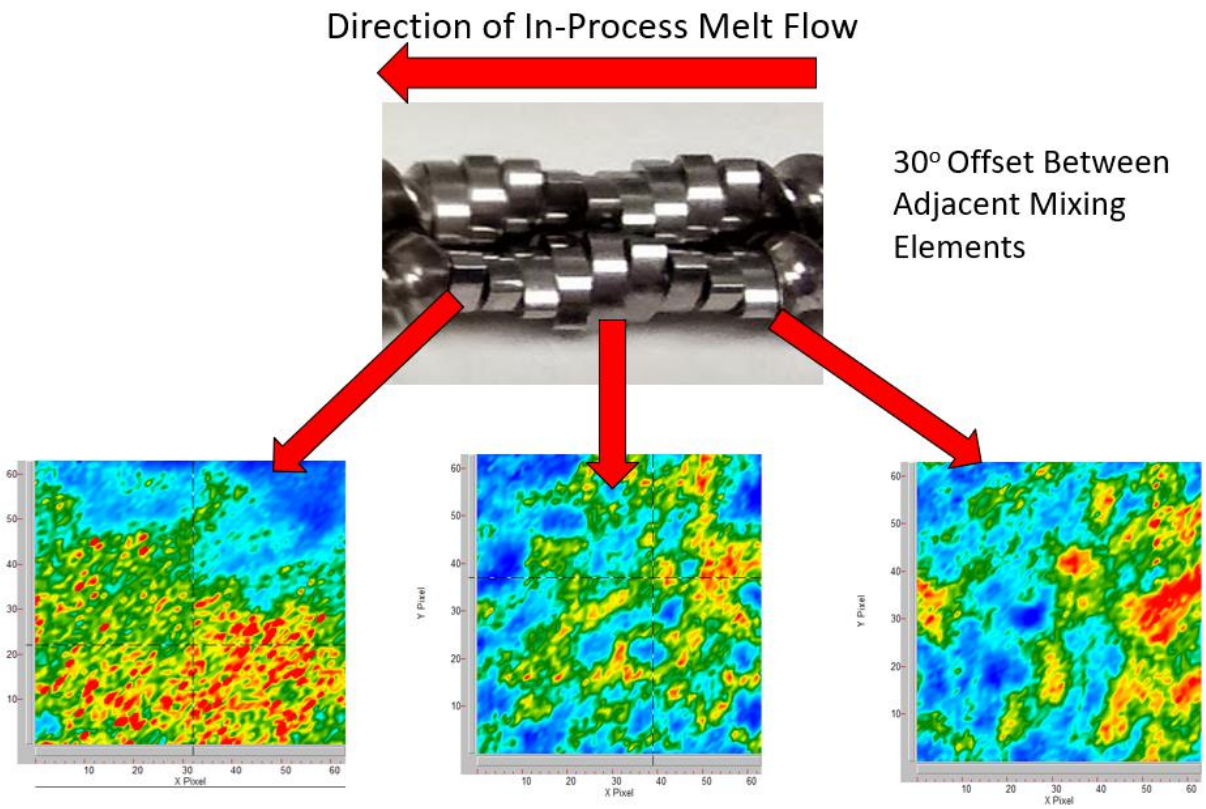

Figure 4-6: IR chemical images take of CBZ from the Beginning, Middle and End of Mixing zone.

In Figure 4-6 it can be seen that CBZ is undergoing dispersive mxing similar to that of CC in Figure 4-4. The DSC data supports this also as the AUC values are relatively unchanged (3.2, 3.0 & 2.6 J/g), again indicating that the dispersive mixing being imparted to the in-process material is not yet sufficient to convert the crystalline lattice to its amorphous form.

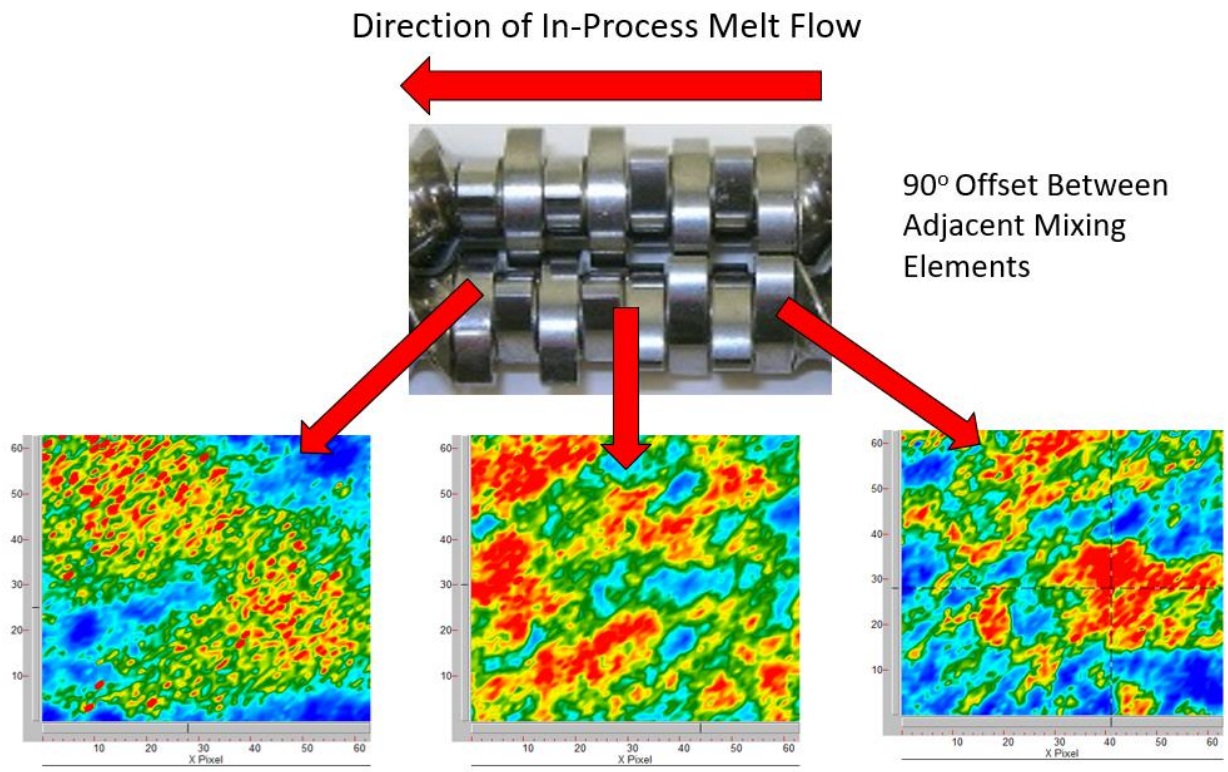

Figure 4-7: IR chemical images take of CBZ from the Beginning, Middle and End of Mixing zone.

Figure 4-7 shows that CBZ is being distributed thoughout the matrix as would be expected from perpendicular mixing elements; however, the DSC data indicates that that more material is undergoing amorphous conversion due, in part, to the intense deformations imparted as the polymer melt is divided and recombined (AUC 1.3, 0.68 and 0.68 J/g respectively). Despite the conventional knowledge that perpendicular are primarily responsible for distributive mixing, it would seem that the in-process material may respond differently due to its compositional changes.

4.5 Conclusion

FT-IR spectral imaging could be a useful offline tool for the investigation of the relationship between screw configuration and API distribution/dispersion within a polymer matrix. It is worth noting that only realtively simple missing blocks were examined in this study and far more complex designs are commonly employed during a typical Hot-Melt Extrusion process. This in combination with the effects noted here, namely the loss of crystallinity in the CBZ samples, may indicate that particular formulations are more or less sensitive to the stresses imparted by the process.

CHAPTER 5.

SUMMARY & CONCLUSIONS

In chapter 2, the use of an extruded intermediate was investigated in a somewhat novel sense (*i.e.* maintaining the API crystallinity) while approaching subsequent product development from a more conventional prospective. Here it was noted that care must be taken to ensure the physical identity of an API crystalline lattice. Additionally, incorporating milled extrudates into oral solid dosage forms poses interesting challenges due to the large differences in density as opposed to particle size. Chapter 3 explores the previously unreported use of a twin-screw extruder for the production of a dry granulation using quality by design principles. This study, in tandem with another study by a colleague, represents the first of its kind as no prior art could be found. Here the use of a twin-screw extruder is explored as an alternative dry granulating technology. Chapter 4 is an attempt to take a more granular look into the effects of screw design by examining the effect of paddle offset angle on dispersion and distribution of two APIs within a polymer matrix. This, in tandem with DSC data for phase identification, produced both anticipated (as in the case of caffeine citrate) and unanticipated results (demonstrated by carbamezapine).

The underlying theme of the research performed in order to arrive at this dissertation is simple; investigations into twin-screw extruder screw configuration. More broadly, this work investigates the interplay between a formulation's constituents and the extruder that is processing them. At the time that this research was conducted, the current pharmaceutical literature concerning screw-configuration seemed to regard it as more of an art rather than a science. On the other hand, the

information available from food, metals, ceramics, engineering literature approached screw geometry from a predominately mathematical perspective. In the current, neither of these approaches work well. Until mathematical based simulation models are more fully matured, the topic of screw configuration, and extrusion in general, should be treated with a combination of theory and practical experience. Finally, while the melt extrusion process is completely amenable to the FDA's push toward the QbD paradigm shift, some understanding and flexibility will be required on the agency's end to fully realize this processing technology. More specifically, the quantities listed in the Inactive Ingredient Database (IID) are simply insufficient to fully implement this processing technology as a viable approach.

BIBLIOGRAPHY

1. White, J.L., Potente, H., Berghaus, U. 2003. Screw Extrusion: Science and Technology; Progress in Polymer Processing. Hanser Publishers. ISBN 1569903174
2. Everhart, J.L., 1964. Impact and Cold Extrusion of Metals. Chemical Publishing Company. ISBN 082060013X
3. Rauwendaal, C. Polymer Extrusion. 2001. Society of Plastics Engineers Books. Hanser Gardner Publishers. ISBN 1569903212
4. Handle, F. 2009. Extrusion in Ceramics: Engineering Materials and Processes. Springer. ISBN 3540271007
5. Guy, R. 2001. Extrusion Cooking: Technologies and Applications. Woodhead Publishing. ISBN 0849312078
6. Moscicki, L., 2011. Extrusion Cooking Techniques: Applications, Theory & Sustainability. Wiley-VCH. ISBN 978-3-527-32888-8
7. Janssen, L. 2004. Reactive Extrusion Systems. CRC Press. ISBN 082474781X
8. White, J.L. 1995. Rubber Processing: Technology, Materials, Principles. Hanser Publishers. ISBN 1569901651
9. Ghebre-Sallassie, I. *et al.* 2003. Pharmaceutical Extrusion Technology (Drugs & the Pharmaceutical Sciences). CRC Press. ISBN 0824740505
10. Repka, M. A., Langley, N., DiNunzio, J., 2013. Melt Extrusion, Materials, Technology and Drug Product Design. Springer. ISBN 978-1-4614-8432-5
11. F Handle (ed.), *Extrusion in Ceramics, Engineering Materials and processes,* Springer-Veralg Berlin Heidelberg, 2009.

12. Costeux, S. et al. (2011) Facile TPO dispersion using extensional mixing. Antec 2011.
13. Sekiguchi, K., N. Obi, and Y. Ueda, *Studies on Absorption of Eutectic Mixture. Ii. Absorption of Fused Conglomerates of Chloramphenicol and Urea in Rabbits.* Chem Pharm Bull (Tokyo), 1964. **12**: p. 134-44.
14. Griff, A.L., Plastics Extrusion Technology. 2nd ed. 1968, Malabar: Robert E. Krieger Publishing Company.
15. Yao, W., et al., *Thermodynamic properties for the system of silybin and poly(ethylene glycol) 6000.* Thermochimica Acta, 2005. **437**(1-2): p. 17-20
16. Vippagunta, S.R., et al., *Factors affecting the formation of eutectic solid dispersions and their dissolution behavior.* J Pharm Sci, 2007. **96**(2): p. 294-304.
17. Desai, J., K. Alexander, and A. Riga, *Characterization of polymeric dispersions of dimenhydrinate in ethyl cellulose for controlled release.* Int J Pharm, 2006. **308**(1-2): p. 115-23.
18. Karavas, E., E. Georgarakis, and D. Bikiaris, *Application of PVP/HPMC miscible blends with enhanced mucoadhesive properties for adjusting drug release in predictable pulsatile chronotherapeutics.* Eur J Pharm Biopharm, 2006. **64**(1): p. 115-26.
19. Crowley, M.M., et al., *Physicochemical properties and mechanism of drug release from ethyl cellulose matrix tablets prepared by direct compression and hot-melt extrusion.* International journal of pharmaceutics, 2004. **269**(2): p. 509-522.
20. Aitken-Nichol, C., F. Zhang, and J.W. McGinity, *Hot melt extrusion of acrylic films.* Pharmaceutical Research, 1996. **13**(5): p. 804-808.
21. Follonier, N., E. Doelker, and E.T. Cole, *Evaluation of hot-melt extrusion as a new technique for the production of polymer-based pellets for sustained release capsules containing high*

loadings of freely soluble drugs. Drug Development and Industrial Pharmacy, 1994. **20**(8): p. 1323-1339.

22. Chen, M., et al., *Influence of Processing Parameters and Formulation Factors on the Bioadhesive, Temperature Stability and Drug Release Properties of Hot-Melt Extruded Films Containing Miconazole.* AAPS PharmSciTech, 2014. **15**(3): p. 522-529.
23. Keleb, E., et al., *Continuous twin screw extrusion for the wet granulation of lactose.* International journal of pharmaceutics, 2002. **239**(1): p. 69-80.
24. Van Melkebeke, B., et al., *Melt granulation using a twin-screw extruder: a case study.* International journal of pharmaceutics, 2006. **326**(1): p. 89-93.
25. Thompson, M. and J. Sun, *Wet granulation in a twin‐screw extruder: Implications of screw design.* Journal of pharmaceutical sciences, 2010. **99**(4): p. 2090-2103.
26. El Hagrasy, A., et al., *Twin screw wet granulation: influence of formulation parameters on granule properties and growth behavior.* Powder technology, 2013. **238**: p. 108-115.
27. Kerns, E.H., *High throughput physicochemical profiling for drug discovery.* J Pharm Sci, 2001. **90**(11): p. 1838-58.
28. Behm, F.M., et al., *Low-nicotine regenerated smoke aerosol reduces desire for cigarettes.* J Subst Abuse, 1990. **2**(2): p. 237-47.
29. Chitkara, D. and N. Kumar, *BSA-PLGA-based core-shell nanoparticles as carrier system for water-soluble drugs.* Pharm Res, 2013. **30**(9): p. 2396-409
30. Bastin, R.J., M.J. Bowker, and B.J. Slater, *Salt selection and optimisation procedures for pharmaceutical new chemical entities.* Org. Proc. Res. Dev., 2000. **4**(5): p. 427-35.
31. Martin, F.A., et al., *Ketoconazole Salt and Co-crystals with Enhanced Aqueous Solubility.* Cryst. Growth Des., 2013. **13**(10): p. 4295-4304

32. Law, D., et al., *Properties of rapidly dissolving eutectic mixtures of poly(ethylene glycol) and fenofibrate: the eutectic microstructure.* J Pharm Sci, 2003. **92**(3): p. 505-15.

33. Kossena, G.A., et al., *Low dose lipid formulations: effects on gastric emptying and biliary secretion.* Pharm Res, 2007. **24**(11): p. 2084-96.

34. Collnot, E.M., et al., *Mechanism of inhibition of P-glycoprotein mediated efflux by vitamin E TPGS: influence on ATPase activity and membrane fluidity.* Mol Pharm, 2007. **4**(3): p. 465-74.

35. Chemburkar, S.R., et al., *Dealing with the Impact of Ritonavir Polymorphs on the Late Stages of Bulk Drug Process Development.* Org. Proc. Res. Dev., 2000. **4**(5): p. 413-417.

36. Chiou WL, Riegelman S (1971) Pharmaceutical applications of solid dispersion systems. J Pharm Sci 60:1281–1302. doi: 10.1002/jps.2600600902

37. Ayenew, Z., Puri, V., Kumar, L., Bansal, A. Trends in Pharmaceutical Taste Masking Technologies: A Patent Review. Recent Patents on Drug Delivery & Formulation, 2009, 3, 26-39.

38. Banker, G.S.; Rhodes, C.T. 2002. Modern Pharmaceutics 4th ed. New York: Dekker, pp. 674-675.

39. Hirani, J., Rathod, D., Vadalia, K., Orally Disintegrating Tablets: A Review. Trop. J. Pharm. Res 2009 161-172.

40. Egilius, L. H., Rapoport, A. M., Dodick, D. W., Charlesworth, B. 2004, Acute Treatment of Migraine with Zolmitriptan 5mg Orally Disintegrating Tablets. CNS Drugs 18, 15, 1133-1141.

41. Kinon, B. J., Hill, A. L., Liu, H., Kollack-Walker, S., 2003, Olanzapine orally disintegrating tablets in the treatment of acutely ill non-compliant patients with schizophrenia, Int. J. Neuropsychopharmacology. 6, 2, 97-102.

42. Pahwa, R., Pipiani, M., Sharma, P. C., Kaushik, D., Nanda, S., 2010. Orally Disintegrating Tablets-Friendly to Pediatrics and Geriatrics. Archives of Applied Science Research. 2, 2, 35-48.

43. Stange, U., Führling, C., 2014. Formulation, Preparation and Evaluation of Novel Orally Disintegrating Tablets Containing Taste-Masked Naproxen Sodium Granules and Naratriptan Hydrochloride. J. Pharm Sci, 103, 1233-1245.

44. Strickley, R., Iwata, Q., Wu, S., Dahl, T. 2007. Pediatric drugs-a review of commercially available oral formulations. J Pharm Sci. 97, 1731-1774.

45. Gupta, M., Kovar, A., Meibohm, B., 2005, The Clinical Pharmacokinetics of Phosphodiesterase-5 Inhibitors for Erectile Dysfunction. J. Clinical Pharmacology 45, 987-1003.

46. Viagra ® (sildenafil citrate tablets) [package insert]. Pfizer, Inc. NY, NY. 1998

47. Revatio ® (sildenafil citrate tablets) [package insert]. Pfizer, Inc. NY, NY. 2005

48. Yi, E., Kim, J., Rhee, Y., Kim, S., Lee, H., Park, C., 2014, Preparation of sildenafil citrate microcapsules and *in vitro/in vivo* evaluation of taste masking efficiency. Int. J. Pharmaceutics, 466, 286-295.

49. O'Donnell J, Mertl SL, Kelly WN. Propylene Glycol Toxicity in a Pediatric Patient: The Dangers of Diluents. J Pharm Prac 2000; 13: 214-225

50. Beers, M. H., Ouslander, J. G., 1989. Risk Factors in Geriatric Drug Prescribing, Drugs, 37, 105-112.

51. Repka, M. A., Thumma, S., Upadhye, S., Kumar, S., McGinity, J., Martin, C., 2007. Pharmaceutical Applications of Hot Melt Extrusion: Part I. Drug Dev and Ind. Pharm. 33, 909-926.

52. Repka, M. A., Langley, N., DiNunzio, J., 2013. Melt Extrusion, Materials, Technology and Drug Product Design. NY, Springer, 4-5; 14-16.

53. U.S. Food and Drug Administration. 2014. Alphabetical List of SCOGS Substances. http://www.fda.gov/Food/IngredientsPackagingLabeling/GRAS/SCOGS/ucm084104.htm

54. Repka, M. A., Shah, S., Lu, J., Maddineni, S., Morott, J., Padwardhan, K., Mohammed, N.2012. Melt Extrusion: Process to Product. Expert Opinion on Drug Delivery, 9, 105-125.

55. Mannur, V. S., Rathi, S. M., Mastiholimath, V. S., Dengale, N. P., Shinde, T. A. 2011. Stability indicating RP-HPLC method development and validation of Sildenafil Citrate in pure form. Int. J. Res. Pharm. Sci. 2, 187-191.

56. Azarmi, S., Roa, W. Löbenberg, R. 2007. Current perspectives in dissolution testing of conventional and novel dosage forms. Int. J. Pharmaceutics. 328, 12-21.

57. U.S. Food and Drug Administration. 2014. Dissolution Methods. http://www.accessdata.fda.gov/scripts/cder/dissolution/dsp_SearchResults_Dissolutions.cfm?PrintAll=1.

58. Melkinov, P., Cobri, P., Cuin, A., Cavicchioli, M. Guimareas, W. 2003. Physicochemical properties of Sildenafil Citrate (Viagra) and Sildenafil Base. J. Pharmaceutical Sciences, 92, 2140-2143.

59. Lu, J., Rohani, S. 2009. Polymorphism and crystallization of active pharmaceutical ingredients (APIs). Curr Med Chem, 16, 884-905.

60. Drug Recalls. FDA.gov; http://www.fda.gov/Drugs/drugsafety/DrugRecalls/default.htm Retrieved on June 22nd, 2015.

61. Sam, T., Koch, H. 2014. Quality Metrics, Quality Culture, Quality Matters. AAPS Newsmagazine, Volume 17, Number 8, Pages 14-20.

62. M. A. Repka, S. Shah, J. Lu et al., “Melt extrusion: process to product,” Expert Opinion on Drug Delivery, vol. 9, no. 1, pp. 105–125, 2012.

63. M. A. Repka, S. K. Battu, S. B. Upadhye et al., “Pharmaceutical applications of hot-melt extrusion: part II,” Drug Development and Industrial Pharmacy, vol. 33, no. 10, pp. 1043–1057, 2007.

64. M. A. Repka, S. Majumdar, S. K. Battu, R. Srirangam, and S. B. Upadhye, “Applications of hot-melt extrusion for drug delivery,” Expert Opinion on Drug Delivery, vol. 5, no. 12, pp. 1357–1376, 2008.

65. Shah, S. Maddineni, S., Lu, J. 2012. Repka, M.A. Melt Extrusion with Poorly Water Soluble Drugs. International Journal of Pharmaceutics. Volume 453. Issue 1. Pages 233-252.

66. Keleb, E.I. *et al*. 2002. Continuous twin screw extrusion for the wet granulation of lactose. International Journal of Pharmaceutics. Volume 239. Issues 1-2. Pages 69-80.

67. Hagrasy, A., Hennenkamp, J., *et al.* 2013. Twin screw wet granulation: Influence of formulation parameters on granule properties and growth behavior. Powder Technology. Volume 238. Pages 108-115.

68. Keleb, E.I. 2004. Twin screw extrusion as a simple and efficient tool for wet granulation. Internaitonal Journal of Pharmaceutics. Volume 273. Issue 1-2. Pages 183-194.

69. Thompson, M.R., Son, J. 2010 Wet granulation in a twin screw extruder: Implications of screw design. Journal of Pharmaceutical Sciences. Volume 99. Issue 4. Pages 2090-2103.

70. Melkebeke, B.V., Vermeulen, B., Vervaet, C., Remon, J.P. 2006. Melt Granulation using a Twin Screw Extruder: A Case Study. International Journal of Pharmaceutics. Volume 326. Issues 1-2. Pages 89-93.

71. Keen, J., McGinity, J., *et al.* 2015. Continuous twin screw melt granulation of glyceryl benhenate: development of controlled release tramadol hydrochloride tablets for improved safety. International Journal of Pharmaceutics. Volume 487. Issues 1-2. Pages 72-80.

72. Patil, H., Tiwari, R., Upadhye, S. Vladyka, R. Repka, M., 2015. Formulation and development of pH-independent/dependent sustained release matrix tablets of ondansetron HCl by a continuous twin-screw melt granulation process. International Journal of Pharmaceutics. In-Press. Available Online.

73. Tan, D., Chin, W., Tan, E., Hong, S., Gu, W., Gokhale, R. 2014. Effect of binders on the release rates of direct molded verapamil tablets using twin-screw extruder in melt granulation. International Journal of Pharmaceutics. Volume 463. Issues 1. Pages 89-97.

74. Mu, B. Thompson, M.R. 2012. Examining the mechanics of granulation with a hot melt binder in a twin-screw extruder. Chemical Engineering Science. Volume 81. Pages 46-56.

75. Vercruysse, J., Burggraeve, A., Fonteyne, M., Cappuyns, P., Delaet, U., Van Assche, I., De Beer, V., Remon, J.P., Vervaet, C. 2015. Impact of screw configuration on the particle size distribution of granules produced by twin screw granulation, International Journal of Pharmaceutics, Volume 479, Issue 1, Pages 171-180.

76. Shen Yu, Gavin K. Reynolds, Zhenyu Huang, Marcel de Matas, Agba D. Salman, Granulation of increasingly hydrophobic formulations using a twin screw granulator, International Journal of Pharmaceutics, Volume 475, Issues 1–2, 2014, Pages 82-96.

77. Tim Chan Seem, Neil A. Rowson, Andy Ingram, Zhenyu Huang, Shen Yu, Marcel de Matas, Ian Gabbott, Gavin K. Reynolds, Twin screw granulation — A literature review, Powder Technology, Volume 276, 2015, Pages 89-102.

78. H. Li, M.R. Thompson, K.P. O'Donnell, Understanding wet granulation in the kneading block of twin screw extruders, Chemical Engineering Science, Volume 113, 2014, Pages 11-21.

79. James J. Cartwright, John Robertson, Dorie D'Haene, Matthew D. Burke, Jeffrey R. Hennenkamp, Twin screw wet granulation: Loss in weight feeding of a poorly flowing active pharmaceutical ingredient, Powder Technology, Volume 238, 2013, Pages 116-121.

80. Kai T. Lee, Andy Ingram, Neil A. Rowson, Comparison of granule properties produced using Twin Screw Extruder and High Shear Mixer: A step towards understanding the mechanism of twin screw wet granulation, Powder Technology, Volume 238, 2013, Pages 91-98.

81. J. Vercruysse, D. Córdoba Díaz, E. Peeters, M. Fonteyne, U. Delaet, I. Van Assche, T. De Beer, J.P. Remon, C. Vervaet, Continuous twin screw granulation: Influence of process variables on granule and tablet quality, European Journal of Pharmaceutics and Biopharmaceutics, Volume 82, Issue 1, 2012, Pages 205-211.

82. Kai T. Lee, Andy Ingram, Neil A. Rowson, Twin screw wet granulation: The study of a continuous twin screw granulator using Positron Emission Particle Tracking (PEPT) technique, European Journal of Pharmaceutics and Biopharmaceutics, Volume 81, Issue 3, 2012, Pages 666-673.

83. D. Djuric, B. Van Melkebeke, P. Kleinebudde, J.P. Remon, C. Vervaet, Comparison of two twin-screw extruders for continuous granulation, European Journal of Pharmaceutics and Biopharmaceutics, Volume 71, Issue 1, 2009, Pages 155-160.
84. Nolte, Elle. 2010. Advanced Granulating Technology Improves Process Efficiencies. Pharmaceutical Processing. http://www.pharmpro.com/articles/2010/08/advanced-granulating-technology-improves-process-efficiencies. Accessed 6/20/2015.
85. Kindelsperger, B. 2010. Continuous Low Moisture Wet Mass Granulation, A Demonstration of Potential. Pharmaceutical Manufacturing. http://www.pharmamanufacturing.com/articles/2010/102/. Accessed 6/20/2015.
86. United States Pharmaceopia 38 - National Formulary 33. General Chapters: <1174>, Powder Flow. http://www.uspnf.com.umiss.idm.oclc.org/uspnf/pub/index?usp=38&nf=33&s=1&officialOn=August%201,%202015. Accessed 8/24/2015.
87. U.S. Department of Health and Human Services. U.S. Food and Drug Administration. Dissolution Methods. http://www.accessdata.fda.gov/scripts/cder/dissolution/dsp_SearchResults_Dissolutions.cfm?PrintAll=1. Accessed 8/24/2015.

VITA

Joseph Thomas Morott Jr., son of Joseph Thomas Morott Sr. and Toni Sue Sullivan Ph.D., was born in Ozark, AL on December 15th, 1981. He received the degree of associate of arts (A.A.) from Wallace Community College in Dothan, AL in 2008. He received the degree of Bachelor of Science (B.S.) in Professional Chemistry from Belmont University in Nashville, TN in May 2010. In August of 2010 he entered the Department of Pharmaceutics & Drug Delivery within the School of Pharmacy at the University of Mississippi. While therein he received admission into the Rho Chi Pharmacy National Honor Society, the 2015 Graduate Achievement Award in Pharmaceutics, and the Pre-Doctoral Award for Outstanding Contributions to the Hands-On Tableting Course, where he served as the Hot-Melt Extrusion Lab Instructor from September 2013 until September 2015. He graduated with the degree of Doctor of Philosophy (Ph.D.) in the Pharmaceutical Sciences, Emphasis in Pharmaceutics.